Study of Erosion-Corrosion Under Impingement by a Fluid Jet

by

KAZI BAYZID KABIR

A thesis

submitted to the Department of Chemical Engineering

for partial fulfillment of the requirements

for the degree

of

MASTER OF SCIENCE IN ENGINEERING
(CHEMICAL)

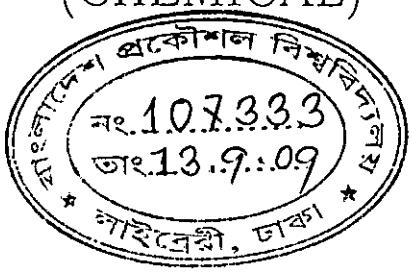

DEPARTMENT OF CHEMICAL ENGINEERING

BANGLADESH UNIVERSITY OF ENGINEERING
AND TECHNOLOGY, DHAKA

CERTIFICATION OF THESIS WORK

We the undersigned, are pleased to certify that **Kazi Bayzid Kabir**, a candidate for the degree of **Master of Science in Engineering (Chemical)** has presented his thesis work on the subject **"Study of Erosion-Corrosion Under Impingement by a Fluid Jet"**. The thesis is acceptable in from and content. The student demonstrated a satisfactory knowledge of the field covered by this thesis in an oral examination held on **August 29, 2009**.

Dr. Iqbal Mahmud — Chairman
Professor Emeritus
Department of Chemical Engineering
BUET, Dhaka-1000

Dr. Ijaz Hossain — Member
Professor and Head
Department of Chemical Engineering
BUET, Dhaka-1000

Dr. M.A.A.S. Choudhury — Member
Assistant Professor
Department of Chemical Engineering
BUET, Dhaka-1000

Dr. Nooruddin Ahmed — Member (External)
UGC Professor
BUET, Dhaka-1000

Abstract

Influence of flow on corrosion behavior of stainless steel, brass and aluminum was studied using electrochemical measurement techniques. Flow effect was identified by comparing erosion-corrosion situations with pure corrosion studies. For this purpose, polarization techniques and open-circuit potential measurements were applied in both quiescent and flow conditions. A closed flow-loop in combination with submerged impinging jet system was used to simulate flow conditions similar to industrial fluid flow at bends and disturbed conditions. The experimental setup showed satisfactory performance within the range of operation.

Polarization behavior was observed in artificial seawater, sodium carbonate and ferrous sulfate. Active-passive behavior was observed for stainless steel in all environments (except in ferrous sulfate with ferric chloride). Brass and aluminum showed active-passive behavior with sodium carbonate. However, in flow condition passive zone of aluminum was totally absent. The polarization curves were found to shift with increasing flow rates indicating increase in corrosion rate.

Open-circuit potential (OCP) transient of the observed metals/alloys indicated the nature and extent of corrosion on the sample by the environment. OCP was obtained in artificial seawater and sodium carbonate solution. Three distinct type of curves were found for all the metal-environment combinations. Increasing OCP potential indicated noble metal behavior while decrease in OCP indicated corrosion of the material in the exposed environment. Directional shift in the OCP indicated changes in the surface phenomena. Hence, shape of these curves provides information about the nature and extent of metal environment interaction. Experimental observations showed the applicability of open circuit measurement for on-line corrosion monitoring.

Acknowledgements

The author expresses his sincere thanks to Dr. Iqbal Mahmud for proposing the present research topic. The author also like to express his profound respect to him for his valuable guidance and supervision throughout the entire work.

The author is grateful to Dr. Md. Moniruzzaman, Associate Professor of Materials and Metallurgical Engineering Department, BUET for providing the potentiostat for the research work. The author would like to gratefully acknowledge the contribution of the MME department for their technical and instrumental support in analysis of metal samples.

The author would like to gratefully acknowledge Mr. Ali Akbar of Chemical Engineering Department, BUET for his cooperation with purchase of materials and chemicals, and setting up the experimental rig.

Acknowledgements are also made for the help rendered by the staff of the Chemical Engineering Department, BUET especially Mr. Abdul Mannan for producing thousands of liters of distilled water and Mr. Abbas, Mr. John Biswas, Mr. Shahjahan and Mr. Mahbub for their help during the research work.

Contents

List of Figures

List of Tables

Abbreviations

AD	Analog-to-Digital
ASTM	American Society for Testing and Materials
BCL	Battelle Columbus Laboratories
CPI	Chemical Process Industries
CS	Carbon Steel
CR	Corrosion Rate
DO	Dissolved Oxygen
ECN	Electrochemical Current Noise
EPN	Electrochemical Potential Noise
EN	Electrochemical Noise
EPRI	Electric Power Research Institute
EPS	Expanded PolyStyrene
ER	Erosion Rate
NBS	National Bureau of Standards
NPSH	Net Positive Suction Head
OCP	Open Circuit Potential
OES	Optical Emission Spectroscopy
PVC	Poly Vinyl Chloride
PTFE	PolyTetraFluoroEthylene
RCE	Rotating Cylinder Electrode
RDE	Rotating Disk Electrode
SCE	Saturated Calomel Electrode
UNS	Unified Numbering System

Symbols

C	corrosion rate	mm^3/hr
C_{b,O_2}	bulk O_2 concentration	mol/m^3
C_{eq}	equilibrium Fe^{2+} concentration	mol/m^3
C_∞	bulk Fe^{2+} concentration	mol/m^3
D	diffusion coefficient	m^2/s
D_{O_2}	diffusion coefficient for O_2 in water	m^2/s
d	diameter	m
E	erosion rate	mm^3/hr
e	height of surface roughness	m
i_a	activation controlled current density	A m^{-2}
i_{corr}	corrosion current density	A m^{-2}
i_d	diffusion controlled current density	A m^{-2}
k_{-1}	reverse reaction rate	dm^3/s
k_1	forward reaction rate	dm^3/s
k_m	mass transfer coefficient	m/s
k_R	reaction rate constant	
l	characteristic dimension	m
r	radius	m
S	synergistic wastage rate	mm^3/hr
T	total wastage rate	mm^3/hr
u	mean velocity	m/s
u_p	particle velocity	m/s
v	mean velocity	m/s

y	distance $\perp$ to the surface	m

GREEK SYMBOLS

δ	diffusion boundary layer thickness	m
η_c	turbulence eddy viscosity	kg/m s
ρ	density	kg/m^3
μ	dynamic viscosity	kg/m s
τ_w	shear stress	N/m^2
ω	angular velocity	radians/s

DIMENSIONLESS NUMBERS

f	fanning friction factor
Re	Reynolds number $\left(= \frac{du\rho}{\mu}\right)$
Sc	Schmidt number $\left(= \frac{\mu}{\rho D}\right)$
Sh	Sherwood number $\left(= \frac{kl}{\rho D}\right)$
y^+	viscous length

Chapter 1

Introduction

1.1 Background

Corrosion is a phenomena as old as the history of metal. Oxides are thermodynamically more stable than the metal and hence, metals corrode spontaneously to form their oxides. Costs involved with corrosion (direct or indirect) are huge (Appendix A) and therefore a lot of effort is put into corrosion research.

Chemical process industries deal with various chemicals and most of the processes are continuous or semi-continuous. A relative motion exists between the moving fluids and the construction materials, In such a situation, corrosion process is intensified by the combined mechanical and chemical effects of the environment. This synergistic effect is termed as erosion-corrosion.

Historically, erosion-corrosion became a problem with the copper alloy condensers of British naval ships [1]. Erosion-corrosion of copper alloys has been an ongoing problem since then. The other major problem areas are (a) power plants where steels are exposed to water or water/steam mixtures in the temperature range 90-280°C; (b) the oil and gas industries where steels are exposed to various liquid, gas and sometimes solids; (c) pulp and paper industries where materials are exposed to sulfur containing chemicals.

Erosion-corrosion can occur in different situations: in absence or presence of solids and gases. Hence, there is no widely acceptable mechanism of erosion-corrosion. However, there are suggestions that the corrosion process is enhanced by increased mass transfer and/or mechanical force impacts on the surface [2, 3]. Therefore, models to predict erosion-corrosion are not readily available. Experimental studies are best way to predict occurrence of erosion-corrosion. In addition, some monitoring techniques have been also developed for online monitoring [4].

The most severe erosion-corrosion problem in single-phase flow occurs under conditions of disturbed turbulent flow at sudden changes in the flow geometry, such as bends, heat-exchanger-tube inlets, orifice plates, valves, fittings, and in turbomachinery including pumps, turbine, and propellers. *In situ* experiments can be performed to analyze erosion-corrosion behavior of metals. However, such large scale experiments would require huge time. On the other hand, small-scale laboratory studies require less time and cost less. Design of experiments with appropriate correlation to the actual large-scale system, therefore, can be very effective.

Several systems has been proposed for studying erosion-corrosion. Among them rotating disk electrode (RDE) has been used by numerous researchers. Rotating cylinder electrodes also found to be attractive and recognized as a useful to tool to study velocity sensitive corrosion [5, 6]. Though, flow, heat and mass transfer equations for these systems are well developed they are far from the geometric similarity of the actual industrial systems.

Liquid impingement systems have three variations, namely, free-jet, submerged jet and jet-in-slit [7]. Free-jet systems are well adopted for studying erosion-corrosion by liquid droplets and slurry erosion-corrosion [8–11]. Jet-in-slit test has also been used for flow-induced localized corrosion and slurry erosion-corrosion studies [7, 12]. However, the impinging fluid has to travel through air before impinging onto the metal surface for both these systems unlike the real conditions in process flow where the metal surfaces are exposed to fluid impacts in submerged conditions. As a result submerged jet systems have been adopted by many researchers [13, 14]. For the current study the latter approach has been selected.

Use of corrosion coupons are simplest form of corrosion monitoring. Corrosion coupons are carefully machined thin metal bars inserted into external coupon holder in the test environment. Coupons are pre-weighed before testing. After exposure, coupons are weighed and/or examined microscopically to assess the mode and extent of damage.

On the other hand, Electrochemical techniques provide a viable method for rapid prediction or evaluation of corrosion. Their applicability arises from the fact that most aqueous corrosion processes involving metals require the transfer of charge across the metal-solution interface. Electrochemical measurements in flowing solution can provide data on (a) the rate of general corrosion and the possibility of other forms of attack, (b) mechanism, (c) the characteristics hydrodynamic parameters, and (d) the composition of the solution by electro-analytically monitoring compositions or measuring red-ox potential, pH etc. [15]. For the current study electrochemical techniques (e.g. polarization and open circuit potential measurements) have been used to take their advantages (e.g. shorter test period, online monitoring etc.) compared to weight-loss method (coupon test).

1.2 Objective of the Study

The objective of the study was to identify the effect of flow on corrosion behavior of several metal/alloys, namely, stainless steel, brass and aluminum, in different corrosive environments. The study included observation of open circuit potential and polarization diagram in absence and presence of flow.

1.3 Scope of the Study

Selection of the metal/alloys and corrosive environment were dictated by the their availability and cost. Corrosive environments were created by dissolving commercial grade chemicals in distilled water Huge chemical requirements and high cost prevented use of analytical grade chemicals.

The experimental system was first characterized to check it's suitability to perform the study. After proper surface preparation metal/alloy specimens were exposed to corrosive fluids, first under stagnant conditions and then with flow conditions. Electrochemical measurements were made to identify flow effects.

1.4 Thesis Organization

Chapter 1 is the introduction to this thesis. Summary of the background and thesis organization are also included in this chapter.

Chapter 2 provides an overview of erosion-corrosion. Hydrodynamic factors affecting corrosion are briefly discussed. Current understanding of erosion-corrosion mechanism, relative roles of erosion and corrosion and remedial measures for erosion-corrosion are explained.

Chapter 3 describes methodology for erosion-corrosion testing. Different systems used for erosion-corrosion study are discussed. Correlating criteria for experimental results with the large-scale systems are provided. Electrochemical instrumentation of corrosion study are briefly discussed. Different corrosion monitoring techniques are also discussed.

Chapter 4 includes experimental methods and materials. Material specifications and detailed description of the experimental rig are provided.

Chapter 5 provides the results of the experimental studies. The observed results are also discussed.

Chapter 6 states the conclusions drawn from the current work and suggests possible direction for future research.

Chapter 2

Literature Review

2.1 Introduction: Forms of Corrosion

Depending on the environmental conditions and the nature of the metal involved corrosion can take many forms. Corrosion can be classified in five broad groups. When all areas of the metal corrode at the same rate it is called **uniform corrosion**. In case of **localized corrosion**, certain areas of the metal surface corrode at higher rate than others due to heterogeneities in the metal, the environment or in the geometry of the structure as a whole. **Pitting** occurs due to highly localized attack at specific areas resulting in small pits that penetrate into the metal and may lead to perforation. In **selective dissolution**, one component of an alloy (usually the most active one) is selectively removed. **Conjoint action of corrosion and mechanical factors** also causes localized attack or fracture due to the synergistic action of mechanical factors and corrosion. Erosion-corrosion, fretting corrosion, impingement attack, cavitation damage, stress corrosion cracking, hydrogen cracking, etc. falls into this category. Potable water distribution networks, fossil fuel and nuclear power industries, transportation sector, chemical processing, pulp & paper, pharmaceutical, food & beverages, and petroleum & petrochemical industries use metals and therefore encounter frequent occurrence

of various forms of corrosion. Figure 2.1 shows types of corrosion that can occur in chemical process industries (CPI) [16].

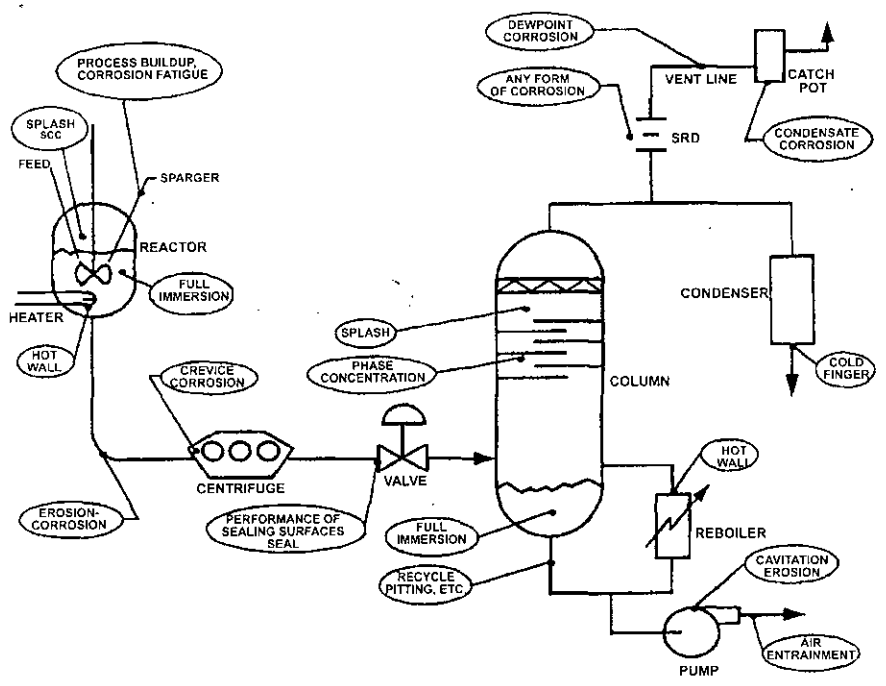

FIGURE 2.1: Various types of corrosion in chemical process industries

This dissertation mainly focuses on flow induced corrosion, i.e., erosion-corrosion.

2.2 Erosion-Corrosion

Relative movement between metals and environments has an effect on rate of corrosion, unless both anodic and cathodic processes are activation controlled [3]. Flow induced corrosion problems, encompassing flow enhanced dissolution and impingement attack, are generally termed as erosion-corrosion.

Erosion-corrosion is the conjoint action involving corrosion and erosion in the presence of a moving corrosive fluid, leading to accelerated loss of material [17]. The relative contribution of erosion and corrosion to the corrosion rate may vary

depending on the type of erosion-corrosion. Table 2.1 shows a spectrum of erosion-corrosion mechanisms from dissolution dominant to purely mechanical damage [18].

TABLE 2.1: Spectrum of erosion-corrosion processes

Dissolution dominant
Flow thins protective film to equilibrium thickness which is a function of both mass transfer rate and growth kinetics. Erosion-corrosion rate is controlled by the dissolution rate of the protective film.
Film is locally removed by dissolution, surface shear stress or particle/bubble impact; but it can repassivate. Erosion-corrosion rate is a function of the frequency of film removal, bare metal dissolution rate and subsequent repassivation rate.
Film is removed and does not reform. Erosion-corrosion rate is the rate the bare metal can dissolve.
Film is removed and underlying metal surface is mechanically damaged which contributes to overall metal loss i.e. erosion-corrosion rate is equal to bare metal dissolution rate plus possibly synergistic effect of mechanical damage.
Film is removed and mechanical damage to underlying metal is the dominant damage mechanism.
Mechanical damage dominant

2.3 Flow Fundamentals Related to Corrosion

Corrosion of metals and alloys is a surface phenomenon and is affected by metal's interaction with the surroundings. Therefore, what goes to the metal surface has a significant effect on corrosion. Transport of materials to the surface can be diffusive or convective. In stagnant condition, diffusion is the means of transport. However, presence of fluid movement about the metal surface (or vice versa) would result convective mass transfer in addition to diffusion.

Fluid flow over a solid surface can be characterized as either laminar or turbulent (based on Reynolds number). Most of the practical transport processes involve turbulent flow. Therefore, solid-fluid interaction in turbulent flow must be well known to understand mass transfer and force impact by fluid on the surface.

Disruption of boundary layer can give rise to some unwanted observations. Therefore, hydrodynamics of the system can play an important role in material loss i.e., erosion-corrosion.

Various hydrodynamic factors related to corrosion are discussed in brief in the following sections.

2.3.1 Hydrodynamic Boundary Layer

Fluid is assumed as ideal (i.e, frictionless and incompressible) in most of the theoretical investigations in the field of fluid mechanics. However, the concept of a *perfect* fluid fails completely when solid surfaces interact with the fluid. Existance of intermolecular attractions in real fluids causes the fluid to adhere to the solid surface and gives rise to shearing stress. Tangential or frictional forces of such a fluid are well connected with the viscosity of the fluid.

For a real fluid, the effects of viscosity are obvious at the solid boundary and diminish rapidly with distance from the boundary. This relatively thin layer of distorted velocity is defined as boundary layer. Outside the boundary layer behavior of the real fluid is similar to the ideal fluid.

The turbulent layer can be divided into three regions [19]:

- inertial sublayer ($y^+ > 30$)
- buffer layer ($30 > y^+ > 5$)
- viscous sublayer ($y^+ < 5$)

where y^+ is the dimensionless viscous length.

Velocity profile for turbulent flow over a plane surface or in a pipe (also known as universal velocity profile) is shown in Figure 2.2[20].

Turbulent boundary layer plays a very important role in the corrosion process, since the movements of corroding chemical species to the wall, chemical reaction

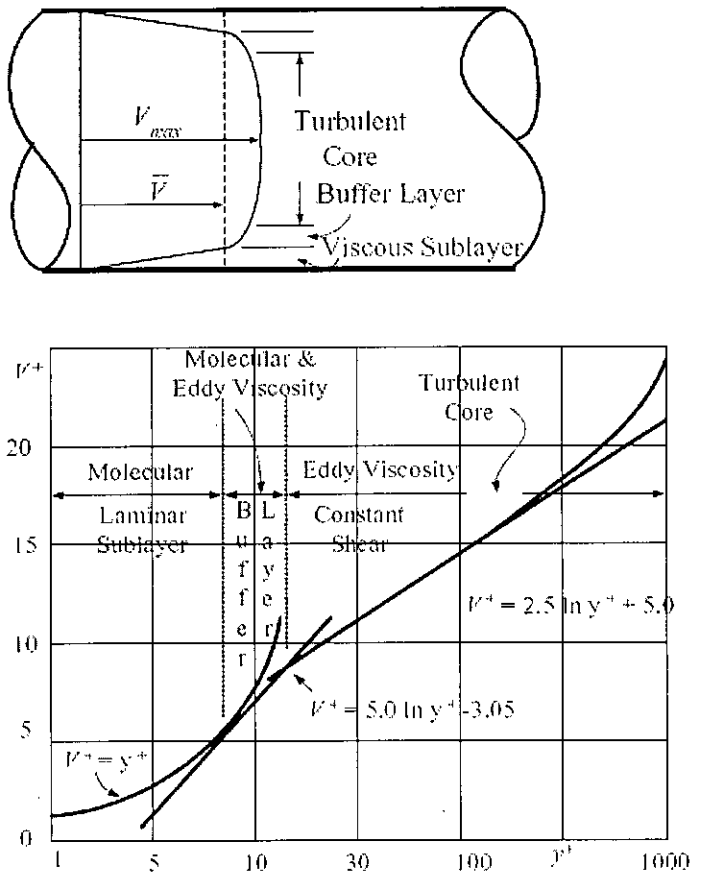

FIGURE 2.2: The universal velocity profile

with the wall and transfer of corrosion products from the wall take place in this region. Any kind of disturbances in the boundary layer (e.g. turbulent bursts and sweeps) have significant effect on important hydrodynamic parameters such as wall pressure and wall shear stress and thereby have major effects on corrosion processes [21].

2.3.2 Wall Shear Stress

Wall shear stress is important to erosion-corrosion phenomena where shear-induced forces damage the surface deposits or passive films. The mathematical definition

of wall shear stress, τ_w, is given by [22]:

$$\tau_w = \mu \left(\frac{\partial u}{\partial y} \right)_0 \tag{2.1}$$

where μ is the dynamic viscosity, u is the mean velocity and y is the distance perpendicular to the surface.

However, Wood [4] suggested an alternative definition which includes the effect of turbulence also:

$$\tau_w = (\mu + \eta_e) \left(\frac{\partial u}{\partial y} \right)_0 \tag{2.2}$$

where η_e is the turbulence eddy viscosity.

Wall shear stress that causes the removal of the protective corrosion films is called critical shear stress [23]. Efird measured the critical shear stresses for copper alloys using plates parallel to tube flow. However, there are suggestions that the obtained values are too low to mechanically disrupt the protective layer and the film removal is actually associated with mass transport induced surface dissolution, not the wall shear stress [4, 24].

2.3.3 Mass Transfer Coefficient

Mass transfer coefficient can be defined as:

$$k_m = \frac{D}{\delta} \tag{2.3}$$

where k_m is the mass transfer coefficient, D is the diffusion coefficient for a chemical species and δ is the diffusion boundary layer thickness. Mass transfer (movement of corrosive species to the metal surface and the movement of corrosion products away from the metal surface) can significantly affect the reaction rates. Therefore, mass transfer coefficient plays important role in corrosion rates, particularly in erosion-corrosion conditions.

Corrosion rate can be calculated from the mass transfer coefficient by the application of well established mass transfer correlations of dimensionless groups:

$$\mathrm{Sh} = \alpha \mathrm{Re}^{\beta} \mathrm{Sc}^{\gamma} \tag{2.4}$$

where, Sc is the ratio of momentum diffusivity to mass diffusivity (Schmidt number) and Sh is the ratio of convective mass transport to diffusive transport (Sherwood number). α, β and γ are the experimental constants and function of specimen composition and geometry. Values of these constants can be found in the literature [15].

2.3.4 Relationship between Mass Transfer Coefficient and Wall Shear Stress

Both mass transfer coefficient and wall shear stress are function of fluid velocity and therefore closely related. The relationship can be obtained using Chilton-Coulburn analogy:

$$\frac{k_m d}{D} = f \mathrm{Re}(\mathrm{Sc}^{1/3}) \tag{2.5}$$

where, f is the fanning friction factor and d is the characteristic length (diameter for pipe flow).

The wall shear stress for pipe flow is given by:

$$\tau_{\mathrm{w}} = f(\rho u^2/2) \tag{2.6}$$

where, ρ is the fluid density.

Using Equation 2.5 and 2.6, the following relationship between mass transfer coefficient and wall shear stress can be obtained:

$$k_m = \text{constant} \left(\frac{\tau_{\mathrm{w}}}{\rho}\right)^{0.5} \mathrm{Sc}^{-2/3} \tag{2.7}$$

2.4 Factors Affecting Erosion-Corrosion

2.4.1 Environmental Influences

2.4.1.1 Surface Films

Formation and retention of protective films are very important from the standpoint of resistance to erosion-corrosion. Protective films can be either thick porous diffusion barriers or invisible passive films. Diffusion barriers (e.g. red rust on carbon steel or cuprous oxide on copper) are formed by anodic dissolution of metal. On the other hand, passive layers are formed by direct oxidation of metals without entering into the solution (e.g. Cr_2O_3 passive film on stainless steel). Passive films are expected to withstand more severe conditions than the softer thicker diffusion barriers which are more easily damaged. However, effect of other factors such as temperature, pH also needs to be taken into consideration [4].

2.4.1.2 pH

pH plays an important role since the solubility of the protective oxide film in the solution depends on it. Skold and Larson [25] studied the effect of pH on corrosion rate of mild steel and found that maximum corrosion rate occurs somewhere between pH values of 7.5 and 8.5 in flow conditions. A similar peak of corrosion rate at pH 8.0 was obtained by Luce and Fontana [26] in their study of the effect of pH on erosion-corrosion of mild steel in distilled water using circular rotating disks at high velocity.

2.4.1.3 Oxygen Concentration

Effect of oxygen concentration on erosion-corrosion depends on controlling corrosion mechanism. When corrosion process is mass-transfer controlled, the corrosion rate is directly proportional to bulk oxygen concentration, C_{b,O_2} or C^n_{b,O_2} [4]. The

value of n depends on flow and geometry of the system. For example, the Berger-Hau correlation [27] can be used to calculate corrosion rate (CR in mm/y) using mass transfer rate of dissolved oxygen to a film-free carbon-steel pipe wall:

$$\mathrm{CR} = 4923 C_{b,\mathrm{O_2}} (D_{\mathrm{O_2}}/d) \mathrm{Re}^{0.86} \mathrm{Sc}^{0.33} \tag{2.8}$$

where, D_{O_2} is the oxygen diffusion coefficient.

2.4.1.4 Temperature

Temperature has effect on pH, oxygen and carbon dioxide solubility, solubility of ionic species, and reaction kinetics. Therefore, temperature can be very influential in determining erosion-corrosion rates.

Effect of temperature on erosion-corrosion can be explained with the help of Figure 2.3 [28]. At lower temperature, erosion plays major role. As the temperature increases, the rate of corrosion product formation increases. Gradually, corrosion starts to play its role along with erosion, as the corrosion product is continually removed and reformed. However, at critical temperature, the corrosion product layer becomes sufficiently thick and strong enough to resist erosion. From this point, the erosion-corrosion rate decreases with time. The effect of alloy corrosion resistance is also shown in the figure. Here, alloy 1 is more susceptible than alloy 2. Hence, change in erosion-corrosion rate is slower and alloy 2 has a different and higher critical temperature.

2.4.1.5 Biofouling

Metal surface, when immersed into an aquatic environment, quickly adsorbs dissolved organic and inorganic substances. Biofouling of the metal surface follows as the surface is then colonized by microorganisms including bacteria, microalgae and fungi. Biofilm formation and generation of extracelluar polymeric substances (e.g.

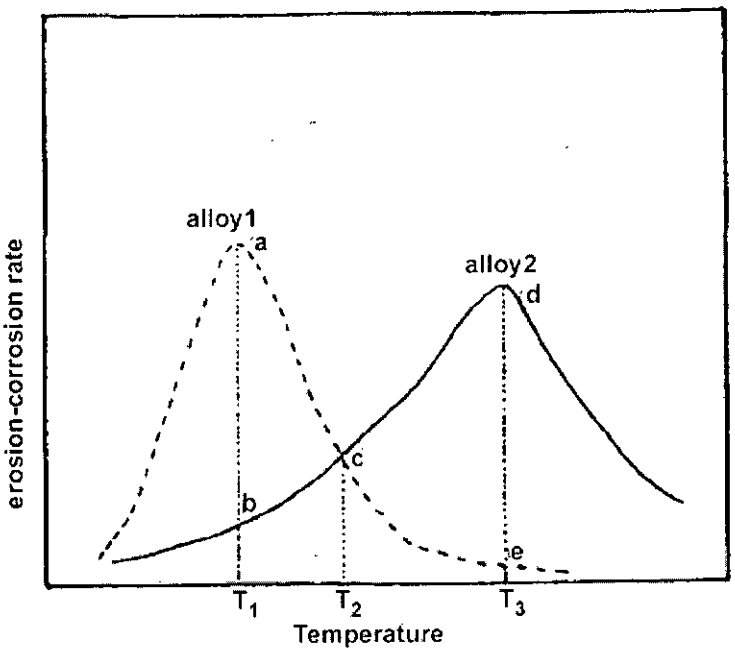

FIGURE 2.3: Effect of temperature on erosion-corrosion of two alloys of different corrosion resistance

polysaccharides, uronic acid) can play an important role in the erosion-corrosion of metals [29].

2.4.1.6 Velocity

Velocity plays a very important role in erosion-corrosion of metals/alloys. Velocity can highly affect the corrosion mechanism. Protective layer can easily break-down at high velocities, specially in presence of suspended solids.

Increased velocity can increase or reduce attack, depending on the mechanism involved. Corrosion of steel increases with velocity due to increased supply of oxygen or carbon dioxide or hydrogen sulfide. On the other hand, in nitric acid attack on type 347 stainless steel decreases as velocity increases. Under stagnant conditions this steel in nitric acid is attacked autocatalytically because of formation of nitrous acid as a cathodic reaction product. Increasing velocity sweeps away the nitrous acid and thus removes one of the corrosive agents in the environment [30].

2.4.2 Nature of Metal or Alloy

Properties of metals/alloys (such as chemical composition, metallurgical history, hardness etc.) can influence their performance under erosion-corrosion conditions.

- Addition of alloying elements can significantly improve the resistance to erosion-corrosion. For example, addition of chromium greatly improves erosion-corrosion resistance of cupro-nickels [3].
- Hardening by heat treatment results in changes in microstructure and heterogeneity and generally decreases resistance to corrosion. For example, type 304 stainless steel is more resistant then the precipitation-hardened stainless steel [30].

2.4.3 Geometric factors

Flow through valves, orifice plates, bends, elbows and heat exchanger tube inlets disturb fully developed flow patterns and destroys the equilibrium hydrodynamic and diffusion boundary layer. Boundary layer disruption at disturbed flow locations gives rise to localized erosion-corrosion. Disturbed flow pattern at heat exchanger tube inlets gives rise to disproportionately wasteful tube replacement as only the first three to four tube diameters at the tube inlet are affected with the remaining tube often being in its original condition when replacement is required [31].

Surface roughness can significantly increase the mass transfer rate. Dawson and Trass [32] used electrodes of different surface roughness to correlate Reynolds number with Sherwood number. The experimental results obtained at Sc=1000 showed that the Sherwood number at rough surfaces are higher than the smooth surface for similar Reynolds number.

Liquid erosion-corrosion depends only on the normal component of velocity. Therefore, liquid erosion-corrosion is reduced as impacts become more glancing. However, when the surface becomes roughened by erosion, the tangential component also makes some contribution [33].

For slurry erosion-corrosion, impact of solid particle on the surface at an oblique angle can generate more surface roughness. This is mainly due to the cutting mode impact of particles at oblique angles rather than the indentation mode at normal incidence. The surface is more susceptible to pitting type of corrosion when impact angle is in between 30-40° [9, 34].

2.4.4 Galvanic Effect

Assembly of dissimilar metals in contact with flowing system can influence erosion-corrosion. More anodic surface is then dissolved at an enhanced rate compared to uncoupled reaction. However, effect of other factors such as anode-cathode area ratio, temperature, flow-field intensity are also needed to be taken into considerations.

Galvanic effect on erosion-corrosion was studied by Al-Hosani *et al.* by coupling copper-based alloys to Mo-stainless steels in Arabian Gulf seawater. The corrosion rates were found to be between 1.33 and 3.0 times in flow conditions then those measured in stagnant conditions [35].

2.5 Erosion-Corrosion Mechanisms

The effect of relative motion between the electrolyte and the metal surface is twofold:

- relative movement influence the transport of reactants and products by convection

- moving fluids create shear stress and pressure fluctuations on the surface, and cause wear.

Based on these effects, flow-dependent corrosion can be classified into two wide areas:

1. Corrosion influenced by convective mass transfer, and
2. Corrosion influenced by mechanical flow effects.

Figure 2.4 shows possible regions of erosion-corrosion interactions between different flow regimes and corrosion [36]. The areas of interaction of corrosion and slurry

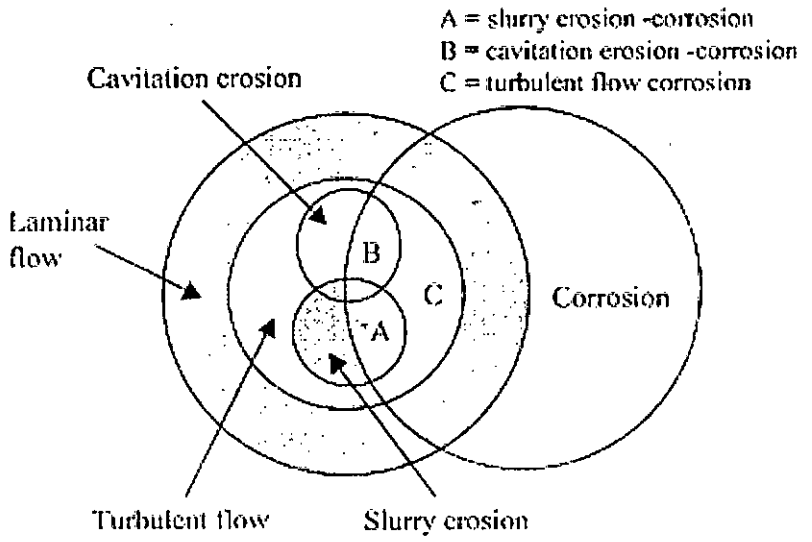

FIGURE 2.4: Interaction of Erosion and Corrosion

impingement(A), cavitation (B) and turbulent flow (C) are termed as erosion-corrosion. Among them, in region C the corrosion is influenced by convective mass transfer. Corrosion in region A and B has effects of mechanical forces which predominates.

2.5.1 Flow-Enhanced Corrosion

Mass transfer of reactants to and from the metal surface plays an important role in flow-enhanced corrosion. In this process, the protective layer on the surface is

destroyed by chemical thinning enhanced by greater mass transfer rate. Major problems occur at locations with high mass transfer rates, corresponding to highly turbulent flow conditions found at downstreams of welds and pipe fittings, at pipe joints, downstream of valves and orifice plates, at bends and elbows of piping, and at heat exchanger tube inlets.

In case of flow-enhanced corrosion, the kinetics is usually mixed and can be characterized by three different stages [37]:

- mass transfer of species (oxygen or H^+ from the bulk of the flow to the surface of the solid)
- mass transfer of the same species through porous surface layers
- reaction at the metal surface

The corrosion rate is dependent on the concentration of the transported species, convective mass transfer coefficient, material transport constant through the porous layer and the reaction rate constant at the surface.

Flow-enhanced corrosion for mixed controlled reactions can be represented by the modified Koutecky-Levich model , given by:

$$\frac{1}{i_{\text{corr}}} = \frac{1}{i_a} + \frac{1}{i_d} = \frac{1}{nFk_1} + \frac{k_{-1}}{k_1 nFk_m} \tag{2.9}$$

where i_{corr} is corrosion current density, i_a is activation controlled current density, i_d is diffusion controlled current density, n is number of electrons, F is Faraday constant, k_1 is forward reaction rate and k_{-1} is reverse reaction rate.

From Equation 2.9, it can be seen when the corrosion process is completely diffusion controlled, a linear relationship exists between the erosion-corrosion rate and mass transfer coefficient. However, this simple relationship between mass transfer and erosion-corrosion does not always hold and leads to a dependency on k_m^n. Reasons for this non-linearity are the following and summarized in Figure 2.5 [18]:

- removal of a surface film above a critical mass transfer coefficient
- interactions of anodic and cathodic areas
- coupling of reactions
- mixed control

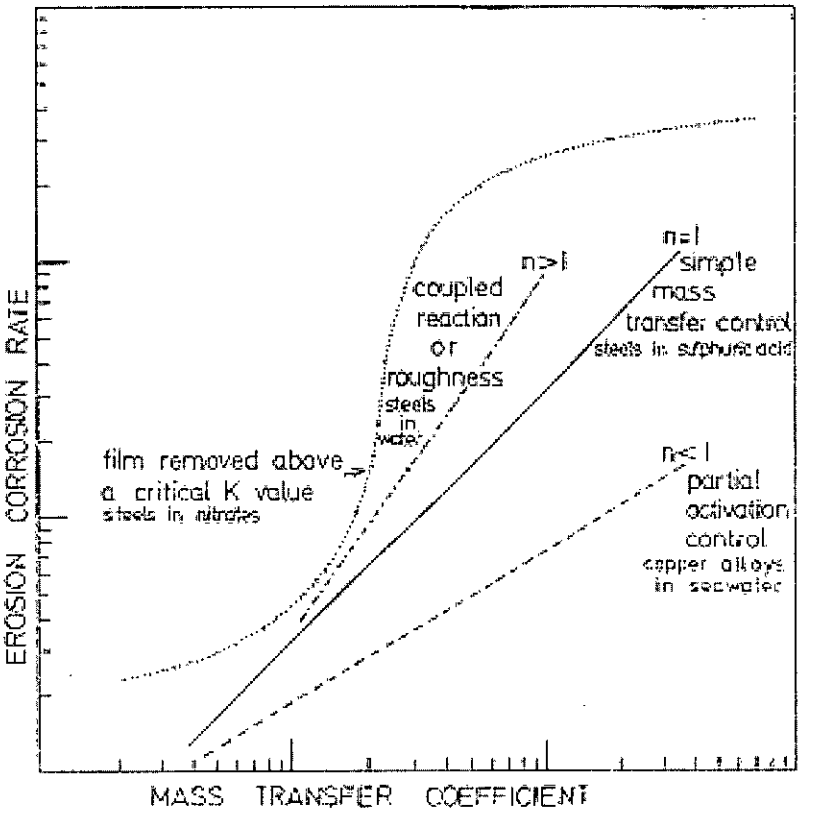

FIGURE 2.5: Relationships between erosion-corrosion rate and mass transfer coefficient

The effect of flow on film dissolution is complex and still not well understood and much more work is required on the fundamentals of the processes involved [2].

2.5.2 Predominantly Mechanical Force Determined Effects

The following mechanical forces can be involved in the destruction of the protective films and the metal at flow-systems:

- turbulent flow causing shear stress fluctuation and pressure impacts
- impact of suspended solid particles
- impact of suspended liquid droplets in high-speed gas flow
- cavitation

2.5.2.1 Turbulent Flow

Occurrence of erosion-corrosion in single-phase turbulent flow can be due to the enhanced mass transfer rate (Section 2.5.1). However, there is another concept: damage of the protective film by the wall shear stress caused by the fluid flow.

The term "breakway" velocity was first introduced by Syrett [38], which gave rise to the concept of critical shear stress for film damage. The value of critical shear stress, τ_w, for pipe flow is given in Equation 2.6. The fanning factor, f can be written as a function of Reynolds number and relative roughness:

$$f = f(\mathrm{Re}, \mathrm{e/d}) \tag{2.10}$$

For fully rough pipe, friction factor is independent of Reynolds number and therefore, $\tau_w \propto u^2$.

Passive films can withstand more severe conditions and are not usually destroyed by single-phase fluid flow [39]. Therefore, the acceptable velocity for carbon-steel and low alloy steels are much higher than the copper tubing [2].

2.5.2.2 Solid Particle Impingement

Solid particle erosion occurs when hard particles are entrained in a gas or liquid medium impinging on the metal surface at a significant velocity. In addition to thick diffusion barriers, this type of impact can also damage thin passive films leading to erosion-corrosion [2].

A simple relationship between the erosion rate (ER) and particle velocity can be obtained, since ER is a function of the kinetic energy of the particles (proportional to u_p^2) and the frequency of impacts (proportional to u_p):

$$\mathrm{ER} \propto u_p^3 \tag{2.11}$$

In addition to impact velocity, kinetic energy is also a function of impact angle, particle size and density. Materials, based on the dependence of their erosion rate on angle of impingement, are broadly classified as ductile or brittle. Ductile materials (such as metals) have maximum erosion-corrosion rate at low impact angles (typically 15-40°) [40]. Effect of impact angle on erosion corrosion can be explained with the help of Figure 2.6 [9]. At normal incidence, the effect

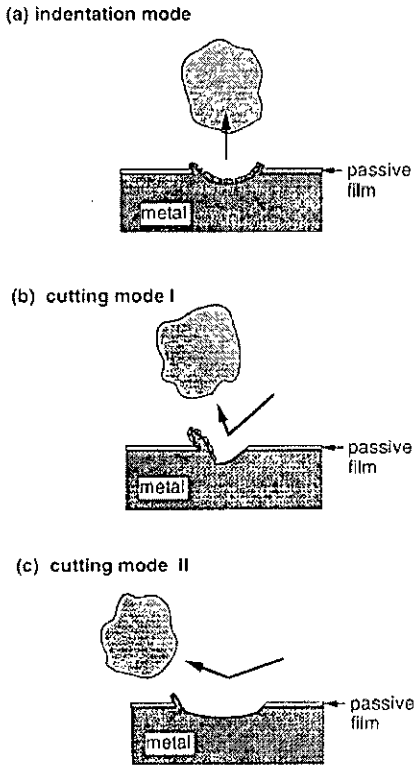

FIGURE 2.6: Plastic deformation by particle impact; (a) indentation mode, (b) cutting mode I, and (c) cutting mode II

of particle impact is shown in Figure 2.6 (a). However, at an oblique angle of impingement, particles create scars on the specimen surface. In most of the cases,

direct material removal does not occur, but a lip of material remains attached at the end of the impact crater. The craters are deeper but the diameter of the scar is small compared to the impinging particle diameter Figure 2.6. Such mode of deformation is known as *cutting mode I*. At lower impact angles, the scars produced by the particles are shallower and elongate more in the direction of the particle motion. At *cutting mode II*, (Figure 2.6 (c)) corrosion rate decreases with decreasing impact angle.

For particle size above 100 μm, the size of erodent particles has little effect on the erosion rate. However, the erosion rate rapidly decreases with particle size smaller than 100 μm. As the particle size decreases, lower flow velocity is required to maintain the particles in the suspension and reduce impact frequency [2, 40].

For fully turbulent pipe flow, average particle impact angle is 5°. This corresponds to *cutting mode II* that cause very little erosion. Nesic showed that for disturbed turbulent flow a wide range of impact angles is encountered [41]. Therefore, erosion-corrosion significantly increases in presence of disturbance. Carbon steel pipe carrying sand-slurry undergoes very severe erosion-corrosion after eight days exposure to disturbed flow whereas the erosion rate is <1 mm/y for nondisturbed flow [42].

For up to 5 mass% solid concentration, erosion rate increases linearly with solid concentration. However, at higher concentrations the effect decreases because of particle-particle interaction [43]. Another important factor is the relative hardness of the surface and the impinging particles. When the particles are softer than the surface, erosion rate is significantly lower [2].

2.5.2.3 Liquid Impingement Erosion

Liquid impingement erosion occurs when a surface is continually exposed to impacts by liquid drops or jets. Blade erosion of steam turbines, aircraft rain erosion are some examples of liquid impingement erosion.

Liquid droplet impingement at high velocities on a solid surface can have two effects which leads to the damage of the surface:

- high contact pressure at the area of impact and
- liquid jetting flow along the surface

For example, impact pressure for water at 500 m/s is about 1250 Mpa, which is above the yield strength of many alloys [44].

When liquid droplets make contact with the surface, contact is made at a point. At that instant, a shock wave of the impact pressure is formed which then begins to travel up into the droplet (Figure 2.7 (a)). Then the contact area spreads out and its perimeter starts to move radially outward at a speed greater than the impact velocity (Figure 2.7 (b)). When the contact angle becomes greater than a critical contact angle,
phi_c, the shock front detaches itself from the solid surface and moves up along the surface of the droplet. The compressed liquid then jet out to relieve the contact pressure Figure 2.7 (c)).

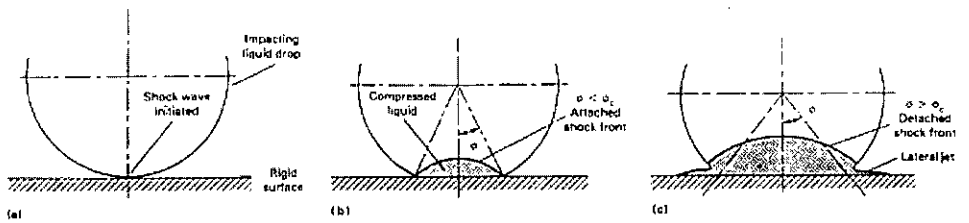

FIGURE 2.7: Liquid drop impact: (a) initial contact, (b) compressive stage with attached shock front, and (c) detached shock and jetting stage

However, fluid-solid interaction becomes more complicated after the formation of peaks and craters by erosion. Initial contact point will then affect both the impact pressure and the jetting pattern. A droplet falling on a peak or slope may not develop full impact pressure. On the other hand, droplet falling in a crater may produce increased pressure due to shock wave collisions [44].

2.5.2.4 Cavitation

Repeated nucleation, growth, and violent collapse of cavities or bubbles in a liquid is termed as cavitation. Cavitation can occur in any liquid system in which flow pattern or vibrations can cause pressure fluctuations.

Nucleation of bubbles occur when the pressure of the flowing liquid falls down below the vapor pressure of the liquid. The bubbles then grow to a stable size and be transported to the down-stream with the flow. These bubbles becomes unstable and collapse violently when they reach a high pressure region in the down-stream. Bubbles can also form and collapse in stationary liquid system that is subjected to vibrational pressure fluctuations.

The collapse velocity is a function of the hydrostatic pressure under which the cavity collapses, the volume of the initial cavity and the liquid density. For a 1 mm radius cavity collapsing at 1 atm overpressure in the water collapse velocity is in the range of 100 to 150 m/s and collapse time is approximately 100 ns.

Collapse of cavities can occur either in contact with the solid surface or away from the surface. Cavities collapsing away from the surface usually collapse symmetrically and produce a shock wave into the surroundings (Figure 2.8 (b)). On the other hand, when cavities collapse in contact with surface it forms a liquid microjet directed toward the solid surface (Figure 2.8 (a)).

Initially, it was thought that these shock waves or jet impacts generated from bubble collapse are the most likely causes of cavitation. However, impacts of either kind do not have the ability to produce damages that are observed during cavitation. It must be noted that in all practical cases large number of cavities are generated at the same time in the low pressure zone. When these clusters are subjected to increased pressure then they collapse in a concerted manner. The collapse of the cavity clusters enhance the effects of other cavities. This results in a significant increase in surface damage. Similar phenomena has also been observed for cavitation in stationary fluids due to vibrational pressure fluctuations [45].

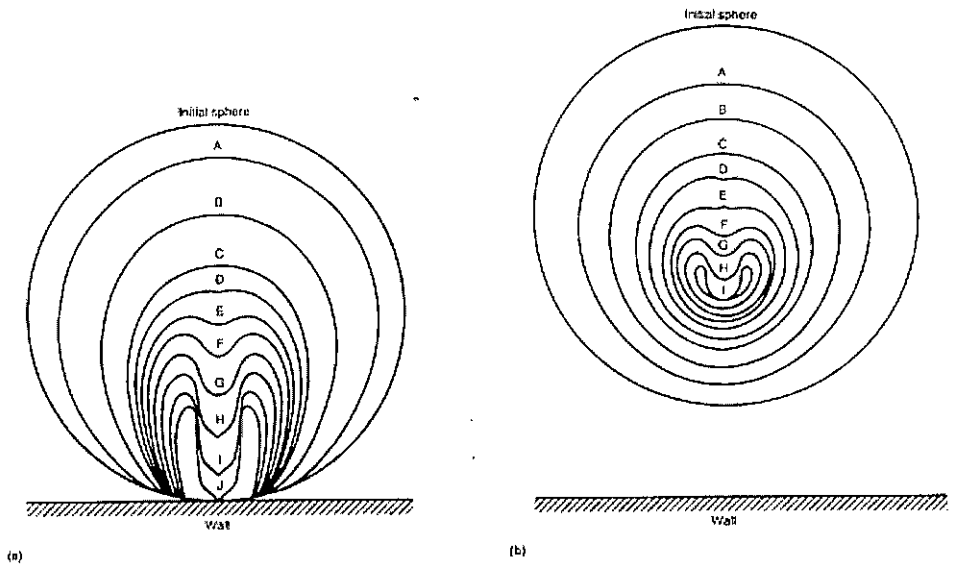

FIGURE 2.8: Collapse of cavity: (a) in contact with the surface, (b) away from the surface

2.6 Synergistic Effects of Erosion and Corrosion

Erosion and corrosion of metals can involve various mechanical and chemical processes (Section 2.5). Simultaneous involvement of mechanical and chemical processes and mutual interaction between them significantly increase loss of material, which is beyond the individual contribution of mechanical wear and corrosion. Wood has defined *synergy* as the difference between erosion-corrosion and the summation of its two parts [4].

Madsen [46] conducted three types of tests to determine the synergistic effect: (a) pure erosion test to measure the erosion rate; (b) pure corrosion tests to measure the corrosion rate; (c) combined tests to measure erosion-corrosion. Synergistic effect was then found using the equation:

$$S = T - (E + C) \tag{2.12}$$

where S is the synergistic effect, T is total erosion-corrosion rate, E is pure erosion rate and C is pure rate of corrosion.

Wood and Hutton [47] analyzed experimental data published by previous workers including Madsen [46, 48–50] and derived two expressions by plotting S/C vs. E/C on log-log scale.

$$\frac{S}{C} = \exp\left[1.277 \ln\left(\frac{E}{C}\right) - 1.9125\right] = 0.1477\left(\frac{E}{C}\right)^{1.277} \tag{2.13}$$

$$\frac{S}{C} = \exp\left[0.755 \ln\left(\frac{E}{C}\right) + 1.222\right] = 3.3940\left(\frac{E}{C}\right)^{0.755} \tag{2.14}$$

Equations 2.13 and 2.14 can be used to predict synergistic effects, for medium- and high-synergistic systems respectively, when pure erosion and corrosion rates are known.

Synergy between erosion and corrosion was further divided into two components: increase in mechanical wear due to corrosion, S', and increase in corrosion due to mechanical wear, S'' [51–53]:

$$S = S' + S'' \tag{2.15}$$

Watson *et al.* [52] further proposed three dimensionless factors to demonstrate wear-corrosion synergism. The total synergism factor is:

$$\frac{T}{T - S}$$

The corrosion augmentation factor represents the ratio of corrosion with wear to corrosion only and is a measure of effect of wear on corrosion:

$$\frac{C + S''}{C}$$

The wear augmentation factor represents the ratio of wear plus the synergism of corrosion on wear to wear only and demonstrates effect of corrosion on wear:

$$\frac{E + S'}{E}$$

Ferng *et al.* [54] used local flow models to predict erosion-corrosion locations in

steel piping. They assumed erosion-corrosion as a coupled phenomena between chemical corrosion and mechanical wear which depends on piping layout, fitting geometry, local distribution of flow properties, and flow chemistry.

Based on their assumptions Ferng *et al.* divided the erosion-corrosion model into two major parts: the chemical corrosion model and the mechanical erosion model.

The chemical corrosion model assumed a mixed control corrosion process of dissolution of magnetite on the metal surface and the mass-transfer rate of Fe^{2+}:

$$R = \frac{C_{eq} - C_{\infty}}{\frac{1}{2k_R} + \frac{1}{k_m}} \tag{2.16}$$

where, R is the total mass loss rate, C_{eq} is the soluble ferrous ion concentration in equilibrium with the magnetite, C_{∞} is the soluble Fe^{2+} concentration at the bulk water, and k_R is the reaction rate constant.

On the other hand, the erosion model assumed that the oxide layer caused by corrosion is removed by the action of numerous liquid droplet impacts:

$$m = C_s N F_\theta(\theta) \frac{\rho_f u^2}{H_v} \tag{2.17}$$

where m is the wear rate, C_s is the system constant, N is the impingement frequency, F_θ is a characteristic function, θ is the impact angle, ρ_f is the fluid density, u is the normal velocity, and H_v is the pipe wall hardness.

The model showed satisfactory results when compared with the practical measurements.

Bozzini *et al.* [55] developed a model based on the same approach of separating erosion-corrosion into major parts. The erosion rate model was developed taking into account the mass flow rate of impacting stream, the impact surface area, and the impact angle. However, the corrosion model used a coefficient to include the synergistic damage, f_a ($0 \leq f_a \leq 1$). The effective current density is thus given

by the following equation:

$$i_{\text{corr}} = f_a i_a + (1 - f_a) i_u \tag{2.18}$$

where the subscripts 'a' and 'u' stand for affected and unaffected, respectively. The stripping coefficient, f_a is defined as:

$$f_a = \left(\frac{\text{no. of impacts}}{\text{control area}}\right) \times \left(\frac{\text{damaged area}}{\text{impact}}\right) \times \text{recovery time} = \lambda A_a \tau \tag{2.19}$$

where λ is the particle flux, A_a is the affected surface area and τ is the passive recovery time.

Bozzini *et al.* analyzed their model to give the single and joint effects of operating parameters (e.g. flow velocity, particle injection rate) on erosion-corrosion damage. They showed that synergistic effects can be negative also as annealed CS shows a reduction in overall corrosion rate with erosion present.

Conflicting results are reported in the literature while performing the tests under different operating conditions. Wood [56] found negative synergy for UNS S32750 in 3.5% NaCl solution at E_k=0.05 μJ (kinetic energy of impacting particles), while Neville and Hue [57] reported positive synergy for the same metal with E_k of 4 μJ. Based on these conflicting results Wood concluded that there is a complex relationship between synergy and kinetic energy, surface roughness, passive film state and there might be either of the positive or negative interaction for different situations. Wood listed various interactive mechanisms and their possible influences (negative or positive) on erosion (S') or corrosion (S'')[58].

All the studies conducted on the synergistic effects are mainly for slurry-erosion or cavitation erosion. The synergy in flow enhanced corrosion are rarely studied and therefore is a potential field to explore.

2.7 Erosion-corrosion Mapping

Erosion-corrosion is a generic term used for processes involving mechanical wear and corrosion. The complexity in mechanism of erosion-corrosion are already discussed in earlier sections (Table 2.1, Section 2.6). Such wide spectrum of mechanisms prompted researcher to classify erosion-corrosion into several regimes.

Interaction between erosion-corrosion was first described by Hogmark *et al.* [59] . They suggested six possible regimes of erosion-corrosion:

1. corrosion
2. erosion-affected corrosion
3. erosion of the corrosion product without flaking
4. flaking of corrosion products at individual impacts
5. simultaneous erosion of the corrosion product and the metal substrate
6. erosion

However, the above regimes are only based on results from microscopy and the transitions between the regimes were not defined.

Kang *et al.* [60] proposed four regimes based on erosion-oxidation studies of pure metals Figure 2.9. Regime to regime transitions was defined by using an equation relating scale growth due to oxidation and scale removal due to erosion:

$$\frac{\mathrm{d}\xi}{\mathrm{d}t} = k_{c,e}/\xi - k' \tag{2.20}$$

where ξ is the instantaneous scale thickness, t is time, $k_{c,e}$ is the parabolic rate constant in presence of erosion and k' is the erosion constant. Later, Rishel *et al.* [61] subdivided the 'erosion-enhanced oxidation zone' into three categories: Type I, Type II and Type III (Figure 2.10).

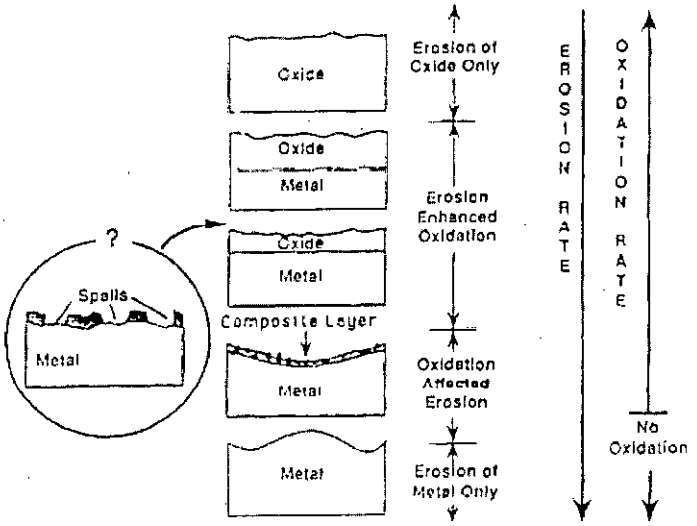

FIGURE 2.9: Different erosion-corrosion regimes according to Kang et al. (1987)

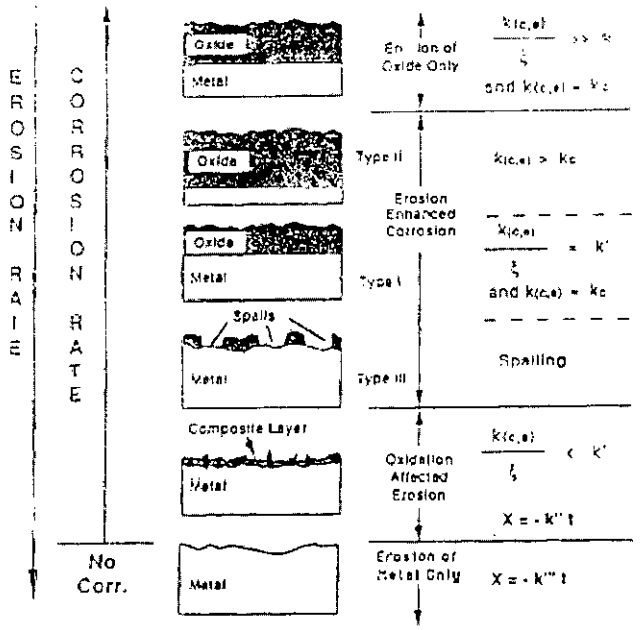

FIGURE 2.10: Different erosion-corrosion regimes according to Rishel et al. (1990)

Sundararajan [62] used the similar approach and developed erosion-corrosion map showing the transitions between erosion-corrosion regimes as a function of both the erosion and corrosion variables Figure 2.11.

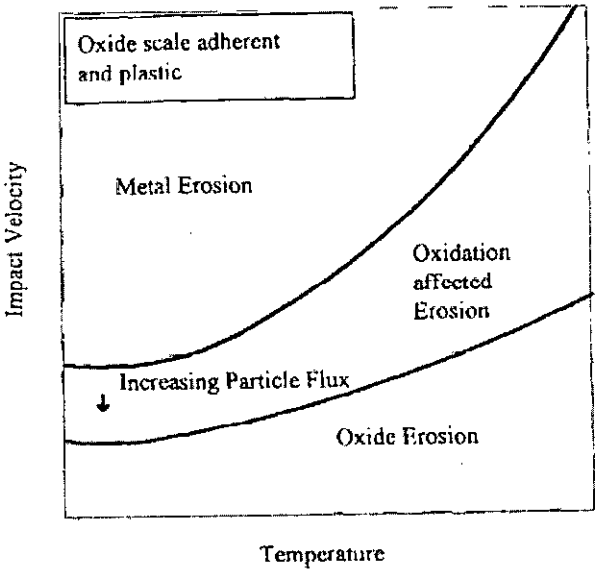

FIGURE 2.11: Erosion-corrosion map developed by Sundararajan (1990)

Stack along with other researchers have used erosion and corrosion models from the literature along with Pourbaix diagrams to develop erosion-corrosion maps [63–68]. Particle velocity-applied potential, particle velocity-pH, particle velocity-particle concentration maps were developed. In addition, process control maps showing the level of wastage in particular environments were developed. A sample process control map is shown in Figure 2.12

Erosion-corrosion maps can be very helpful for selecting material in a particular environment. Erosion-corrosion maps also provide valuable information relating to control of environmental parameters. Process control maps also provide very useful information for optimizing process parameters to minimize erosion-corrosion rate.

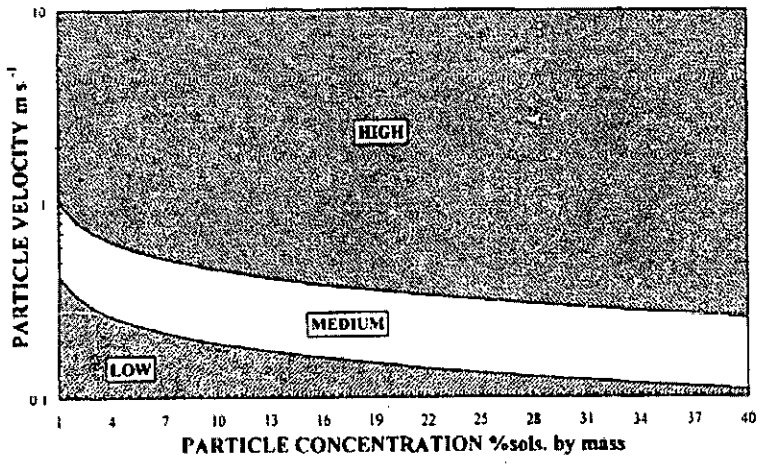

FIGURE 2.12: Particle velocity-particle concentration wastage map showing the transition between the wastage levels at an applied potential of -0.7 V

2.8 Erosion-corrosion Prediction and Control

2.8.1 Prediction

Occurrence of erosion-corrosion can be predicted by using Keller's approach. An equation relating erosion-corrosion with temperature, velocity, geometric factors etc., was developed by Keller [69]. This approach has been further modified by Electric Power Research Institute (EPRI) and a computer program (CHECWORKS) has been developed. This software can be used to predict erosion-corrosion occurrence [3].

Another approach to predict erosion-corrosion is to simulate the practical case in the laboratory and generate erosion-corrosion data that can be used by correlating the experimental data to the actual case. This approach of erosion-corrosion will be discussed in the next chapter.

Online monitoring of erosion-corrosion is possible by adoption of advanced electrochemical techniques. Electrochemical noise (EN) is defined as the fluctuations of electrical quantities such as cell current, electrode potential in electrolytic system.

Sources of EN in corrosion systems can be fluctuations of the concentration of the reacting species at the metal-electrolyte interface, fluctuations in surface morphology, fluctuations in electrode activity, fluctuations in electrolyte velocity etc. By measuring electrochemical current noise (ECN) and/or electrochemical potential noise (EPN) can be used to predict changes in flow regime for multiphase flow. EN has also been used for characterizing the kinetics of the breakdown and healing processes of passive films continuously abraded by impinging solid particles from the analysis of EN transients. Details of this technique can be found in literature [70, 71].

2.8.2 Control

2.8.2.1 Design

Improved design can considerably lower the erosion-corrosion rate. Controlling the velocity by increasing the flow area and the minimization of the abrupt changes in the flow system geometry by using long radius elbows, gradual changes in the flow cross-section, and specifying maximum weld root protrusion are good practices to minimize erosion-corrosion problem. Damage of heat-exchanger-tube-inlet can be avoided by using plastic inserts.

For slurry erosion-corrosion, damage rate can be controlled by optimizing the particle size (e.g. by grinding). Appropriate design to reduce the amount of impacting liquid, the droplet size and the angle of impact is beneficial for liquid impingement attack. Cavitation damage of pumps can be avoided by maintaining a substantial safety margin between NPSH available and NPSH required.

2.8.2.2 Materials

Using more erosion-corrosion resistant but costly materials can be beneficial. For example, copper tubing in hot water distribution system can be substituted by stainless steels. However, stainless steel should be avoided for chloride containing

environments. Alloy containing 20-28% Cr and 2-2.5% C with 2% Mo have good resistance to slurry erosion-corrosion at pH values down to 4. For more corrosive environments, alloy should contain less C. Stellite, 12% Cr martensitic stainless steel and 17Cr-4Ni precipitation hardened stainless steels are good choice for preventing liquid impingement erosion. In addition to nickel-based and titanium alloys, high density polyethylene has good cavitation-erosion resistance.

2.8.2.3 Inhibitors

Inhibitors are successfully used in recirculating cooling water system and steam condensate return line. However, excessive costs in once through systems has limited the applicability of inhibitors.

Chromates and nitrates act as passivating inhibitor at high concentrations. On the other hand chromates at low concentrations act as cathodic inhibitors. However, chromates are carcinogenic and it's toxicity made the use limited (< 0.05 ppm in effluent) in some jurisdictions [2].

Non-chromate inhibitors (e.g. zinc oxide, sodium tripolyphosphate, nitrilotris (methylene) triphosphoric acid(NTMP)) has been successfully used for recirculating cooling water systems but showed little benefit when used in sand or coal slurries.

2.8.2.4 Environmental Modifications

Environmental conditioning such as deaeration or raising the pH can be applied. However, it must be noted that at elevated pH corrosion might increase due to pitting corrosion. Modification of operating variables such as temperature, flow rates can be beneficial where wet steam is involved.

2.8.2.5 Cathodic Protection

Cathodic protection can be used if possible and has sufficient throwing power down the inside of pipes.

Chapter 3

Laboratory Testing of Erosion-Corrosion

3.1 Introduction

Prediction of erosion-corrosion occurrence and determination of the relative roles of corrosion and erosion are prerequisite for the control of erosion-corrosion. Appropriate design modifications and material selection are very much dependent on these technical know-how.

Information about erosion-corrosion can be obtained from various case studies in the practical fields. However, collection of such data would require a large time span.

An alternative and suitable way to produce erosion-corrosion data is to design laboratory experiments. Experimental data is then used for the industrial case with the use of appropriate correlation. Design of experiments is based on the underlying principles. Therefore, prediction of the mechanism and selection of appropriate correlation coefficients have significant role on the validity of the data produced.

This chapter focuses on the testing and monitoring of flow-enhanced erosion-corrosion.

3.2 Basis of Experiment Design

Effect of velocity on corrosion is a known phenomena. The effect of flow on corrosion can be governed by various factors (discussed in details in Chapter 2). However, design of experiments for studying erosion-corrosion is aimed at the following:

1. effect of mass transfer
2. effect of shear
3. effect of differential mass transfer
4. effect of multiphase flow

For cathodically controlled processes (corrosion by H^+, organic acids, oxygen, Fe^{3+} ions etc.) mass transfer of the corrosive species to the wall through the diffusion boundary layer determine the corrosion rate [72, 73]. Anodically controlled processes can also have flow effects where the flow affects the dissolution or thinning of the corrosion-product film (corrosion of carbon-steel lines carrying hot deoxygenated water or wet steam in power plants)[2]. Such corrosion in large-scale systems can be well approximated by choosing flow systems with comparable mass-transfer coefficient.

Wall shear stresses above critical values can cause damage to the protective films. Moreover, hydrodynamic shear may influence the persistence of filming inhibitors since they are more loosely bound to the surfaces than the oxide films. Shear induced corrosion in large-scale systems can be studied by choosing flow systems with comparable surface shear.

Differential cell may form between regions of same metal due to exposure to differing flow fields. Anodic sites may corrode uniformly or in the form of pits. Study of differential mass transfer effect is very difficult since detailed knowledge of local flow field in addition to mechanism of anodic and cathodic process is required.

Corrosion in the power plants and petrochemical industries occur mainly in multiphase flow conditions. Multiphase flow corrosion mechanism may differ from the mechanisms of single-phase flow corrosion (e.g., mass transfer, surface shear). However, simulation of the large-scale systems can be performed by incorporating involved mechanisms (e.g. liquid droplets, slug flow)and comparable operating conditions.

3.3 Experimental Systems

3.3.1 Rotating Disk

Rotating disk electrode (RDE) is simply a metal coupon machined into a cylinder and encased in epoxy or PTFE such that only the circular face is exposed to the corrosive environment. Relative motion between the surface and electrode is produced by rotating the electrode about its axis (Figure 3.1).

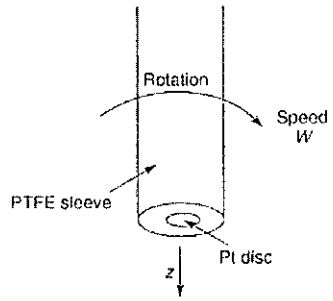

FIGURE 3.1: Rotating disk electrode

The RDE draws the solution up toward the electrode along the z-axis and then flings it out radially across the electrode surface (Figure 3.2). The electrode surface is uniformly accessible with this centrifugal flow [15].

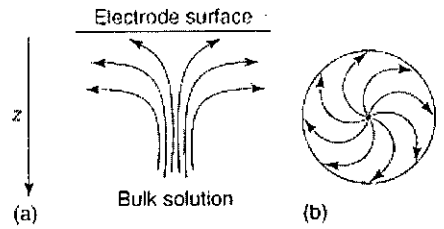

FIGURE 3.2: Rotating disk electrode

From simple geometry and circular symmetry about the z-axis, the hydrodynamic and convective diffusion equations can be analytically solved. Therefore, RDE is an ideal tool to study systems with complex reactions [74]. Because of it's simplicity RDE has been used by many researchers.

Equation for current distribution on the disk for laminar conditions was developed by Levich [75] equation and given by(in dimensionless form):

$$\mathrm{Sh} = 0.6205\mathrm{Re}^{0.5}\mathrm{Sc}^{0.33} \tag{3.1}$$

where $\mathrm{Re} = \dfrac{\omega r^2}{\nu}$ and $\mathrm{Sh} = \dfrac{k_m r}{D}$.

At higher Reynolds number, three different flow regimes can exist simultaneously on the disk surface. Chin and Litt conducted detailed study of transition between flow regimes and found that if Re$< 1.7 \times 10^5$ flow is laminar; if $1.7 \times 10^5 <$Re$< 3.5 \times 10^5$ flow is transitional and flow is turbulent for Re$> 3.5 \times 10^5$ [76].

Simultaneous presence of different flow regimes leads to formation of differential concentration cell as different section of the surface is exposed to different flow fields. Greater corrosion have been observed at the periphery, when copper disk was rotated in seawater; the central regions have been relatively unattacked. Iron disks have shown greater corrosion in the central region than on the periphery. These observations are related to the differential oxygen cell formation. Corrosion rate at the periphery (where the flow is turbulent)increased due to higher oxygen transfer rate. On the other hand, iron disks actually passivated at the periphery

faster than central regions [73]. Therefore, RDE is an appropriate tool for erosion-corrosion study if the disk is not too large to cause the flow to become transitional or turbulent at the periphery.

3.3.2 Rotating Cylinder

Erosion-corrosion occurs preferably in turbulent flow conditions. However, RDE is only applicable for corrosion studies in laminar flow. Rotating cylinder electrode (RCE) is an alternative for RDE and have been successfully used to study flow enhanced corrosion [5, 77, 78]. Basic components of a RCE is shown in Figure 3.3[79].

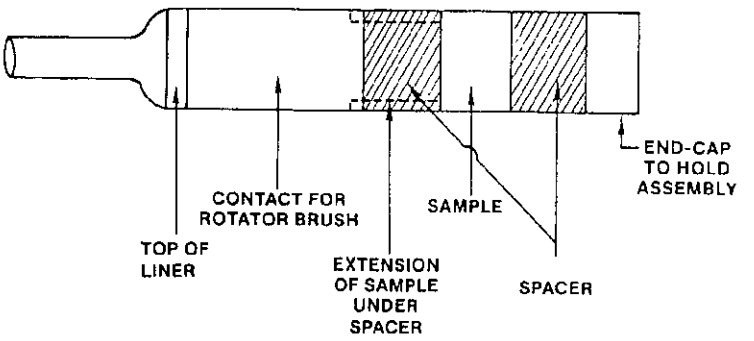

FIGURE 3.3: Rotating cylinder electrode

Practical aspects and hydrodynamics of RCE is now well known [75, 80, 81]. Laminar flow occurs only at low rotational speed with a critical Reynolds number of ~ 200 $\left(\mathrm{Re} = \dfrac{\omega d^2}{2\nu}\right)$.

Dimensionless group correlation was first reported by Eisenberg et al. [82]:

$$\mathrm{Sh} = 0.0791\mathrm{Re}^{0.7}\mathrm{Sc}^{0.356} \tag{3.2}$$

Correlation reported by other workers have similar form of $\mathrm{Sh} = a\mathrm{Re}^b\mathrm{Sc}^c$ with b in between 0.6-0.748 and c in between 0.27-0.41 [6]. However, all these correlations

were developed assuming hydrodynamically smooth surface. These correlations can vary depending upon the type of surface roughness [5].

Two approaches can be used to study erosion-corrosion using RCE: similarity in the wall shear-stress and similarity in mass-transfer coefficients between RCE and the large-scale systems [6]. However, for fully developed turbulent flow, the two approaches are linked (Equation 2.7).

RCE has seen increasing use as a corrosion examining tool for last 50 years. Examples of using RCE for corrosion evaluation for different alloys and environments are listed by Silverman [6]. Easy construction, simple application procedure and well-understood hydraulics have made RCE probably the simplest device to study corrosion in the turbulent flow conditions.

3.3.3 Impinging Jet

Impinging jet systems consist of a electrolytic jet impinging at 90° onto a metal specimen [83] as shown in Figure 3.4. In impinging jets, hydrodynamic characteristics and mass transfer depends on both jet to plate distance (H/d) and the radial position on the plate (r/d) and therefore dimensionless group correlation is somehow different from other geometries:

$$\mathrm{Sh} = a\mathrm{Re}^{a}\mathrm{Sc}^{b} f(H/d) f(r/d) \tag{3.3}$$

Hydrodynamic characteristics of fluid jet impinging on a flat plate is shown in Figure 3.5. Stagnation zone is marked as region A. The velocity component changes from axial to radial component in this region, with a stagnation point at the center and ends at $\sim r/r_0 = 2$. The stagnation zone has been well characterized in terms of mass transfer and resembles a rotating disk (region of uniform accessibility) [15, 73]. However, this region is poorly defined on the basis of wall shear stress since the flow vectors changes with increasing radial distance [84].

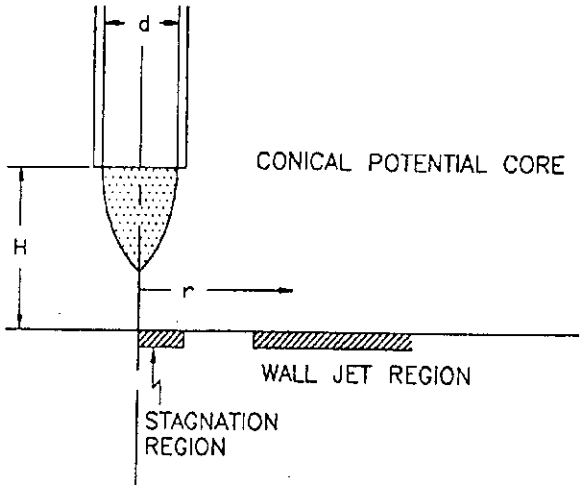

FIGURE 3.4: Impinging jet system

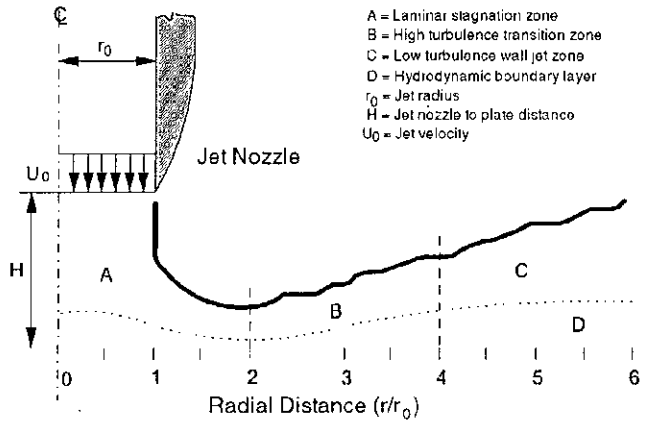

FIGURE 3.5: Flow field for a circular jet impinging on a flat plate

Region B extends radially upto $r/r_0 = 4$ [85]. Fluid flow in this region is characterized by high turbulence, large velocity gradient at wall and high wall shear stress. This region is of interest for studying erosion-corrosion in high-turbulence area. This region has not been mathematically well characterized. However, published work conducted in this region shows that wall shear stress is proportional to the square of the velocity [86, 87]:

$$\tau_w = 0.179 \rho U_0^2 \mathrm{Re}^{-0.182} \left(\frac{r}{r_0} \right)^{-2.0} \tag{3.4}$$

where, Reynolds number is defined as $Re = \frac{2r_0U_0}{\nu}$.

Turbulence subsides in Region C as the wall jet thickness gradually increases. Flow in this region is hard to correlate with pipe flow since the momentum transfer and fluid entrainment is in the opposite direction from the pipe flow [84]. However, equation developed by Giralt and Trass, Equation 3.4, is still valid for this region.

Jet impingement study has been effectively employed to study flow enhanced corrosion, effect of gas entrainment, disturbed flow, and slug flow as well as effects of flow on corrosion inhibitor [84, 88–90]. It must be mentioned that the selection of appropriate specimen size is critical to the observed results. To study effect of uniform mass transfer the coupon must lie within the stagnation region. If the specimen size is greater than the jet diameter than the corrosion process becomes complicated with the possibility of differential oxygen cell formation since the mass transfer rate varies outside the stagnation region [73].

Examples of several setups using impinging jet for corrosion studies can be found in the literature [13, 14, 90].

3.3.4 Flow-Loop Systems

Flow-loop systems can be once-through or recirculating. However, recirculating systems are preferred because of high operating cost of once-through systems. Simple flow-loop systems can be designed by combining fluid flow and heat transfer.

Different geometries can be used in the test section. Flow-loops using orifice [15], circular tubes [15, 91], square channels [92], elbows [93] have been designed to study erosion-corrosion. However, while designing the test section it is necessary to ensure that the pressure drop in the test section must not exceed the pressure drop for which the pump is selected.

In addition to erosion-corrosion study, flow-loop systems can also be used for studying performance of inhibitors [91, 94].

3.4 Selection of Experimental System

Experimental systems discussed in Section 3.3 have been more or less used for erosion-corrosion study. Selection of systems by the researchers were governed by the underlying mechanism and the relative merits and demerits of the systems.

Rotating disk electrodes, though extensively used, have some major drawbacks. Even at high rotational speeds, RDE operates under laminar flow, whereas industrial systems operate under turbulent flow. RCE can operate satisfactorily under turbulent flow conditions. For both, RDE and RCE maintaining low-resistance electrical connection is difficult [73].

Compared to rotating electrodes, impinging jets more closely simulates industrial flow systems, where the fluid is moving and the metal surface is stationery. Flow pattern developed for the impinging jet systems are similar to that developed at bends and other location of flow disturbances. These systems also capable of testing multi-phase flow situations.

Impinging jets can be classified into three categories: free-jet, jet-in-slit and submerged jet. Free-jet and jet-in-slit systems are suitable for studying liquid-droplet erosion and slurry erosion-corrosion. Submerged jet systems are adopted to study flow-enhanced corrosion where corrosion is increased by increased mass transfer and/or increased surface shear.

3.5 Electrochemical Measurements in Corrosive Environments

Corrosion of metals or alloys in aqueous environment is electrochemical process. Therefore, a wide range of electrochemical techniques have been developed. Electrochemical techniques have several advantages when compared to weight loss measurements: sensitivity to low corrosion rates, short experiment durations and

well-established theoretical understanding. Some of the electrochemical techniques commonly applied are listed below:

- potential measurements
- current measurements
- polarization measurements
- electrochemical impedance spectroscopy (EIS)
- electrochemical noise (EN), etc.

Among them, potential and polarization measurements are described in the following sections.

3.6 Open Circuit Potential Measurements

Open circuit potential (OCP) is the electrode potential at which no net current flow through the external circuit of the electrochemical cell. OCP of a corroding metal/alloy is measured as voltage between the metal/alloy (working electrode) and a reference electrode using a high-impedance voltmeter. Principle of OCP measurements are shown in the Figure 3.6. To measure OCP, a reference electrode (R) is also immersed in the electrolytic solution. To minimize, the ohmic drop it is necessary to place the reference electrode as close as possible to the electrode surface (W). In practice, a reference electrode is inserted into a Luggin probe(HL) and the tip of the probe is placed at about $2d$ from the surface, where d is the external diameter of the capillary [95]. With such arrangements potential can be measured using voltmeter (U); amplification of the signal, if necessary, is done by using amplifiers (MV).

Measurement of OCP can provide:

- A method for determining whether the corrosion system is in the active or the passive state [96].

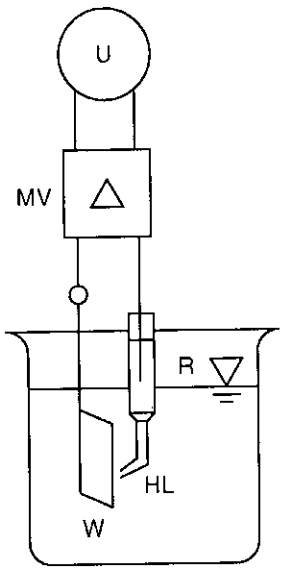

FIGURE 3.6: Electrical circuit for OCP measurements

- Determination of the potential distribution on the corroding surface (heterogenous mixed electrodes) [97].
- Data for corrosion monitoring in a plant or in the field [98, 99].
- Information on the free corrosion potential as the starting point for the application of electrochemical protection methods.
- Data for control of the protection potential during electrochemical protection [100].

3.7 Polarization Measurements

Correlations between current and potential in corrosion systems are referred to as current-potential curves or the polarization curves. For polarization measurements a three-electrode cell is necessary. The metal/alloy under investigation, working electrode (W), connected with a counter electrode (C) and a reference electrode (R) in presence of electrolytic environment. Such a cell is shown in Figure 3.7.

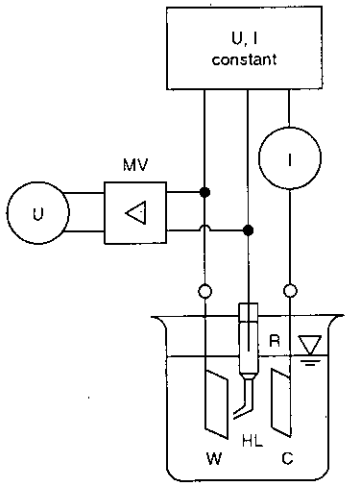

FIGURE 3.7: Electrochemical cell for polarization measurements

Depending on the position of the working potential to the open-circuit potential, polarization measurements can be classified into two broad groups:

- Measurements in the vicinity of the open-circuit potential, and
- Measurements far away from the open-circuit potential (>100 mV)

Measurements near the open-circuit potential are used for the determination of polarization resistance, and potential and current measurements on corrosion cell. Determination of polarization curves and pitting, passivation and repassivation potentials for localized corrosion (e.g. crevice corrosion, SCC, fatigue) are performed by measurements far from the open-circuit potential. Active, passive and transpassive regions can be distinguished from these measurements.

The polarization resistance, R_p is defined as the slope of the polarization curve at the corrosion potential:

$$R_p = \left(\frac{dE}{di}\right)_{E \to E_{\text{corr}}} \tag{3.5}$$

Measurement of polarization resistance is also known as linear polarization resistance (LPR) measurements assuming a linear relationship between current density and potential exists around E_{corr}. This resistance is related to the corrosion current

density, i_{corr}, by Stern-Geary equation [101]:

$$i_{\text{corr}} = \frac{B}{R_p} = \left(\frac{1}{2.3R_p}\right)\left(\frac{\beta_a\beta_c}{\beta_a + \beta_c}\right) \tag{3.6}$$

where β_a and β_c are the Tafel slopes for anodic and cathodic reactions respectively.

Value of B is dependent on the systems and required to determine experimentally. Experimental values of B for different systems have been summarized by Grauer et al. [102]. LPR has found useful application for on-site real time corrosion monitoring by providing rapid determination of corrosion rate. Some common applications of LPR are:

- Cooling water systems
- Potable water treatment and distribution systems
- Amine sweetening
- Waste water treatment systems
- Pickling and mineral extraction processes
- Pulp and paper manufacturing

Potentiostats are used to maintain the working electrode at a constant potential while measuring the polarization curves. The potentiostat acts as an electronic regulating device and can produce any required potential-time function. Using potentiostats following measurements can be performed:

- Potential hold experiments in which the potential is held constant for a given time of the experiment
- "Potentiostatic" experiments for imposing quasistationary states in which the applied potential is maintained for a certain time. The applied potential is then changed to the next value.

- Potentiodynamic (potentiokinetic) experiments with a linear change of potential with time.

- Potential on, potential off, potential reversal, potential step experiments with very rapid changes in potential.

Another important measuring arrangement for corrosion studies is the galvanostatic polarization circuit. Galvanostatic polarization measurements can be performed with the same arrangement used for potentiostatic measurements (Figure 3.7). A potentiostat can supply constant current by maintaining a constant voltage across a resistor. The supplied current then flows through the measuring circuit that is connected in series with the resistor.

However, it must be noted that the potentiostatic and galvanostatic curves for active-passive metal are not same and passive region cannot be accessed from galvanostatic polarization curves (shown in Figure 3.8) [95].

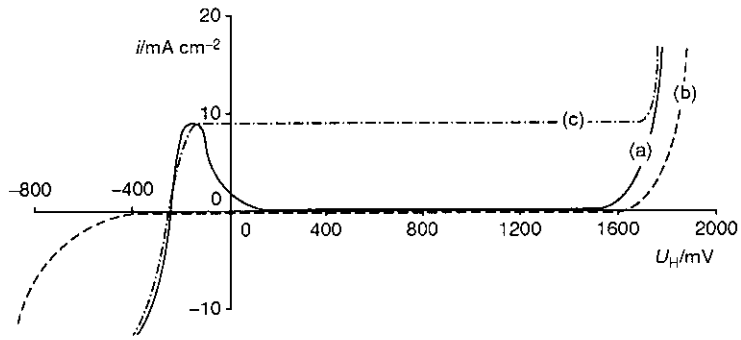

FIGURE 3.8: Current density-potential curves for 13% Cr Steel: (a) 0.2 M H_2SO_4, potentiostatic; (b) 0.2 M Na_2SO_4, potentiostatic; (c) 0.2 M H_2SO_4, galvanostatic

Applications of galvanostatic and potentiostatic measurements are:

- Characterization of the electrochemical systems taking part in the corrosion process (metal electrode and redox systems, systems with active and passive behavior, electrode kinetics) [103, 104].

- Determination of the dependence of dissolution rates on potential, in particular the estimation of critical potentials such as the pitting potential [105, 106], repassivation potential [107].
- Determination of the potential dependence of rupture time and crack propagation rate in SCC and corrosion fatigue [108].
- Potential dependence of selective corrosion of structural components in intergranular corrosion [109].
- Potential dependence of dissolution rates during cathodic [110] and anodic protection [111].
- Estimation of corrosion rates solely from current–potential curves.

Polarization measurements can cause irreversible changes in the electrode surface that can be observed from the hysteresis effect of backward polarization scans [30]. These changes can be small or large depending on the length of time and magnitude of impressed current and potential changes.

3.8 Electrochemical Instrumentation

3.8.1 Reference Electrodes

In corrosion tests selection of reference electrodes depends on the corrosive environment and the aim of the test (Table 3.1). The reference electrode selected should be as similar as possible to the system under investigation. This will ensure contamination minimization of the reference electrode (e.g. chloride ions diffusing into the sulphate solution of a copper/copper sulphate reference electrode will change the potential of the reference electrode) and avoid misleading corrosion test results by ions from the reference electrode entering the test solution (e.g. chloride ions in a pitting corrosion test in sulphate solution) [112].

TABLE 3.1: Field of application of various reference electrodes

Electrode system	Electrolyte	Field of application
$Hg/Hg_2Cl_2/Cl^-$	KCl *sat.*	general
$Hg/Hg_2Cl_2/Cl^-$	KCl $1M$	general
$Hg/Hg_2Cl_2/Cl^-$	KCl $0.1M$	general
$Hg/Hg_2SO_4/SO_4^{2-}$	K_2SO_4 *sat.*	sulfate containing media
$Hg/HgO/OH^-$	NaOH $1M$	alkaline media
$Ag/AgCl/Cl^-$	KCl $0.1M$	general
$Ag/AgCl/Cl^-$	KCl $3M$	hot media
Hg Tl/TlCl	KCl $3.5M$	hot media
$Cu/CuSO_4$	$CuSO_4$ *sat.*	Soils, water

3.9 Potentiostat

A potentiostat is a basic equipment required to control a three-electrode cell. It functions by maintaining the potential of the working electrode at a constant level with respect to a reference electrode by varying current through an auxiliary electrode. The potentiostat of Figure 3.9 shows the basic principles of potential control [113].

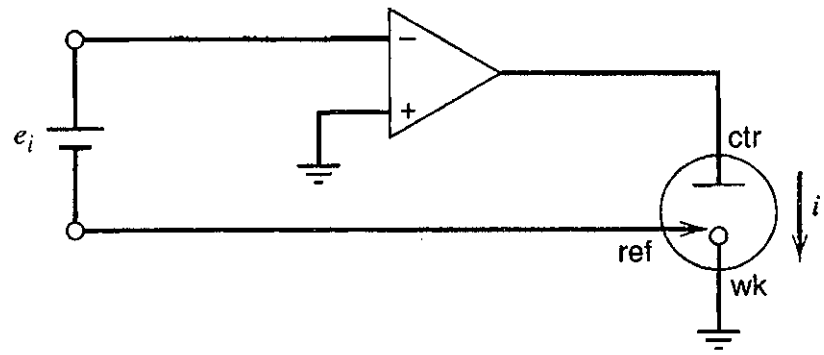

FIGURE 3.9: A simple potentiostat connected to a three-electrode cell

As shown in the Figure, the reference electrode is connected to the inverting input of the operational amplifier. Since the inverting input is a virtual ground, the reference electrode is at $-e_i$ *vs.* ground. The current through the cell is controlled by the amplifier so that the reference electrode is always at $-e_i$ *vs.* ground. Since the working electrode is grounded, $e_{wk}(vs.\ \text{ref}) = e_i$.

However, the controlled voltage always contains a *uncompensated resistance loss* due to voltage drop in the solution. This loss can be made negligibly small by careful placement of the reference electrode with respect to the working electrode.

3.10 Galvanostat

A galvanostat is an electronic instrument that controls the current through an electrochemical cell at a preset value. In the galvanostat shown in Figure 3.10, the working electrode is at virtual ground. Current through the cell depends on the

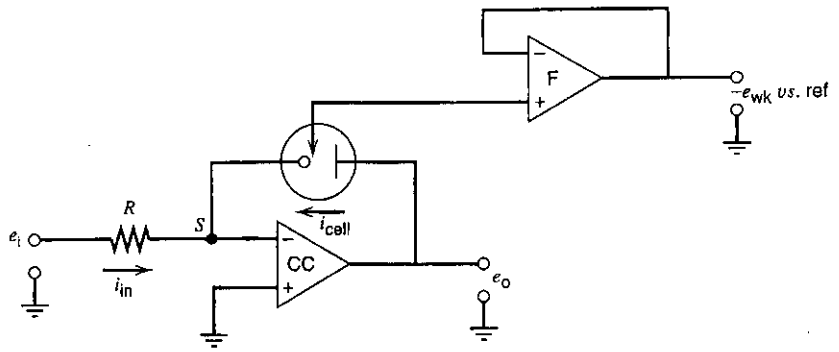

FIGURE 3.10: A simple galvanostat

input potential. The reference electrode is connected to the noninverting input of F. Thus voltage follower, F, gives the reference electrode's potential versus ground, which is $-e_{wk}$.

Chapter 4

Materials and Methods

4.1 Introduction

A submerged impinging jet system was used to study effect of flow on corrosion. Stainless steel, brass and aluminum were exposed to different aqueous solutions at different fluid velocities as well as in quiescent condition. Weight loss method was applied to study the behavior of the experimental rig. Later electrochemical methods (e.g. polarization, open circuit potential transient) were also used.

4.2 Experimental Setup

Closed-loop system designed by Easin [114], after several modifications, was used for the current study. Modifications involve removal of the metallic bend and tee-section, removal of exiting specimen holder and replacing it with a perspex specimen holder.

A schematic diagram of the test rig is shown in Figure 4.1. A 150 liter tank was used to store aqueous solution. Water was circulated from the reservoir by a centrifugal pump (material of construction: polypropylene). Poly vinyl chloride

(PVC) pipeline and fittings were used to avoid corrosion which would be experienced with steel or copper tubes.

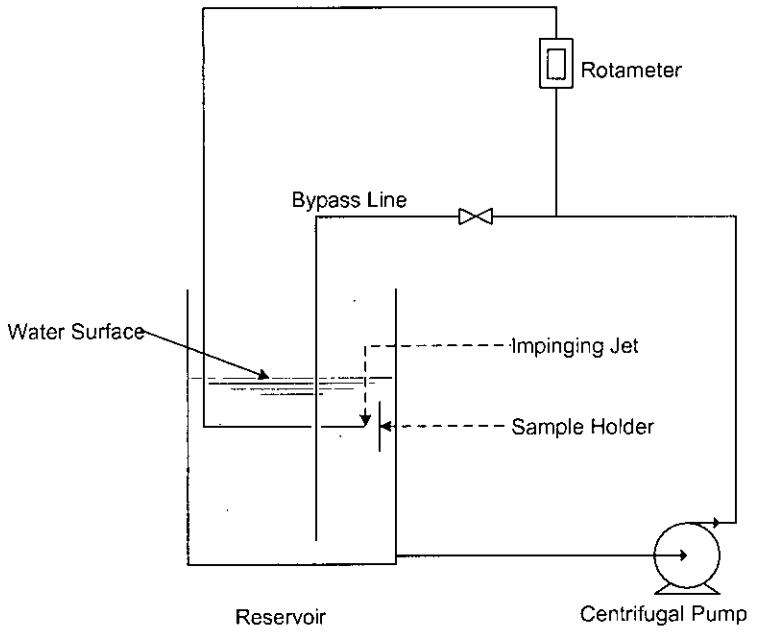

FIGURE 4.1: Erosion-corrosion test rig with submerged impinging jet

To manipulate water velocity at the nozzle exit a bypass line with valve was used. Water circulation rate through the system was adjusted by varying the opening of this valve. A pre-calibrated rotameter was installed to measure the water flow rate. A nozzle of 0.5-inch diameter was used to create the impinging jet. Capacity of the pump did not permit use of nozzles with smaller diameters.

The specimen holder, made of perspex sheet, could be rotated about its vertical axis. This enabled conducting impinging test runs for any impact angle between 0° to 90°. The test rig can be used either as submerged jet or free jet. However, experiments were performed with submerged jet configuration because of it's resemblance with the disturbed flow systems commonly encountered in chemical process industries.

4.3 Materials

4.3.1 Metal and Alloys

Erosion-corrosion of stainless steel, brass and aluminum were investigated. Optical Emission Spectroscopy (OES) was used to determine compositions of the metal and alloys. Table 4.1 shows composition of the metal and alloys used.

TABLE 4.1: Metal/Alloy Compositions

Metal/Alloy	Components	%	Designation
Stainless Steel	Cr	17.187	UNS S20100
	Ni	2.1167	
	C	0.10894	
	Mn	4.9511	
	Si	0.57588	
	P	0.04515	
	S	0.0106	
Aluminum	Al	>99	-
Brass	Cu	62.753	CW508L
	Zn	36.972	

4.3.2 Reagents

Commercial grade Na_2CO_3, $FeSO_4$, $FeCl_3$ and raw seasalt were used for preparation of solutions. These chemicals were dissolved in distilled water to prepare the solution.

In addition, HCl and HNO_3 were used for corrosion product removal for cleaning the test specimens after experiment.

4.4 Potentiostat/Galvanostat

HA-303 Potentiostat/Galvanostat manufactured by Hokuto Denko Corporation, Japan was used for producing potentiostatic/galvanostatic polarization curves. Saturated Calomel Electrode (SCE) was used as reference electrode while platinum was used as counter electrode. For potentiostat function the equipment was able to provide maximum control voltage of ± 10 V; for galvanostat function the equipment can provide maximum control voltage of ± 1 V, equivalent to ± 3 A current.

4.5 Data Acquisition System

A data acquisition system was developed to collect open circuit potential transient data. The system has two input channels; one with voltage-follower function and the other with five times amplification. A micro-controller was used for Analog-to-digital (AD) conversion. The data acquisition system was connected to a computer through RS-232 port.

4.6 Experimental Procedures

1. Preparation of Working Electrodes

Rectangular working electrodes were made from commercial sheet (composition is given in Table 4.1) of 1.5-mm thickness. Since size of the specimen affects corrosion behavior [73, 115], specimens were made sufficient large enough (102mm $\times$ 76mm) to nullify the size effect.

2. Surface Preparation

The prepared electrodes were polished to obtain a smooth surface, free of any physical defects. All specimens were ground on 600 grit silicon carbide abrasive paper. The specimens were then washed with distilled water, degreased with acetone, dried with hot air and stored in a desiccator before weighing. The rear and

the edges of the samples were coated with expanded polystyrene (EPS) solution in Xylene to make sure that only the front section is exposed to the flow.

3. Coupon Tests

For coupon tests, Specimen was then placed in the specimen holder and exposed to the impinging jet for a fixed period. The specimen was then dismounted and cleaned by washing with distilled water, treated chemically if needed, and degreased by washing with acetone. Then the specimen were dried in hot air, cooled in a desiccator and weighed.

4. Removal of Corrosion Products

Corrosion products can be removed in three ways: mechanical,. chemical and electrolytic. ASTM G1-03 standard procedure was applied for chemical removal of corrosion products. Aluminum was treated with nitric acid for 5 minutes at 25°C. Brass samples were immersed in HCl (sp. gr. 1.19) for 3 minutes at ambient temperature. SS201 was treated with HCl at ambient temperature.

To determine the mass loss of the base metal when removing corrosion products, an uncorroded sample was also cleaned by the same procedure. The extent of metal loss resulting from cleaning process was then utilized to correct the corrosion mass loss.

5. Cell Formation

A cell consisting of working electrcde and a saturated calomel electrode (SCE) was formed for measuring equilibrium potentials. For measurements away from the equilibrium (potentiostatic or galvanostatic control), cell consisting of three electrodes was used. The test specimen was used as working electrode, SCE served as reference electrode while a platinum electrode was used as auxiliary electrode. A luggin capillary with salt-bridge connection was used to hold the reference electrode. Tip of the capillary ended at the surface of the working electrode.

6. Electrochemical Measurements

Measurements from the above mentioned cells were recorded. Tests were performed to conduct galvanostatic, potentiostatic polarization and open-circuit potential measurement.

Chapter 5

Results and Discussion

5.1 Results

5.1.1 Characterization of the Test Rig

The test rig was first characterized to ensure that it has good control over various test parameters (e.g. velocity, impact angle).

Figure 5.1 demonstrates changes in temperature as a function of time of operation. Two separate sets of data were collected; one in the month of July and the other in the month of November. Rise of temperature resulted from operation of the pump for extended period. For both cases maximum temperatures were achieved after about 12 hours from start. Beyond this point the temperature was expected to remain constant. However, cooler ambient temperature at night in November caused temperature to fall slightly before becoming constant.

Variation of oxygen concentration was also recorded. Figure 5.2 shows dissolved oxygen (DO) concentration and the corresponding water temperature. Increased aeration caused by flow agitation at the beginning resulted immediate rise in DO. However, the process was reversed soon due to increase in water temperature.

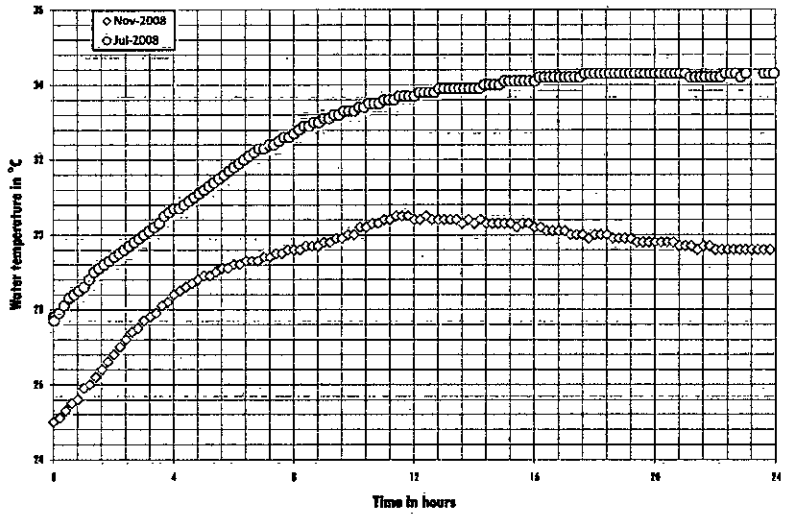

FIGURE 5.1: Water temperature variation with time

After about 4 hours DO concentration reached a minimum. Thereafter, DO concentration increased at a very slow rate for a short period and then remained constant.

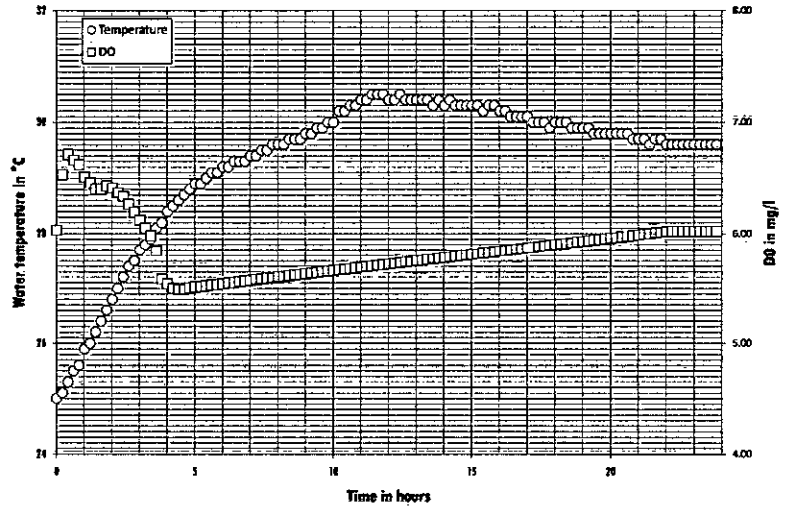

FIGURE 5.2: Dissolved Oxygen as a function of time of the running time of test rig (velocity = 2.63 m s^{-1})

To check the consistency and reproducibility of the rig several tests were performed. Figure 5.3 shows weight loss of SS 201 specimen at impact velocity of 2.63 m s^{-1}

and impact angle of 90°C. It can be assumed that all data points lie on a straight line. The rate of corrosion was also within a very small range.

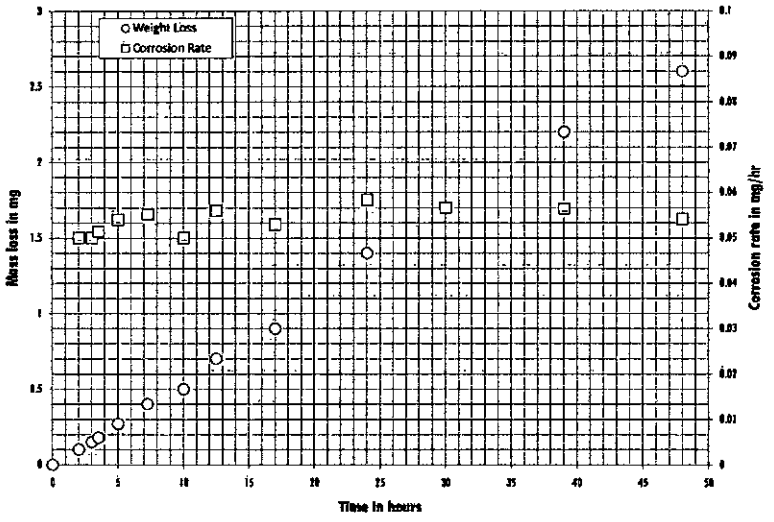

FIGURE 5.3: Cumulative weight loss and rate of corrosion as a function of time (material: SS 201, impact velocity = 2.63 m s^{-1}, impact angle = 90°)

Figure 5.4 shows the relationship between corrosion rate and the impact velocity of water impinging onto copper specimen. This figure clearly shows that at quiescent condition corrosion rate was considerable low and the rate increased with velocity. Specimens without EPS coating on the back and on the edges were also exposed to the flow. These specimens showed higher corrosion rate, resulted from differential cell formation due to less mass transfer at the rear.

Effect of impact angle on corrosion is shown in Figure 5.5. For single phase flow, erosion-corrosion depends only on the normal component of the impact velocity [33]. The experimental data conforms this phenomenon as the corrosion rate has gradually increased with the increasing impact angle having a maximum at 90°.

With current configuration, the setup is able to produce impact velocities up to about 6 m s^{-1}. However, increasing the pumping capacity can definitely increase the impact velocity.

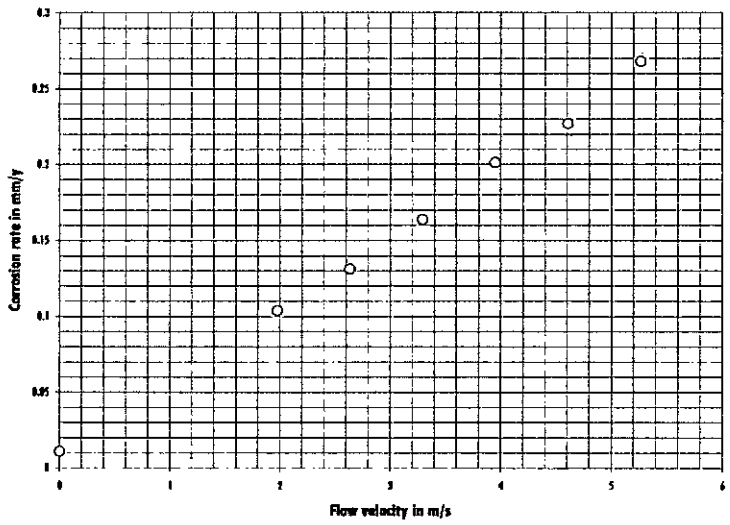

FIGURE 5.4: Corrosion rate with different impact velocities (material: Copper, impact angle = 90°)

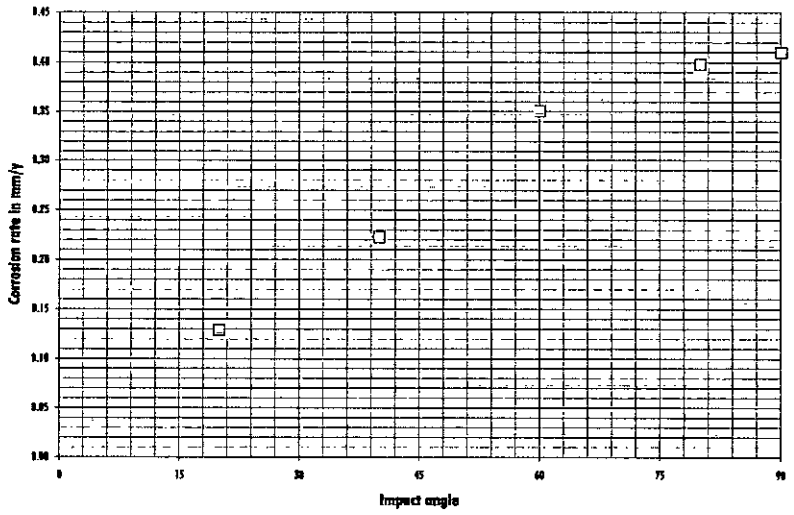

FIGURE 5.5: Corrosion rate with different impact angles (material: Aluminum, velocity = 3.29 m s^{-1})

The experimental data shown above conforms consistency and reproducibility of the test rig. This rig is very simple to operate and have good control over the operating variables. Moreover, fluid flow is well characterized for such systems. As a result, a impinging jet system can be successfully used to develop laboratory tests comparable to actual industrial situations.

5.1.2 Polarization Diagrams

5.1.2.1 Stainless Steel

Figure 5.6 shows potentiostatic polarization curves for SS201 measured in artificial seawater under both quiescent condition and fluid jet impingement. From the figure it is clear that the cathodic reaction is accelerated by the high mass transfer rate under flow conditions.

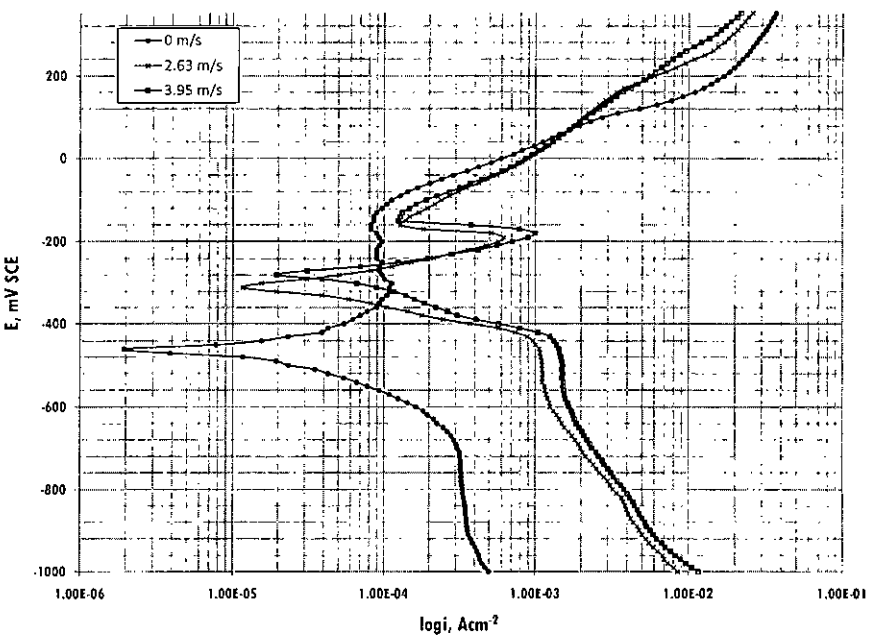

FIGURE 5.6: Potentiostatic polarization curves: SS201 in artificial seawater

At quiescent condition, passivation occurs at approximately -300 mV. Passivation also occurs under flow conditions. However, upon reaching the passivation current the current density starts to increase immediately and the alloy enters the transpassive zone.

Polarization curves in Na_2CO_3 were obtained in two different concentrations (2.5% and 5%). SS201 shows active-passive behavior for both quiescent and fluid impingement conditions. Figure 5.7 shows that there flow rates and concentration of Na_2CO_3 has insignificant effect on $E_{passive}$ and $E_{transpassive}$. However, critical current density and passivation current density have shown increasing trend with increasing velocity. Cathodic polarization curves also have significant flow effect.

Potentiostatic polarization diagrams obtained for SS201 in $FeSO_4$ is shown in Figure 5.8(a). SS201 shows active-passive behavior in the solution. However, the passive zone is found to be very small. The flow conditions greatly increased the cathodic reaction rate. $i_{critical}$ also significantly increased in flow conditions. Anodic polarization curve at EMF more than 800 mV at quiescent condition shows repeated formation and dissolution of oxide film. However, flow conditions do not show similar behavior. Figure 5.8(b) shows polarization diagram for SS201 in $FeSO_4$+$FeCl_3$. The passive zone is completely absent.

5.1.2.2 Brass

Cathodic polarization curves of brass shift to the right as the flow rate increases (Figure 5.9). In the anodic region, the current density steadily increases without any fluctuations. Brass specimens used for polarization curve measurement were found to have shallow pits.

Figure 5.10 shows potentiostatic polarization curves for brass measured in Na_2CO_3. When polarized anodically brass shows active-passive behavior. As shown in the figure, at approximately -360 mV critical current density is obtained.A secondary passivation was also observed at -200 mV. The secondary passive zone is obtained

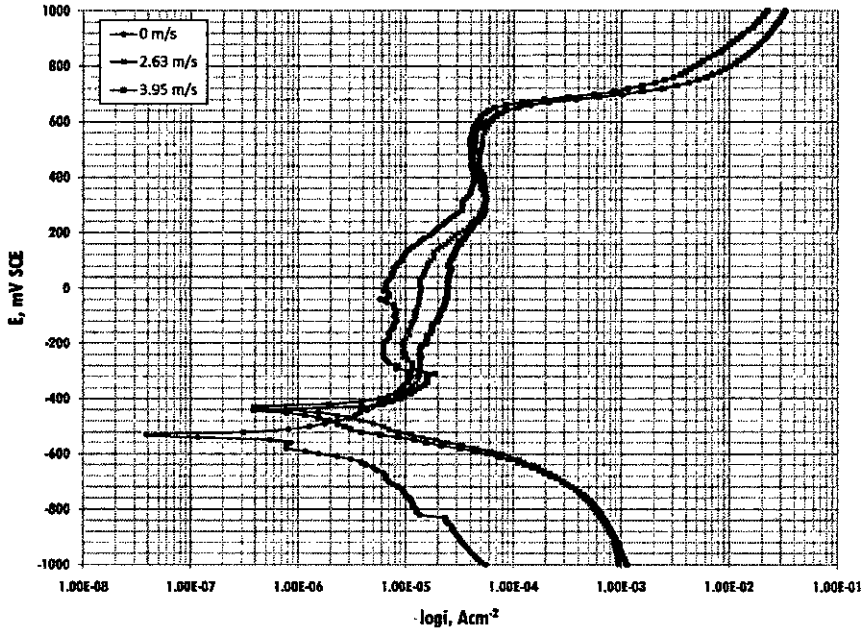

(a)

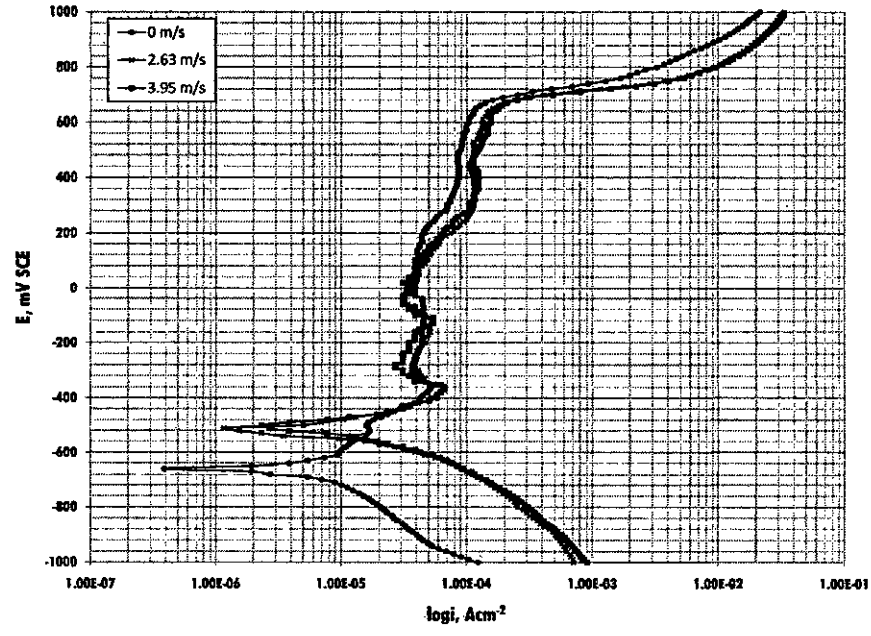

(b)

FIGURE 5.7: Polarization curves of SS201 in (a) 2.5%, and (b) 5.0% Na_2CO_3

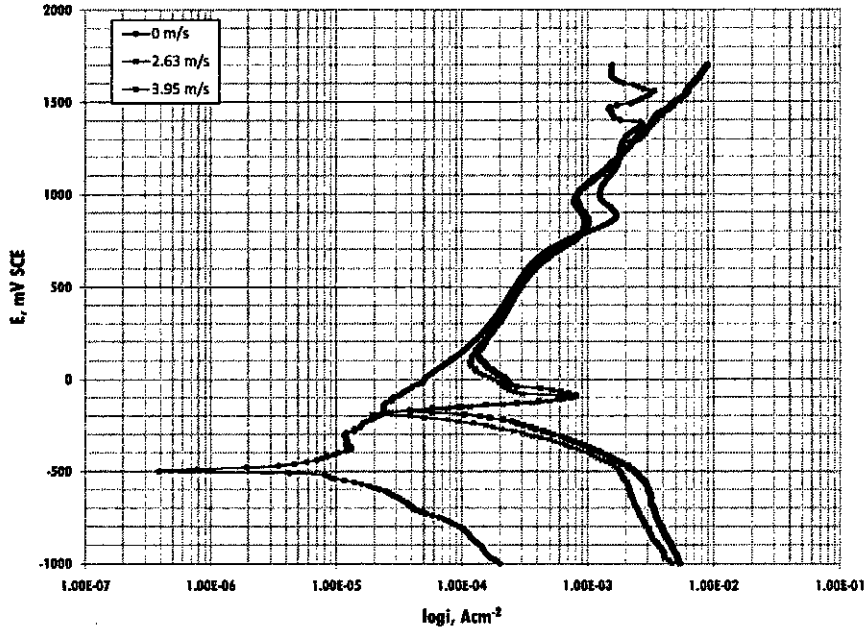

(a)

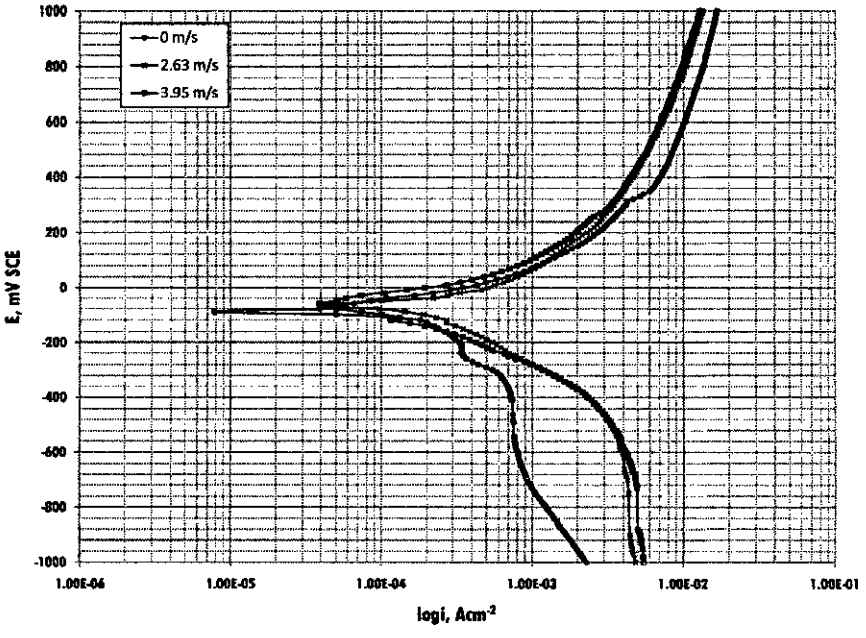

(b)

FIGURE 5.8: Polarization curves of SS201 in (a) $FeSO_4$, and (b) $FeSO_4$+$FeCl_3$

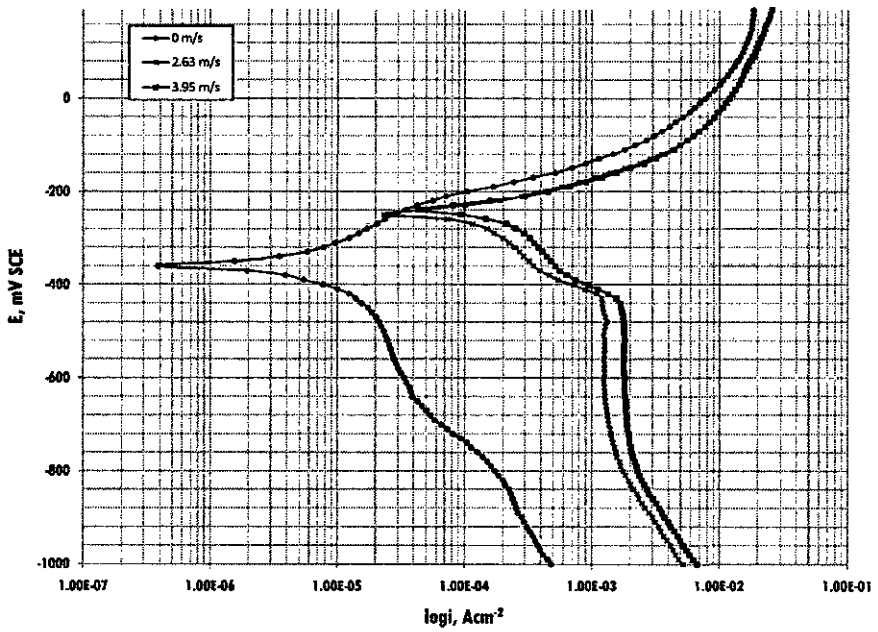

FIGURE 5.9: Potentiostatic polarization curves: Brass in artificial seawater

with small/invisible active nose and the secondary passivation current increased 10 folds for the flow conditions. There were no effect of flow on $E_{transpassive}$.

Figure 5.11(a) shows polarization diagram of brass in $FeSO_4$. The polarization curves for quiescent and flow conditions are qualitatively similar; only the rate of cathodic and anodic processes are faster with flow. Similar behavior is observed with addition of $FeCl_3$. However, reaction rates increased by ten folds in presence of chlorides.

5.1.2.3 Aluminum

Potentiostatic polarization curves for aluminum in artificial seawater is shown in Figure 5.12. Like brass there is a significant increase in the cathodic reaction rate. No passive zone is observed. Al specimens showed formation of numerous pits after removing from the corrosive environment.

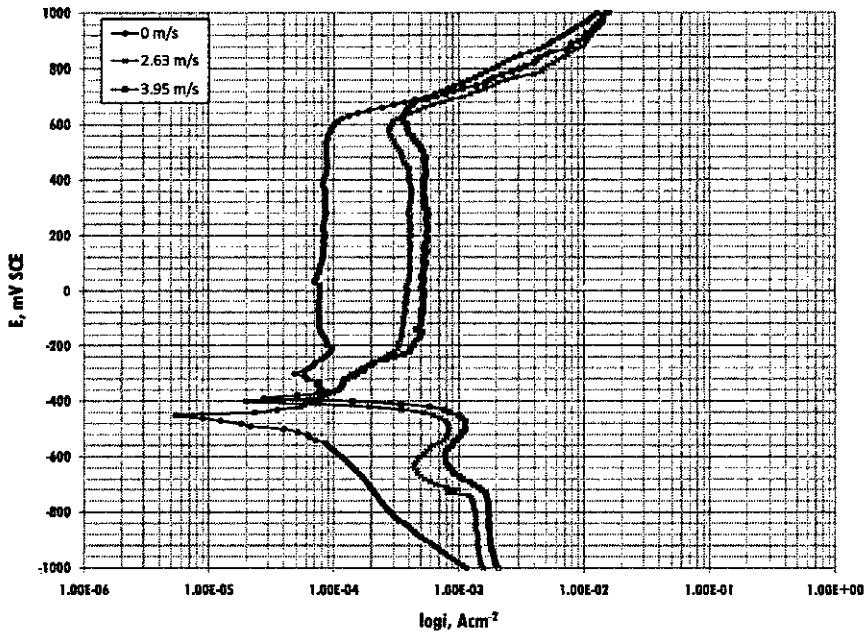

(a)

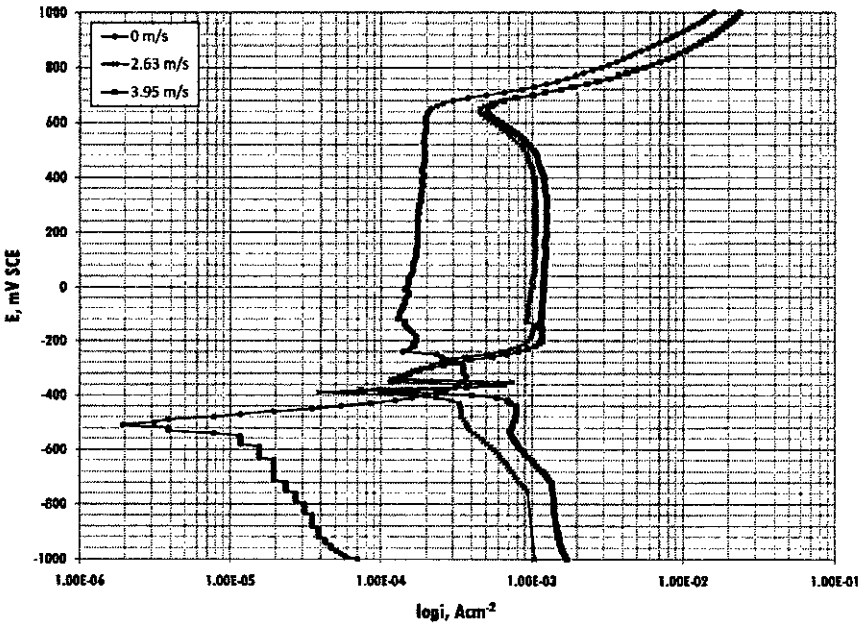

(b)

FIGURE 5.10: Polarization curves of Brass in (a) 2.5%, and (b) 5.0% Na_2CO_3

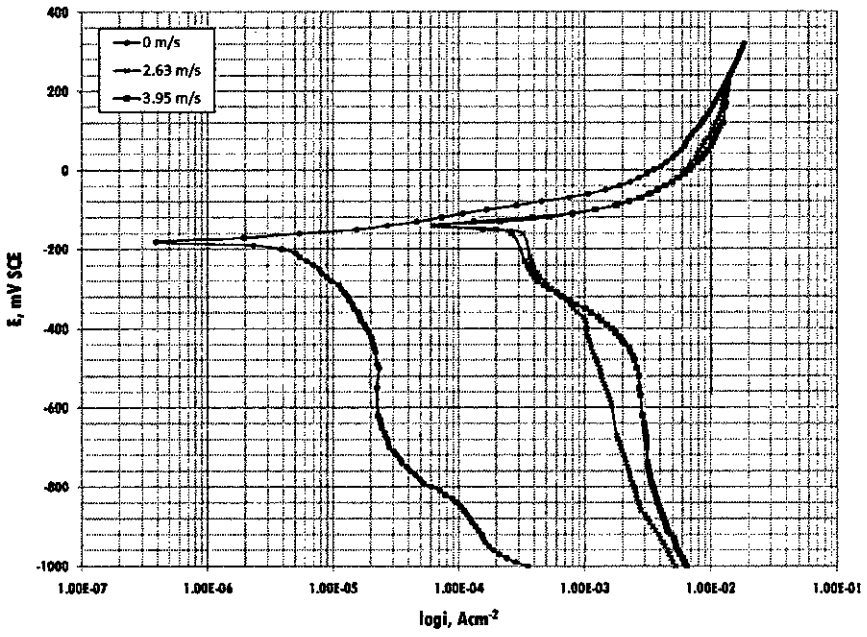

(a)

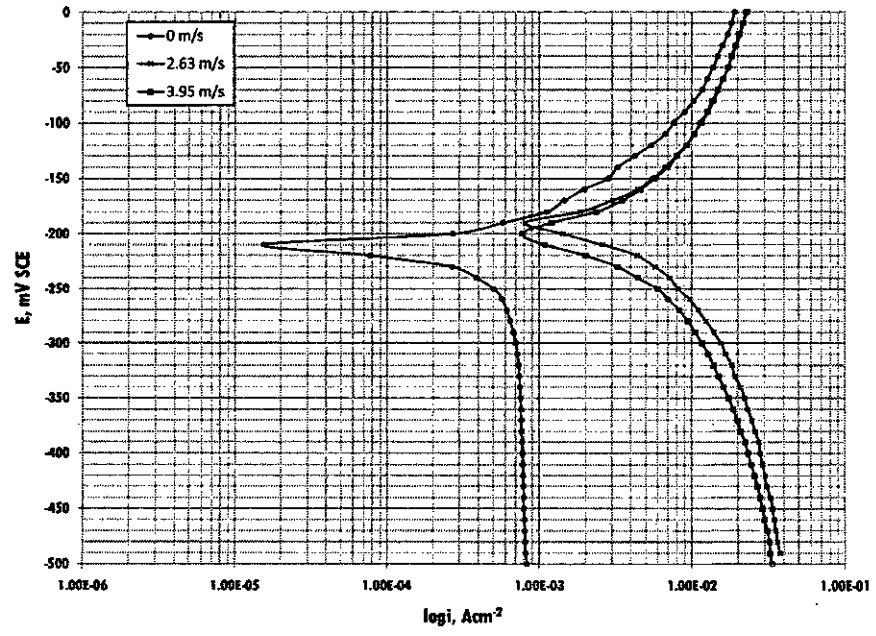

(b)

FIGURE 5.11: Polarization curves of Brass in (a) $FeSO_4$, and (b) $FeSO_4$+$FeCl_3$

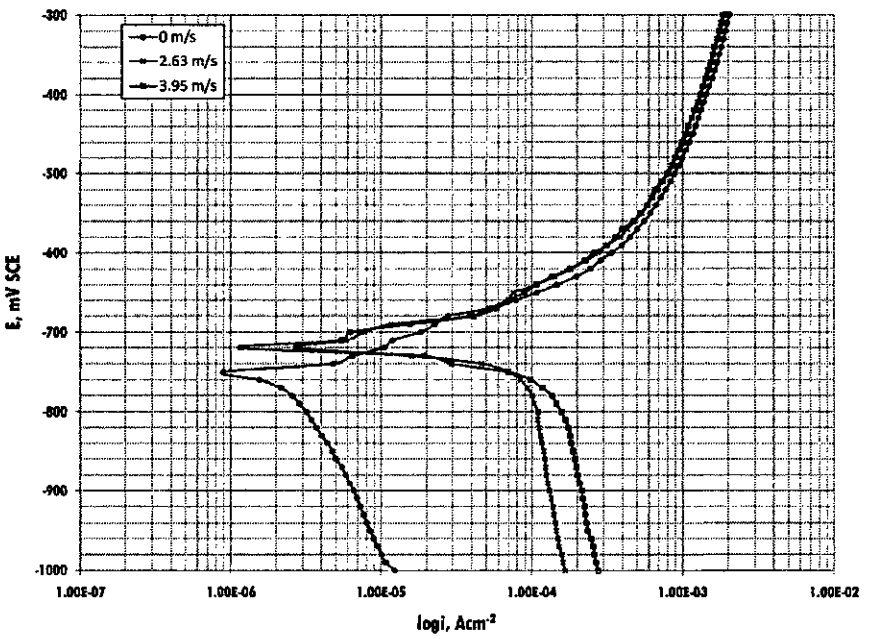

FIGURE 5.12: Potentiostatic polarization curves: Aluminum in artificial seawater

Galvanostatic polarization curves for aluminum in Na_2CO_3 are shown in Figure 5.13. For both concentrations, passivation of aluminum is observed due to anodizing effect of the environment. However, in flow situations no passive zone is observed. Passive zone is completely stripped off by the flow impact and anodic polarization curves are very steep. Cathodic polarization curves showed small variation due to flow.

Polarization behavior of Aluminum in $FeSO_4$ and $FeSO_4$+$FeCl_3$ are shown in figures 5.14(a) and 5.14(b). Like brass, reactions rates are found to increase in presence of chlorides and flow.

5.1.3 Open Circuit Potential

Open circuit potential is often also termed as the equilibrium potential, the rest potential or the free corrosion potential. Open circuit potentials were measured immediately after immersing the specimens in the corroding environment with

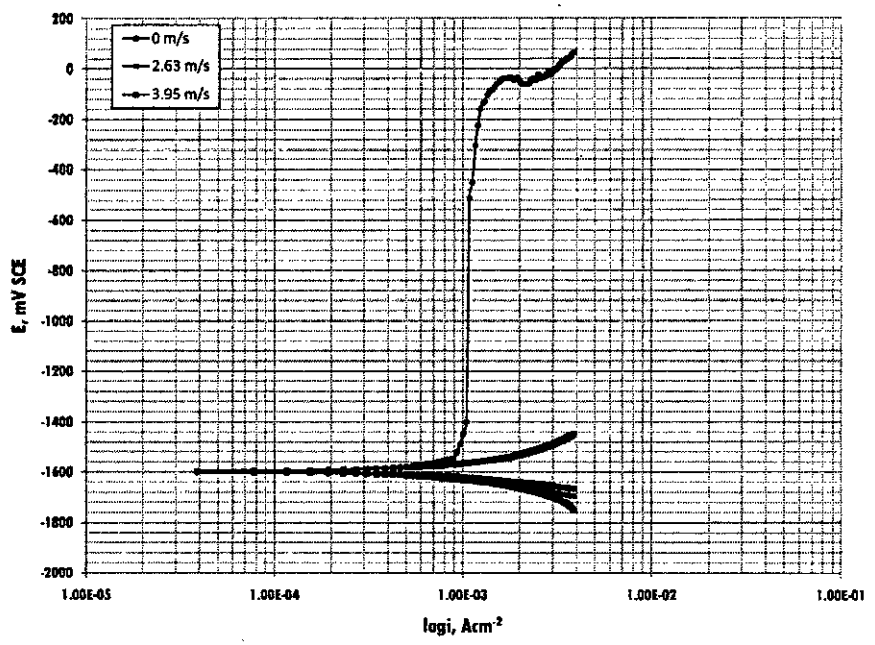

(a)

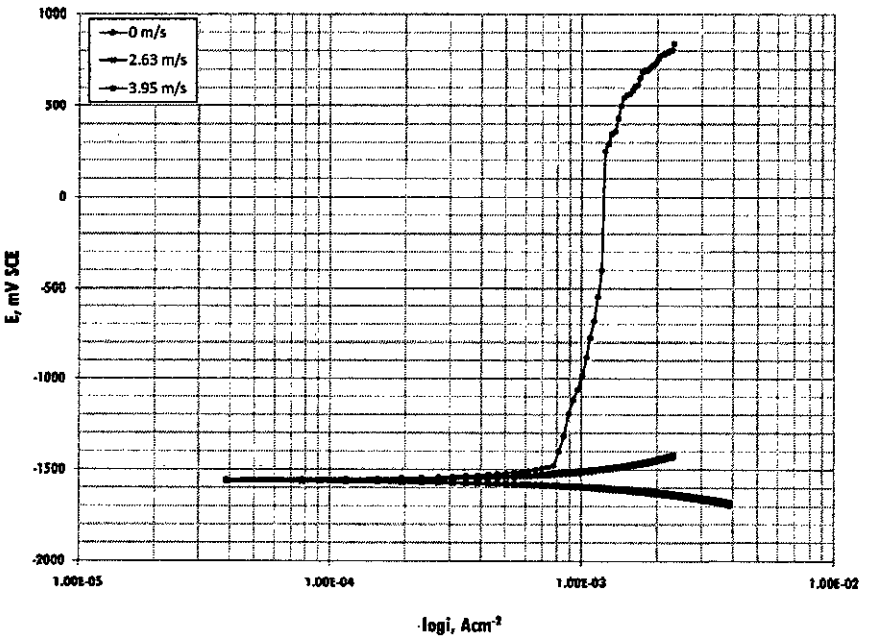

(b)

FIGURE 5.13: Polarization curves of Aluminum in (a) 2.5%, and (b) 5.0% Na_2CO_3

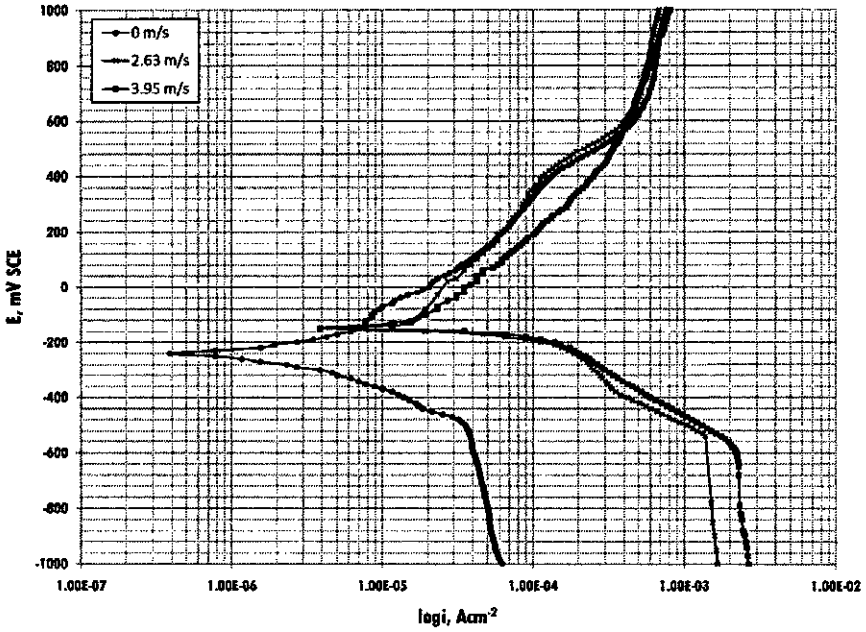

(a)

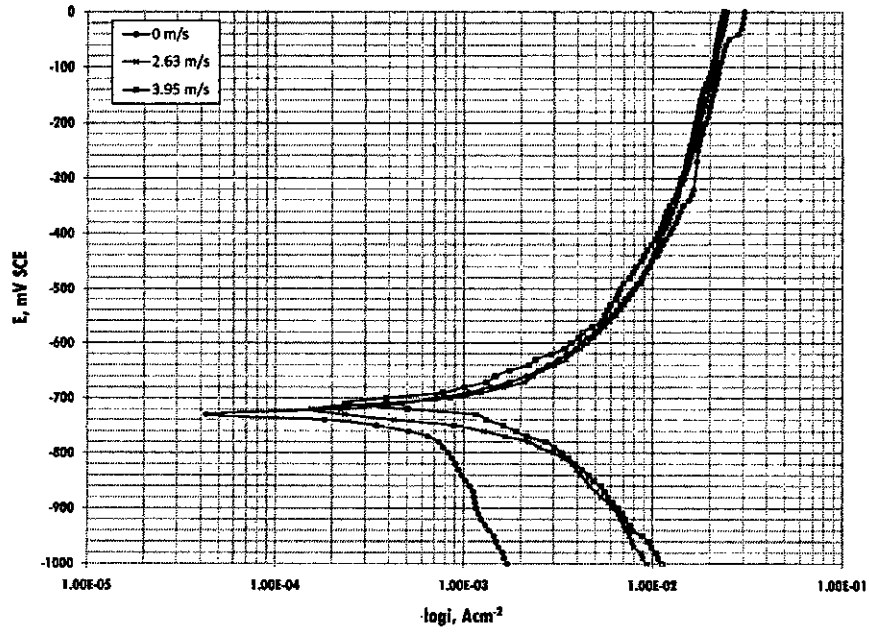

(b)

FIGURE 5.14: Polarization curves of Aluminum in (a) $FeSO_4$, and (b) $FeSO_4$+$FeCl_3$

respect to SCE. OCP for SS201, aluminum and brass in different environments are shown in Table 5.1.

TABLE 5.1: OCP of SS, Brass and Aluminum at different environments

Material	Environment	OCP at different velocities (m/s), mV		
		0	2.63	3.95
SS201	Seawater	-460	-310	-280
	Sodium Carbonate (2.5%)	-530	-440	-430
	Sodium Carbonate (5%)	-630	-550	-510
	Ferrous Sulfate	-500	-180	-170
	Ferrous Sulfate+Ferric Chloride	-90	-80	-90
Brass	Seawater	-360	-250	-230
	Sodium Carbonate (2.5%)	-460	-390	-380
	Sodium Carbonate (5%)	-510	-390	-380
	Ferrous Sulfate	-180	-140	-140
	Ferrous Sulfate+Ferric Chloride	-210	-190	-200
Aluminum	Seawater	-760	-730	-720
	Sodium Carbonate (2.5%)	-1600	-1597	-1600
	Sodium Carbonate (5%)	-1600	-1597	-1600
	Ferrous Sulfate	-240	-150	-150
	Ferrous Sulfate+Ferric Chloride	-730	-720	-710

Open circuit potential can be function of many factors (e.g. metal composition, ion concentrations, temperature). Effect of flow on OCP can be clearly understood from the results. Flow conditions greatly affect the cathodic process (represents the reduction of oxygen at aerated conditions). Higher rate of cathodic process cause the intersection point of the cathodic and anodic polarization curves (hence the OCP) shift to more positive direction as observed for all of the cases. Though the experiments were performed without temperature control, each run was started with similar temperature. Therefore, it can be concluded that the shift in OCP is only due to the presence of flow.

In addition, flow seems to have some effect on the exchange current density. Increasing flow velocity causes higher exchange current density indicating higher rate of corrosion.

5.1.4 Open Circuit Potential Transient

5.1.4.1 Stainless Steel

Figure 5.15 shows OCP of SS201 in seawater as a function of time. Under fluid jet impingement, the potential increases very sharply immediately after exposing to the environment. After first 40 s the rate decreases and shows an exponential behavior until pitting potential of -187 mV (at approximately 1200 s; shown with an arrow in Figure 5.15) is reached. However, the potential then starts to decrease at a slow rate. The rate increases as the time goes on with more and more fluctuations.

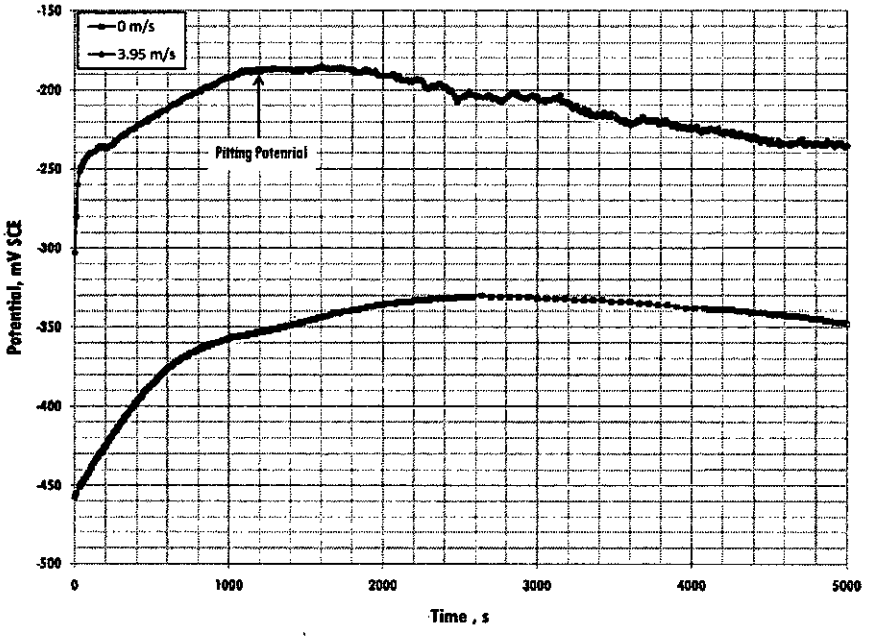

FIGURE 5.15: OCP transient of SS201 in seawater

OCP of SS201 in quiescent condition also increases with time. However, the rate is much slower than the flow conditions. The potential also does not reach the pitting potential within the experimental period of 5000 s. At quiescent condition, the potential reaches a maximum of -330 mV at approximately 3000 s and then shows a very slow decline.

When exposed to 2.5% Na_2CO_3, SS201 and brass show similar trend in OCP. SS201 starts with a potential difference of -510 mV with respect to SCE (Figure 5.16). The potential then starts to increase. However, the rate starts to diminish with time and OCP settles to a value of -373 mV after 5000 s. Under fluid impingement, initial potential shifts to a more positive direction, -440 mV and reaches to -200 mV after 5000 s.

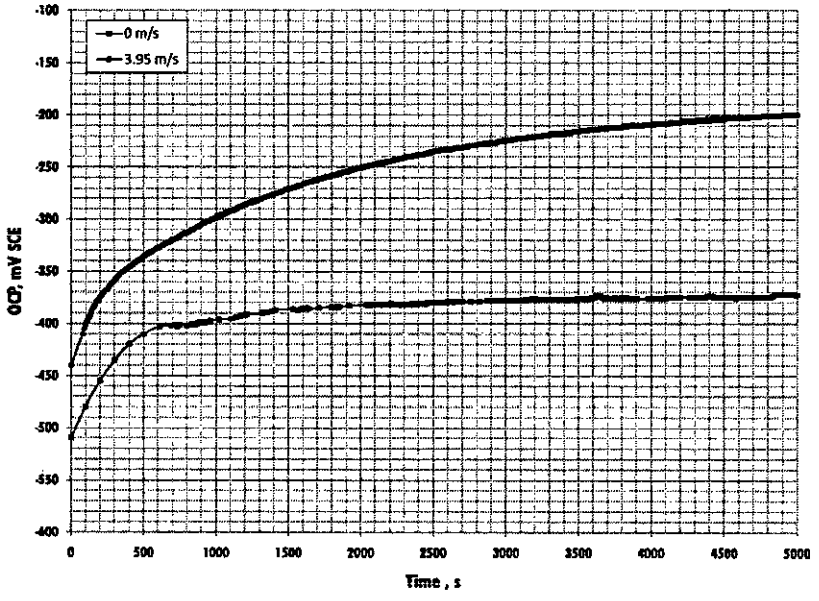

FIGURE 5.16: OCP transient of SS201 in Na_2CO_3

5.1.4.2 Brass

OCP of brass in seawater is shown in Figure 5.17. In both quiescent and fluid impingement condition the the potential change after the initial induction period is very slow leading to almost constant potential after a period of approximately 3500 s. The shape of the curve indicates formation of protective layer on the surface. In flow condition, protective layer of the fluid impact zone continuously get destroyed followed by reformation of the layer.

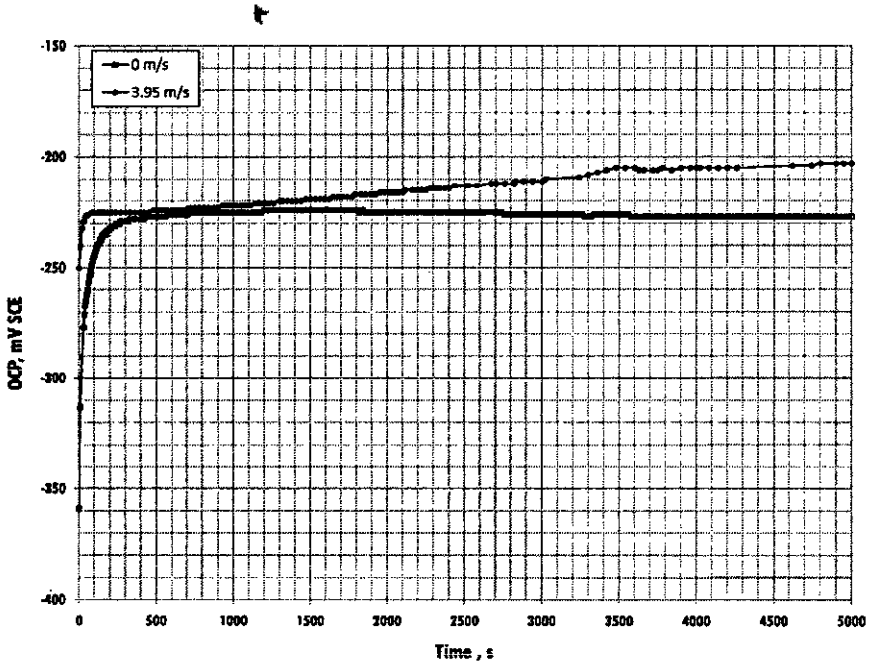

FIGURE 5.17: OCP transient of brass in seawater

Brass has initial OCP of -505 mV for no flow and -435 mV for impact velocity of 3.95 m/s. The OCP then increases and after an induction period of approximately 1000 s shows relatively small variation (Figure 5.18).

5.1.4.3 Aluminum

OCP of aluminum in seawater in totally different from the other two specimens, as shown in Figure 5.19. After exposing the aluminum specimen to artificial seawater the OCP starts to decrease. At quiescent condition, OCP decreases at a steady rate. But, at flow conditions, OCP of aluminum decreases at a very fast rate upto 200 s. The rate, then becomes much slower. However, the curve shows large amount of oscillations indicating destruction and formation of corrosion product layer at the surface. The convex shape of OCP for aluminum indicates that it undergoes severe corrosion when exposed to seawater. Even at the end of a experimental period of 5000 s the rate of decline in OCP is quite considerable.

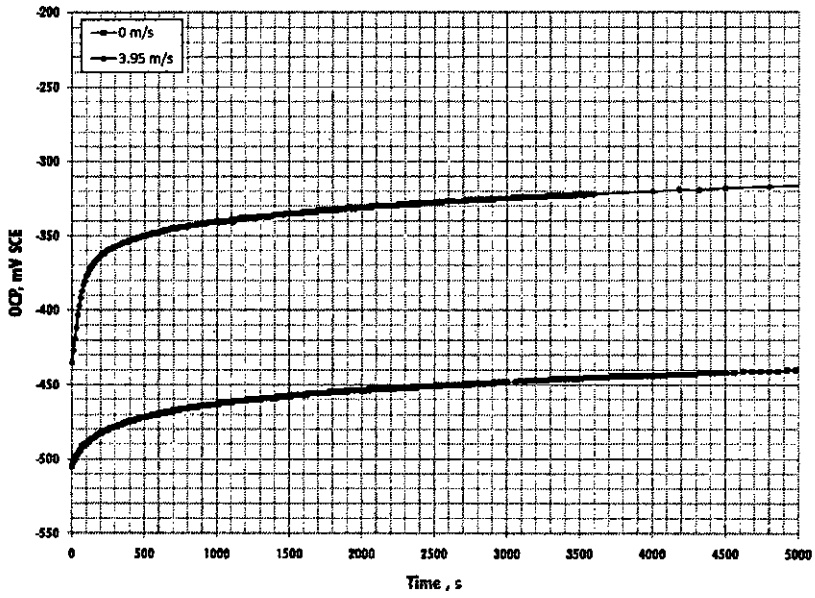

FIGURE 5.18: OCP transient of brass in Na_2CO_3

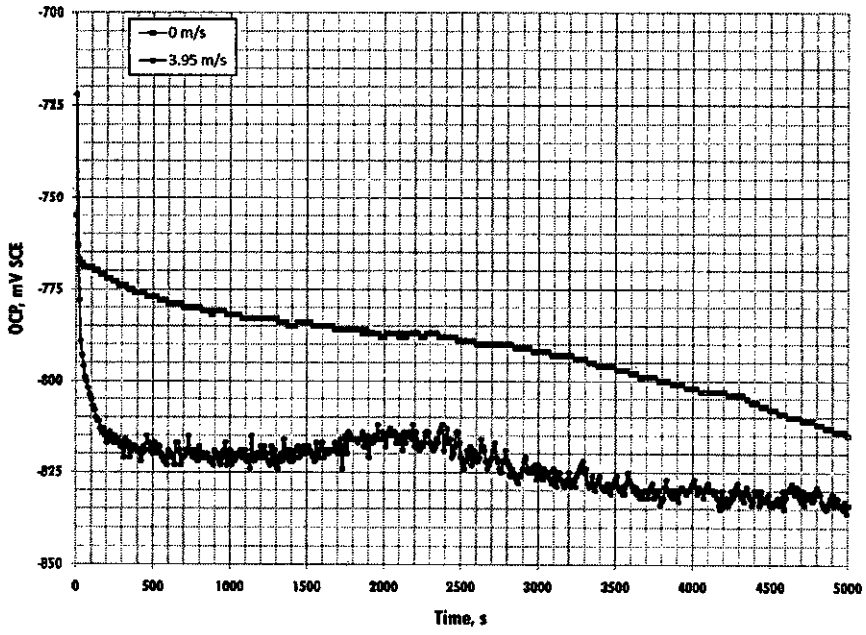

FIGURE 5.19: OCP transient of aluminum in seawater

Like seawater, behavior of aluminum in Na_2CO_3 is quite different from other two alloys as shown in Figure 5.20. For quiescent condition, the OCP initially increases, upto 400 s. For next 400 s the potential remains within -1556 to -1564 mV. After that the potential gradually decreases indicating significant attack on the metal and continues upto 1700 s. This phase is followed by a steady value of OCP for rest of the experimental time. The metal get anodized to give a protective layer and therefor OCP variation is insignificant here.

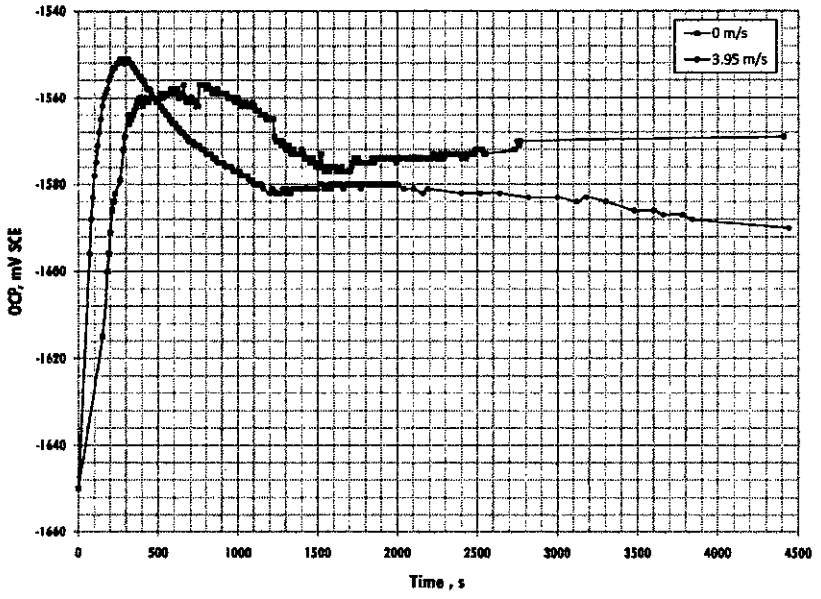

FIGURE 5.20: OCP transient of aluminum in Na_2CO_3

At flow condition, induction period is reached at a faster rate and only in 300 s. Then the potential gradually decreases initially at faster rate. Rate of change in OCP slows down with time, but does not disappear completely. The anodizing effect is therefore absent in case of flow. This observation is similar to the earlier observations made with the galvanostatic polarization curves Figure 5.13.

5.1.5 Physical Observations

Stainless steel specimens used for OCP measurement in artificial seawater showed no apparent change in the surface after the exposure period. However, while

measuring OCP under flow conditions pit formation was observed for stainless steel specimens. SS specimens exposed to sodium carbonate solution showed better resistivity than in the seawater in both quiescent and flow conditions. Passive layer of Cr_2O_3 was invisible with naked eyes.

When brass samples were exposed to seawater a diffusion barrier formed on the specimen surface marked by a visible oxide layer. In quiescent condition, this oxide layer was continuous. However, when exposed to fluid flow three distinct section was observed: stagnation, transition and wall-jet region. Among them stagnation and wall-jet region were covered with the oxide layer. Fluid impact pressure is greater in the transition region (discussed in Section 3.3.3) and therefore oxide layer in this region was thinner and the specimen was directly exposed to the corrosive environment (Figure 5.21). Brass in sodium carbonate showed similar behavior.

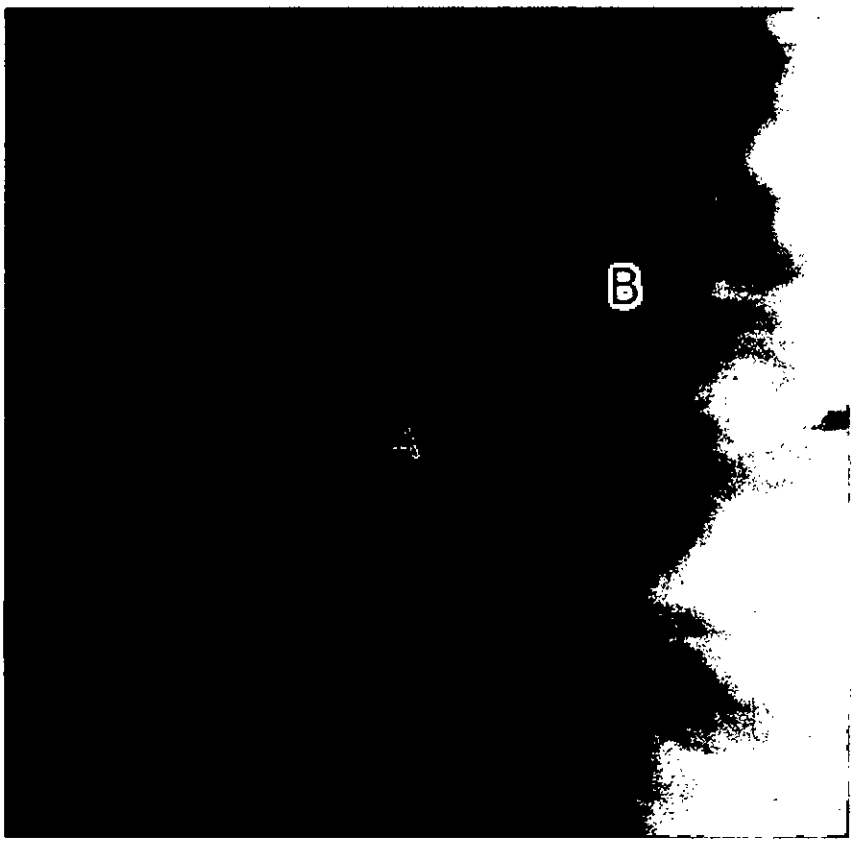

FIGURE 5.21: Brass specimen after flow exposure: (A) Stagnation, (B) Transition and (C) Wall-jet region

Aluminum when exposed to seawater showed higher corrosion rate than the other specimens. Both in quiescent and flow conditions numerous pits were observed. Pits formed on the surface showed an array like formation. Under flow conditions, the corrosion products moved away from the higher turbulence region and deposited on the region of lower turbulence. Hence, surface roughness greatly increased under flow conditions. Aluminum specimens showed better resistivity when exposed to sodium carbonate solution.

While performing polarization measurements applied voltage was shifted far from the rest potential until oxygen evolution occurred. Pits were found in each specimens as the applied potential in all cases were above the pitting potential.

5.2 Discussion

Electrochemical measurements were made to study the effect of flow on corrosion. Tests were performed in the turbulent flow regime since erosion-corrosion occurs mostly under such conditions. All the experiments were performed under steady flow rates (2.63 m/s and 3.95 m/s) without any temperature control.

Reynolds number for an impinging jet is given by:

$$\mathrm{Re} = \frac{du\rho}{\mu} \tag{5.1}$$

where, d is the diameter of the impinging nozzle, u is the solution velocity, and ρ and μ is the density and viscosity of the solution. For a flow velocity of 2.63 m/s using a nozzle of 0.5 in diameter, *Re* under flow impingement is calculated to be 333000. Reynolds number is 500000 for flow velocity of 3.95 m/s for the same system. This value indicates that the flow is turbulent since the critical value for laminar to turbulent flow in a impinging jet system is 2000 [15]. Turbulent flow near the surface enhanced oxygen mass transfer rate to the electrode surface and reduces the thickness of the diffusion boundary layer. Therefore, flow increases oxygen reduction at the surface and also enhance the anodic reaction.

5.2.1 Polarization Diagrams

Staring from cathodic region, metals/alloys were polarized in the anodic direction. The shape of the polarization curves of the specimens varied depending on the specimen and the environment (e.g. corrosive environment, flow velocity).

Effect of flow on cathodic polarization curves were observed in all the cases. With increased velocity, the cathodic current density increased causing the curves to shift to right. The increased mass transfer rate resulted from the flow increased cathodic reaction rates.

Effect of flow on anodic polarization curves varied from case to case and discussed in detail in the following sections.

5.2.1.1 Polarization Curves in Artificial Seawater

SS showed active-passive behavior in artificial seawater. For quiescent condition, the passive zone lies in between -300 mV and -120 mV. The current density in this region has shown oscillatory behavior. Presence of chloride ion in high concentration hindered the passive layer formation. These observed oscillations signify the breakdown of passive layer and instant repassivation until the transpassive zone is reached. Presence of fluid flow shortened the passive zone. Turbulent flow near the electrode increases oxygen transfer to the metal surface through the porous passive layer (in presence of chlorides) and transfer of metal ions from the pores to the bulk solution. Hence, stable pitting starts soon after passivation and the transpassive zone is reached Figure 5.6.

Brass and aluminum showed similar anodic behavior. Current density increased monotonically with increasing applied potential. Brass is more noble in seawater galvanic series then aluminum. Like other copper alloys a visible diffusion barrier of Cu_2Cl_2 is formed on the specimen surface. No such protective layer is formed for aluminum. Severe attack on aluminum in seawater is marked by the presence of numerous pits compared to brass specimen. Pits observed on the brass specimen

are because of selective attack of chloride environment to zinc, as observed for copper-zinc alloys containing less than 85% Cu. Since, the anodic process for brass and aluminum are partially activation controlled they are less responsive to flow (hence mass transfer)then stainless steel.

5.2.1.2 Polarization Curves in Sodium Carbonate

Anodic polarization of SS in Na_2CO_3 showed active-passive behavior. For, both quiescent and flow conditions the typical *S*-shaped curve was observed. Curves obtained conforms the stability of the chromium oxide passive layer in absence of significant amount of chlorides. However, polarization curves moved to the right in flow conditions. The critical current density and the size of the active nose increased with flow rate.

Active-behavior shown by brass in Na_2CO_3 is different from that of SS. A secondary passive zone is observed in addition to the primary passive zone. Primary passivation corresponds to the formation of Cu_2O diffusion barrier. However, in aerated solution Cu_2O reacts with oxygen to form CuO. Initial breakup of passivity therefore occurs because of dissolution of Cu_2O diffusion barrier. However, the surface repassivates with the newly formed Cu_2O-CuO layer. Ratio of Cu_2O to CuO depends of various factors such as corrosive environment, alloy additions etc. In flow conditions, 10 folds increase in current density was observed in the transition zone. Convective transfer of oxygen to the surface has affected both the kinetics and yield of Cu_2O to CuO corrosion as reflected by this increase in current.

In quiescent condition, aluminum also showed passivation when polarized in Na_2CO_3. Due to the limitations of the equipment, galvanostatic polarization curves were generated instead of potentiostatic polarization curves. As a result, the active nose is absent in these curves.

Aluminum readily converts to oxide because of its active nature. The stability of this oxide layer depends on pH, alloying elements. However, similar pH can

have different effect on the oxide layer depending on the nature of the acid or base present in the solution.

In quiescent condition oxide layer acts as a very good diffusion barrier in Na_2CO_3 solution. The passive zone observed was very stable. However, when aluminum was exposed to turbulent flow the oxide layer was completely destroyed due to combined effect of flow impacts and alkaline dissolution of oxide layer into AlO^{2-}. The passive zone is therefore completely absent in turbulent flow conditions.

All these three metal/alloys show a net shift of polarization curve to the right with increased concentration (Figure 5.7, 5.10 and 5.13). Variation in pH of the two environment was very small (10.56 and 10.61). However, the commercial grade of Na_2CO_3 contained chlorides(Cl^-). 2.5% solution found to consist of 54.3 ppm of Cl^-. Chloride content in the solution is doubled with the concentration of Na_2CO_3. The increase in current density is affected by this increased concentration of chloride ion.

5.2.1.3 Polarization Curves in Ferrous Sulfate

Anodic polarization curves for SS in $FeSO_4$ showed a very small passive zone. Impurities present in the commercial grade $FeSO_4$ may have shortened the passive zone. Effect of these impurities can not be explained in detail since exact composition was unknown. Flow conditions increased the active nose of the polarization curve and also increased the critical current density since the process is mass-transfer controlled.

Anodic polarization of aluminum and brass showed similar behavior in the same environment. Current density gradually increased with increase in applied potential.

When $FeCl_3$ was added in the solution along with $FeSO_4$ the polarization curves shifted to the right. The passive zone for SS vanished due to the effect of high chloride content. The current density also increased from the previous case (only $FeSO_4$) because of oxidizing effect of $FeCl_3$.

5.2.2 Open Circuit Potential Transient

As soon as the sample specimens were immersed in the corroding environment OCP was found to vary with time. Variation of OCP depends on the metal/alloy composition, nature of the corrosive environment, flow conditions, temperatures etc. Depending on the conditions OCP can shift either in more noble or less noble direction or can be a combination of both.

While studying the OCP transients of the metal/alloys, three distinct types of potential-time curves are observed.

- **Case A:** Potential becomes more and more noble, the metal or alloy becomes protected by the oxide layer formation: brass and stainless steel in Na_2CO_3.
- **Case B:** Potential becomes noble and then starts to decrease. This is observed when the protective layer of the metal or alloy is modified by the environmental factors (e.g. breakdown of passivation of SS201 in presence of chloride)
- **Case C:** Potential becomes less and less noble, the metal or alloy severely attacked by the environment: aluminum in seawater.

Case A is caused by enhanced cathodic reaction (oxygen reduction) and enhance anodic reaction (growth of the passive film) on the surface. In such cases, corrosion products are formed instantaneously as soon as the specimens are exposed to the corrosive environment. The potential starts to shift to the noble direction. After stable diffusion barrier is developed the material gets isolated from the environment and metal dissolution rate drops considerably. As a result insignificant changes in surface potential is observed.

Case B is observed for SS201 when exposed to flowing seawater. Initially the polarization shifts to the noble direction indicating formation of diffusion boundary layer on the metal surface. However, presence of turbulent flow impacts reduces the diffusion boundary layer and also enhances the oxygen mass transfer rate. The

turbulent flow also washes away anolyte from the surface. This causes migration of more metal ions to the anolyte. Chloride ions then migrates to maintain the electroneutrality. Hence the anolyte has a high concentration of $FeCl_2$ and thereby lowering the anolyte pH. It is shown earlier that at a concentration higher than 3 M $FeCl_2$ dissolution of stainless steel sustains in chloride medium. When this concentration is obtained, pits start to form on the surface. The net effect is shift of polarization curve to the active direction. Formation of pit is followed by repassivation. This explains the oscillations in the potential in this region. However, this phenomena is not as severe as observed for SS under impingement by free jets [10].

Similar curve is found for aluminum in Na_2CO_3. For aluminum, the potential shift in the negative reduction was observed after a certain period of time for both quiescent and flow conditions. Here the oxide film is dissolved by the alkaline dissolution of Al_2O_3 to AlO^{2-}. The rate of dissolution increased in presence of flow and observed by the faster rate of potential shift in the active direction.

Case C is observed for aluminum in seawater. Aluminum is prone to pitting corrosion in presence of chlorides ions and at a pH close to neutrality [116]. The oxide layer dissolves in the solution in the form of Al^{3+} and does not act as effective boundary layer. More severe conditions are observed in turbulent flow conditions. The dissolution rate is increased by accelerated diffusion to and from the surface and the potential continues to decrease.

Chapter 6

Conclusions and Recommendations

6.1 Conclusions

Erosion-corrosion of stainless steel, brass and aluminum was studied under impingement by a submerged fluid jet. Electrochemical techniques (e.g. polarization, open circuit potential measurement) were used instead of conventional weight-loss method. Electrochemical studies provided some advantages over weight-loss method such as quick characterization of corrosion behavior and provided a means for online corrosion monitoring.

The experimental system, a combination of closed flow-loop and impinging jet system, used for the studies showed acceptable performance. However, the system used was very large volume-wise and therefore large volume of liquid handling was necessary.

From the polarization studies following conclusions can be made:

- Stainless steel showed active-passive behavior in artificial seawater, sodium carbonate and ferrous sulfate in quiescent condition. In presence of flow, passive zones were shortened by flow impacts and convective mass transfer.

The passive zone was completely removed when $FeCl_3$ was added with ferrous sulfate due to oxidizing nature of Fe^{3+} and presence of chloride ions.

- Brass showed active-passive behavior for sodium carbonate only. Passive zone similar to quiescent conditions were observed in flow conditions only with higher passivation current for Na_2CO_3. For all cases with Na_2CO_3, two different passive zones were observed second of which corresponds to shift of passive layer from Cu_2O to CuO. Polarization curves of brass in artificial seawater and ferrous sulfate found to be similar to active metals/alloys.

- Aluminum showed active behavior in seawater and ferrous sulfate. However, basic solution of Na_2CO_3 favored formation of passive oxide layer in quiescent condition. When exposed to flow, the passive layer was completely destroyed due to flow impacts and enhanced dissolution of alumina layer resulting absence of passive zone.

The shape of the polarization curve depends on the metal-environment interaction. Therefore, polarization curves can be usefully utilized as a tool for identification of corrosion mechanism(s) involved.

Shape of the open circuit potential transient shows the severity of attack on metal/alloy by the environment. Therefore, it can be used as a tool for on-line monitoring of corrosion. It is a simple and cheap technique for corrosion monitoring. The experimental results obtained in the current study shows that it can be very effective. For example, the curves obtained for brass shows that a diffusion barrier is quickly formed on the surface upon exposure to artificial seawater. Similarly, SS in seawater did not show pitting type of attack in quiescent condition during the period of study. However, pitting was observed for the same specimen in presence of flow. Therefore, open circuit potential also gives a good insight of the effect of flow on corrosion.

6.2 Recommendations for Modifications

- Flow-loop system used for the current study is very large (the water reservoir holds approximately 120 liters of water). Due to large volume of the system a lot of distilled water is required. A similar system can be designed in a smaller scale which can be used with ease of operation.

- The flow-loop system for the test rigs includes long pipes and quite a few directional shifts (e.g. elbows, T-joints) in it's flow path causing large amount of head loss. As a result, pump used in the current system can develop a maximum flow rate of 6 m s^{-1}. Moreover, the impinging-jet of smaller diameter cannot be used in the system because of overall head loss in the system. Modification of flow-path and increasing the pumping capacity can increase the range of experimental study in terms of flow-rates.

- The specimen holder, specimen and the connecting wire (welded/brazed to the back side of the specimen) was completely submerged in the solution. Copper wires, used for electrical connection, can lead to galvanic cell formation when the EPS coating is removed under some undesirable circumstances. This problem can be avoided by using extended hollow specimen holder which will penetrate through the reservoir wall and electrical connection to the specimen can be made through the cylindrical shell without exposing to the solution.

6.3 Recommendations for Future Work

- Experiments were performed in open system. However, industrial flow systems have limited access to oxygen. Use of closed systems can be more practical and corrosion behavior with limited oxygen supply can be observed.

- Effect of temperature on erosion-corrosion can be observed by installing a temperature-control system in the solution reservoir.

- Three-distinct flow regimes are observed in jet systems: stagnation, transition and wall-jet region. Corrosion behavior in these three zones can be studied by the use of three concentric circular ring-electrodes, each of which will lie in three different regions.

Appendix A

Cost of Corrosion

TABLE A.1: Direct economic losses due to corrosion

Country	Year	Direct economic loss/year	Avoidable Cost	Reference
USA	1949	$ 5.5 billion		[117]
	1966	$ 10 billion		[118]
	1975	$ 75 billion	15%	[119]
	1986	$ 176 billion	15%	[120]
	1998-2001	$ 276 billion		[121]
Germany	1968-1969	DM 19 billion	23%	[122]
	1988	DM 85 billion		[123]
	1994	DM 117 billion		[123]
UK	1969-1970	£1.365 billion	23%	[124]
	1975	£2 billion	20%	[125]
	1998-2001	£4.645 billion	14.46%	[119]
Sweden	1964	300-400 million Crowns	25-35%	[123]
Finland	1965	150-200 million Markaa		[119]
USSR	1969	6 billion Rubles		[119]
Australia	1956	A$ 100-120		[126]
	1973	A$ 470 million		[127]
India	1960-61	Rs 1.54 billion		[128]
	1986	Rs 40.8 billion	44%	[129]
	1996-1997	Rs 240 billion		[130]
Japan	1976-1977	JPY 2500 billion		[131]
	1997	JPY 3900 billion (Uhlig's method)		[132]
		JPY 5200 billion (Hoar's method)		[132]
		JPY 9700 billion (NBS/BCL method)		[132]
Canada	1953	C$ 300 million		[133]
	1966	C$ 1 billion		[134]
	1979	$ 10 billion		[123]
South Africa	1985	ZAR 4 billion		[135]

TABLE A.2: Global cost of corrosion for 2004

Direct Cost	$ 990 billion
Indirect Cost	$ 940 billion
Total Cost	$ 1930 billion

Appendix B

Experimental Data

TABLE B.1: Polarization Data: SS201 in artificial seawater

Velocity: 0 m/s		Velocity: 2.63 m/s		Velocity: 3.93 m/s	
Potential	Current Density	Potential	Current Density	Potential	Current Density
mV	A/cm^2	mV	A/cm^2	mV	A/cm^2
-1000	4.95E-04	-1000	8.51E-03	-1000	1.16E-02
-990	4.68E-04	-990	8.05E-03	-990	1.05E-02
-980	4.49E-04	-980	7.35E-03	-980	9.64E-03
-970	4.33E-04	-970	6.97E-03	-970	8.90E-03
-960	4.26E-04	-960	6.81E-03	-960	8.20E-03
-950	4.14E-04	-950	6.31E-03	-950	7.62E-03
-940	4.02E-04	-940	5.92E-03	-940	7.04E-03
-930	3.87E-04	-930	5.53E-03	-930	6.70E-03
-920	3.75E-04	-920	5.30E-03	-920	6.19E-03
-910	3.64E-04	-910	4.99E-03	-910	5.92E-03
-900	3.60E-04	-900	4.80E-03	-900	5.65E-03
-890	3.56E-04	-890	4.64E-03	-890	5.34E-03
-880	3.52E-04	-880	4.37E-03	-880	5.22E-03
-870	3.52E-04	-870	4.22E-03	-870	4.99E-03
-860	3.48E-04	-860	4.06E-03	-860	4.80E-03
-850	3.48E-04	-850	3.95E-03	-850	4.68E-03
-840	3.44E-04	-840	3.87E-03	-840	4.45E-03
-830	3.41E-04	-830	3.75E-03	-830	4.33E-03
-820	3.37E-04	-820	3.68E-03	-820	4.14E-03

Continued on next page

Potential mV	Current Density A/cm^2	Potential mV	Current Density A/cm^2	Potential mV	Current Density A/cm^2
-810	3.33E-04	-810	3.41E-03	-810	3.99E-03
-800	3.33E-04	-800	3.21E-03	-800	3.79E-03
-790	3.29E-04	-790	3.10E-03	-790	3.64E-03
-780	3.25E-04	-780	2.98E-03	-780	3.44E-03
-770	3.25E-04	-770	2.83E-03	-770	3.25E-03
-760	3.25E-04	-760	2.63E-03	-760	3.13E-03
-750	3.21E-04	-750	2.52E-03	-750	2.98E-03
-740	3.21E-04	-740	2.40E-03	-740	2.83E-03
-730	3.21E-04	-730	2.28E-03	-730	2.75E-03
-720	3.17E-04	-720	2.13E-03	-720	2.60E-03
-710	3.17E-04	-710	2.05E-03	-710	2.51E-03
-700	3.06E-04	-700	1.98E-03	-700	2.36E-03
-690	3.02E-04	-690	1.92E-03	-690	2.29E-03
-680	2.90E-04	-680	1.82E-03	-680	2.19E-03
-670	2.79E-04	-670	1.74E-03	-670	2.11E-03
-660	2.63E-04	-660	1.66E-03	-660	2.03E-03
-650	2.48E-04	-650	1.55E-03	-650	1.93E-03
-640	2.24E-04	-640	1.49E-03	-640	1.86E-03
-630	2.13E-04	-630	1.43E-03	-630	1.81E-03
-620	1.93E-04	-620	1.38E-03	-620	1.76E-03
-610	1.82E-04	-610	1.32E-03	-610	1.72E-03
-600	1.63E-04	-600	1.25E-03	-600	1.66E-03
-590	1.43E-04	-590	1.24E-03	-590	1.63E-03
-580	1.24E-04	-580	1.20E-03	-580	1.58E-03
-570	1.08E-04	-570	1.18E-03	-570	1.55E-03
-560	9.29E-05	-560	1.16E-03	-560	1.53E-03
-550	7.74E-05	-550	1.15E-03	-550	1.52E-03
-540	6.58E-05	-540	1.11E-03	-540	1.52E-03
-530	5.42E-05	-530	1.11E-03	-530	1.49E-03
-520	4.26E-05	-520	1.12E-03	-520	1.51E-03
-510	3.48E-05	-510	1.11E-03	-510	1.49E-03
-500	2.32E-05	-500	1.10E-03	-500	1.51E-03
-490	1.93E-05	-490	1.10E-03	-490	1.49E-03
-480	1.16E-05	-480	1.09E-03	-480	1.47E-03
-470	3.87E-06	-470	1.07E-03	-470	1.44E-03

Continued on next page

Potential mV	Current Density A/cm^2	Potential mV	Current Density A/cm^2	Potential mV	Current Density A/cm^2
-460	1.93E-06	-460	1.06E-03	-460	1.43E-03
-450	7.74E-06	-450	1.01E-03	-450	1.38E-03
-440	1.55E-05	-440	9.64E-04	-440	1.32E-03
-430	2.32E-05	-430	8.86E-04	-430	1.25E-03
-420	3.87E-05	-420	7.35E-04	-420	1.04E-03
-410	4.26E-05	-410	5.73E-04	-410	7.89E-04
-400	5.42E-05	-400	3.72E-04	-400	5.73E-04
-390	6.19E-05	-390	2.48E-04	-390	4.06E-04
-380	6.97E-05	-380	1.78E-04	-380	3.06E-04
-370	7.74E-05	-370	1.43E-04	-370	2.63E-04
-360	8.90E-05	-360	1.04E-04	-360	2.21E-04
-350	9.29E-05	-350	8.13E-05	-350	1.86E-04
-340	9.67E-05	-340	5.80E-05	-340	1.59E-04
-330	1.04E-04	-330	3.87E-05	-330	1.39E-04
-320	1.08E-04	-320	1.93E-05	-320	1.16E-04
-310	1.08E-04	-310	1.16E-05	-310	8.90E-05
-300	1.12E-04	-300	1.55E-05	-300	6.58E-05
-290	1.01E-04	-290	3.10E-05	-290	3.87E-05
-280	9.67E-05	-280	5.03E-05	-280	1.93E-05
-270	9.29E-05	-270	8.13E-05	-270	3.10E-05
-260	9.29E-05	-260	1.12E-04	-260	6.97E-05
-250	9.67E-05	-250	1.51E-04	-250	1.24E-04
-240	8.90E-05	-240	2.13E-04	-240	1.93E-04
-230	8.90E-05	-230	2.75E-04	-230	2.83E-04
-220	8.90E-05	-220	3.60E-04	-220	4.18E-04
-210	9.29E-05	-210	4.72E-04	-210	5.57E-04
-200	9.67E-05	-200	5.73E-04	-200	7.04E-04
-190	9.29E-05	-190	6.19E-04	-190	8.90E-04
-180	8.90E-05	-180	5.11E-04	-180	9.95E-04
-170	8.13E-05	-170	1.82E-04	-170	7.82E-04
-160	8.13E-05	-160	1.28E-04	-160	3.75E-04
-150	8.51E-05	-150	1.39E-04	-150	1.24E-04
-140	8.51E-05	-140	1.47E-04	-140	1.28E-04
-130	8.90E-05	-130	1.70E-04	-130	1.32E-04
-120	9.67E-05	-120	1.93E-04	-120	1.47E-04

Continued on next page

Potential mV	Current Density A/cm^2	Potential mV	Current Density A/cm^2	Potential mV	Current Density A/cm^2
-110	1.04E-04	-110	2.17E-04	-110	1.63E-04
-100	1.12E-04	-100	2.40E-04	-100	1.90E-04
-90	1.28E-04	-90	2.71E-04	-90	2.24E-04
-80	1.43E-04	-80	3.10E-04	-80	2.71E-04
-70	1.66E-04	-70	3.48E-04	-70	3.17E-04
-60	2.01E-04	-60	4.22E-04	-60	3.72E-04
-50	2.40E-04	-50	4.84E-04	-50	4.41E-04
-40	2.86E-04	-40	5.57E-04	-40	5.19E-04
-30	3.56E-04	-30	6.39E-04	-30	6.00E-04
-20	4.22E-04	-20	7.24E-04	-20	6.81E-04
-10	5.11E-04	-10	8.20E-04	-10	7.66E-04
0	5.92E-04	0	8.98E-04	0	8.55E-04
10	7.16E-04	10	1.00E-03	10	9.48E-04
20	8.13E-04	20	1.11E-03	20	1.04E-03
30	9.79E-04	30	1.23E-03	30	1.16E-03
40	1.11E-03	40	1.31E-03	40	1.30E-03
50	1.28E-03	50	1.42E-03	50	1.41E-03
60	1.44E-03	60	1.53E-03	60	1.52E-03
70	1.68E-03	70	1.64E-03	70	1.66E-03
80	1.94E-03	80	1.76E-03	80	1.82E-03
90	2.29E-03	90	1.91E-03	90	1.97E-03
100	2.72E-03	100	2.04E-03	100	2.13E-03
110	3.44E-03	110	2.21E-03	110	2.37E-03
120	4.76E-03	120	2.45E-03	120	2.61E-03
130	6.19E-03	130	2.61E-03	130	2.83E-03
140	7.74E-03	140	2.86E-03	140	3.10E-03
150	9.13E-03	150	3.14E-03	150	3.37E-03
160	1.10E-02	160	3.40E-03	160	3.73E-03
170	1.25E-02	170	3.79E-03	170	4.22E-03
180	1.40E-02	180	4.49E-03	180	4.68E-03
190	1.53E-02	190	5.26E-03	190	5.07E-03
200	1.69E-02	200	5.96E-03	200	5.61E-03
210	1.84E-02	210	7.08E-03	210	6.04E-03
220	1.97E-02	220	8.20E-03	220	6.66E-03
230	2.10E-02	230	9.48E-03	230	7.20E-03

Continued on next page

Potential mV	Current Density A/cm^2	Potential mV	Current Density A/cm^2	Potential mV	Current Density A/cm^2
240	2.23E-02	240	1.08E-02	240	7.86E-03
250	2.38E-02	250	1.27E-02	250	8.67E-03
260	2.50E-02	260	1.44E-02	260	9.52E-03
270	2.61E-02	270	1.55E-02	270	1.08E-02
280	2.75E-02	280	1.70E-02	280	1.20E-02
290	2.86E-02	290	1.80E-02	290	1.35E-02
300	3.01E-02	300	1.94E-02	300	1.51E-02
310	3.15E-02	310	2.07E-02	310	1.61E-02
320	3.28E-02	320	2.18E-02	320	1.74E-02
330	3.41E-02	330	2.31E-02	330	1.87E-02
340	3.54E-02	340	2.45E-02	340	2.05E-02
350	3.67E-02	350	2.59E-02	350	2.17E-02

TABLE B.2: Polarization Data: SS201 in 2.5% sodium carbonate

Velocity: 0 m/s		Velocity: 2.63 m/s		Velocity: 3.93 m/s	
Potential	Current Density	Potential	Current Density	Potential	Current Density
mV	A/cm^2	mV	A/cm^2	mV	A/cm^2
-1000	5.53E-05	-1000	9.56E-04	-1000	1.14E-03
-990	5.03E-05	-990	9.48E-04	-990	1.10E-03
-980	4.68E-05	-980	9.29E-04	-980	1.07E-03
-970	4.41E-05	-970	9.25E-04	-970	1.04E-03
-960	4.10E-05	-960	9.13E-04	-960	1.01E-03
-950	3.95E-05	-950	8.90E-04	-950	9.91E-04
-940	3.72E-05	-940	8.78E-04	-940	9.64E-04
-930	3.56E-05	-930	8.67E-04	-930	9.44E-04
-920	3.37E-05	-920	8.55E-04	-920	9.13E-04
-910	3.21E-05	-910	8.44E-04	-910	8.86E-04
-900	3.10E-05	-900	8.20E-04	-900	8.67E-04
-890	2.94E-05	-890	8.05E-04	-890	8.36E-04
-880	2.83E-05	-880	7.70E-04	-880	8.13E-04
-870	2.71E-05	-870	7.47E-04	-870	7.89E-04
-860	2.67E-05	-860	7.20E-04	-860	7.66E-04
-850	2.48E-05	-850	6.93E-04	-850	7.43E-04
-840	2.36E-05	-840	6.70E-04	-840	7.08E-04
-830	2.32E-05	-830	6.39E-04	-830	6.77E-04
-820	1.35E-05	-820	6.15E-04	-820	6.54E-04
-810	1.28E-05	-810	5.88E-04	-810	6.31E-04
-800	1.24E-05	-800	5.65E-04	-800	6.00E-04
-790	1.16E-05	-790	5.38E-04	-790	5.73E-04
-780	1.16E-05	-780	5.15E-04	-780	5.46E-04
-770	1.12E-05	-770	4.88E-04	-770	5.19E-04
-760	1.08E-05	-760	4.61E-04	-760	4.80E-04
-750	1.01E-05	-750	4.30E-04	-750	4.49E-04
-740	9.67E-06	-740	4.06E-04	-740	4.10E-04
-730	9.29E-06	-730	3.79E-04	-730	3.79E-04
-720	8.51E-06	-720	3.52E-04	-720	3.48E-04
-710	7.74E-06	-710	3.21E-04	-710	3.13E-04
-700	6.97E-06	-700	2.98E-04	-700	2.86E-04
-690	6.58E-06	-690	2.67E-04	-690	2.55E-04

Continued on next page

Potential mV	Current Density A/cm^2	Potential mV	Current Density A/cm^2	Potential mV	Current Density A/cm^2
-680	6.58E-06	-680	2.43E-04	-680	2.21E-04
-670	6.19E-06	-670	2.18E-04	-670	1.96E-04
-660	5.42E-06	-660	1.95E-04	-660	1.74E-04
-650	5.03E-06	-650	1.69E-04	-650	1.51E-04
-640	4.26E-06	-640	1.52E-04	-640	1.28E-04
-630	3.87E-06	-630	1.24E-04	-630	1.10E-04
-620	3.10E-06	-620	1.14E-04	-620	9.17E-05
-610	2.32E-06	-610	9.09E-05	-610	7.28E-05
-600	1.55E-06	-600	7.78E-05	-600	5.73E-05
-590	1.16E-06	-590	6.11E-05	-590	4.26E-05
-580	7.74E-07	-580	4.53E-05	-580	3.21E-05
-570	7.74E-07	-570	3.33E-05	-570	2.13E-05
-560	8.51E-07	-560	2.44E-05	-560	1.55E-05
-550	5.42E-07	-550	1.90E-05	-550	1.20E-05
-540	1.16E-07	-540	1.43E-05	-540	8.51E-06
-530	3.87E-08	-530	1.12E-05	-530	5.80E-06
-520	3.10E-07	-520	8.51E-06	-520	3.87E-06
-510	8.13E-07	-510	6.97E-06	-510	3.10E-06
-500	1.28E-06	-500	6.19E-06	-500	2.71E-06
-490	1.78E-06	-490	5.03E-06	-490	2.32E-06
-480	2.32E-06	-480	3.87E-06	-480	1.93E-06
-470	2.94E-06	-470	3.10E-06	-470	1.55E-06
-460	3.41E-06	-460	2.32E-06	-460	1.16E-06
-450	3.75E-06	-450	1.55E-06	-450	7.74E-07
-440	4.41E-06	-440	7.74E-07	-440	3.87E-07
-430	4.95E-06	-430	3.87E-07	-430	3.87E-06
-420	5.61E-06	-420	1.93E-06	-420	6.19E-06
-410	6.58E-06	-410	3.87E-06	-410	7.35E-06
-400	8.13E-06	-400	5.80E-06	-400	8.90E-06
-390	8.13E-06	-390	6.97E-06	-390	9.67E-06
-380	8.51E-06	-380	8.13E-06	-380	1.12E-05
-370	8.90E-06	-370	1.04E-05	-370	1.20E-05
-360	9.29E-06	-360	1.16E-05	-360	1.33E-05
-350	9.67E-06	-350	1.12E-05	-350	1.50E-05
-340	1.04E-05	-340	1.24E-05	-340	1.59E-05

Continued on next page

Potential mV	Current Density A/cm^2	Potential mV	Current Density A/cm^2	Potential mV	Current Density A/cm^2
-330	1.08E-05	-330	1.32E-05	-330	1.59E-05
-320	1.12E-05	-320	1.28E-05	-320	1.59E-05
-310	1.08E-05	-310	1.35E-05	-310	1.86E-05
-300	1.12E-05	-300	1.32E-05	-300	1.36E-05
-290	8.13E-06	-290	1.16E-05	-290	1.36E-05
-280	8.51E-06	-280	1.16E-05	-280	1.36E-05
-270	6.97E-06	-270	1.16E-05	-270	1.36E-05
-260	6.58E-06	-260	1.04E-05	-260	1.36E-05
-250	6.19E-06	-250	9.67E-06	-250	1.39E-05
-240	6.19E-06	-240	1.01E-05	-240	1.35E-05
-230	6.19E-06	-230	9.29E-06	-230	1.35E-05
-220	6.19E-06	-220	9.67E-06	-220	1.36E-05
-210	6.19E-06	-210	9.67E-06	-210	1.40E-05
-200	6.19E-06	-200	9.29E-06	-200	1.55E-05
-190	6.58E-06	-190	9.67E-06	-190	1.56E-05
-180	6.97E-06	-180	1.01E-05	-180	1.58E-05
-170	6.97E-06	-170	1.08E-05	-170	1.58E-05
-160	6.97E-06	-160	1.08E-05	-160	1.70E-05
-150	7.35E-06	-150	1.04E-05	-150	1.76E-05
-140	7.74E-06	-140	1.12E-05	-140	1.74E-05
-130	7.74E-06	-130	1.12E-05	-130	1.78E-05
-120	8.13E-06	-120	1.16E-05	-120	1.93E-05
-110	8.13E-06	-110	1.20E-05	-110	1.99E-05
-100	7.74E-06	-100	1.24E-05	-100	2.05E-05
-90	8.13E-06	-90	1.20E-05	-90	2.10E-05
-80	8.13E-06	-80	1.24E-05	-80	2.16E-05
-70	7.74E-06	-70	1.28E-05	-70	2.25E-05
-60	7.74E-06	-60	1.32E-05	-60	2.29E-05
-50	6.58E-06	-50	1.32E-05	-50	2.32E-05
-40	5.80E-06	-40	1.32E-05	-40	2.35E-05
-30	6.97E-06	-30	1.35E-05	-30	2.42E-05
-20	6.97E-06	-20	1.35E-05	-20	2.42E-05
-10	6.19E-06	-10	1.39E-05	-10	2.44E-05
0	6.58E-06	0	1.39E-05	0	2.47E-05
10	6.58E-06	10	1.35E-05	10	2.48E-05

Continued on next page

Potential mV	Current Density A/cm^2	Potential mV	Current Density A/cm^2	Potential mV	Current Density A/cm^2
20	6.58E-06	20	1.35E-05	20	2.48E-05
30	6.97E-06	30	1.35E-05	30	2.50E-05
40	7.35E-06	40	1.43E-05	40	2.52E-05
50	7.35E-06	50	1.47E-05	50	2.53E-05
60	7.74E-06	60	1.51E-05	60	2.58E-05
70	7.74E-06	70	1.55E-05	70	2.67E-05
80	8.13E-06	80	1.59E-05	80	2.48E-05
90	8.51E-06	90	1.63E-05	90	2.55E-05
100	9.29E-06	100	1.70E-05	100	2.59E-05
110	9.29E-06	110	1.82E-05	110	2.71E-05
120	9.67E-06	120	1.82E-05	120	2.83E-05
130	1.01E-05	130	1.82E-05	130	2.86E-05
140	1.08E-05	140	1.97E-05	140	2.94E-05
150	1.16E-05	150	2.17E-05	150	3.02E-05
160	1.28E-05	160	2.32E-05	160	3.25E-05
170	1.35E-05	170	2.52E-05	170	3.10E-05
180	1.47E-05	180	2.67E-05	180	3.48E-05
190	1.66E-05	190	2.86E-05	190	3.64E-05
200	1.78E-05	200	3.13E-05	200	3.75E-05
210	1.90E-05	210	3.52E-05	210	3.95E-05
220	2.01E-05	220	3.83E-05	220	4.14E-05
230	2.24E-05	230	4.02E-05	230	4.26E-05
240	2.36E-05	240	4.30E-05	240	4.64E-05
250	2.55E-05	250	4.45E-05	250	4.88E-05
260	2.79E-05	260	4.80E-05	260	5.19E-05
270	3.02E-05	270	4.88E-05	270	5.34E-05
280	3.33E-05	280	5.07E-05	280	5.46E-05
290	3.33E-05	290	5.22E-05	290	5.46E-05
300	3.37E-05	300	5.42E-05	300	5.42E-05
310	3.33E-05	310	5.46E-05	310	5.50E-05
320	3.52E-05	320	5.50E-05	320	5.53E-05
330	3.72E-05	330	5.50E-05	330	5.53E-05
340	3.95E-05	340	5.53E-05	340	5.42E-05
350	3.99E-05	350	5.46E-05	350	5.42E-05
360	4.10E-05	360	5.46E-05	360	5.11E-05

Continued on next page

Potential mV	Current Density A/cm^2	Potential mV	Current Density A/cm^2	Potential mV	Current Density A/cm^2
370	4.18E-05	370	5.50E-05	370	5.07E-05
380	4.30E-05	380	5.42E-05	380	5.03E-05
390	4.33E-05	390	5.38E-05	390	4.84E-05
400	4.45E-05	400	5.34E-05	400	4.76E-05
410	4.26E-05	410	5.30E-05	410	4.68E-05
420	4.26E-05	420	5.03E-05	420	4.49E-05
430	4.14E-05	430	4.88E-05	430	4.30E-05
440	3.99E-05	440	4.76E-05	440	4.18E-05
450	4.06E-05	450	4.80E-05	450	4.10E-05
460	4.14E-05	460	4.72E-05	460	4.10E-05
470	4.22E-05	470	4.84E-05	470	4.06E-05
480	4.14E-05	480	4.80E-05	480	4.06E-05
490	4.30E-05	490	4.88E-05	490	4.06E-05
500	4.37E-05	500	4.99E-05	500	4.02E-05
510	4.30E-05	510	5.07E-05	510	4.02E-05
520	4.26E-05	520	5.07E-05	520	3.95E-05
530	4.45E-05	530	5.11E-05	530	3.95E-05
540	4.45E-05	540	5.15E-05	540	3.99E-05
550	4.45E-05	550	5.15E-05	550	4.10E-05
560	4.33E-05	560	5.38E-05	560	4.18E-05
570	4.57E-05	570	5.50E-05	570	4.26E-05
580	4.91E-05	580	5.73E-05	580	4.26E-05
590	5.26E-05	590	5.92E-05	590	4.45E-05
600	5.61E-05	600	6.15E-05	600	4.61E-05
610	6.23E-05	610	6.46E-05	610	4.88E-05
620	6.66E-05	620	7.00E-05	620	4.95E-05
630	7.12E-05	630	7.82E-05	630	5.42E-05
640	8.24E-05	640	8.63E-05	640	5.80E-05
650	1.10E-04	650	1.04E-04	650	6.66E-05
660	1.44E-04	660	1.37E-04	660	8.51E-05
670	2.14E-04	670	2.05E-04	670	1.22E-04
680	3.80E-04	680	3.15E-04	680	1.92E-04
690	6.31E-04	690	6.08E-04	690	3.25E-04
700	1.03E-03	700	9.91E-04	700	5.61E-04
710	1.62E-03	710	1.53E-03	710	8.63E-04

Continued on next page

Potential mV	Current Density A/cm^2	Potential mV	Current Density A/cm^2	Potential mV	Current Density A/cm^2
720	2.37E-03	720	2.51E-03	720	1.16E-03
730	3.29E-03	730	3.17E-03	730	1.55E-03
740	4.18E-03	740	4.21E-03	740	2.07E-03
750	5.19E-03	750	5.07E-03	750	2.51E-03
760	6.23E-03	760	6.00E-03	760	3.03E-03
770	7.00E-03	770	6.93E-03	770	3.56E-03
780	8.24E-03	780	8.05E-03	780	3.95E-03
790	9.09E-03	790	8.94E-03	790	4.33E-03
800	1.01E-02	800	1.02E-02	800	4.76E-03
810	1.14E-02	810	1.12E-02	810	5.22E-03
820	1.23E-02	820	1.20E-02	820	5.65E-03
830	1.35E-02	830	1.31E-02	830	6.42E-03
840	1.46E-02	840	1.42E-02	840	7.20E-03
850	1.57E-02	850	1.52E-02	850	8.05E-03
860	1.68E-02	860	1.65E-02	860	8.67E-03
870	1.79E-02	870	1.75E-02	870	9.29E-03
880	1.91E-02	880	1.87E-02	880	1.00E-02
890	1.99E-02	890	1.98E-02	890	1.08E-02
900	2.12E-02	900	2.11E-02	900	1.17E-02
910	2.26E-02	910	2.22E-02	910	1.28E-02
920	2.40E-02	920	2.33E-02	920	1.35E-02
930	2.50E-02	930	2.44E-02	930	1.50E-02
940	2.60E-02	940	2.54E-02	940	1.65E-02
950	2.73E-02	950	2.64E-02	950	1.70E-02
960	2.86E-02	960	2.76E-02	960	1.81E-02
970	2.95E-02	970	2.88E-02	970	1.89E-02
980	3.10E-02	980	3.00E-02	980	2.05E-02
990	3.19E-02	990	3.12E-02	990	2.09E-02
1000	3.30E-02	1000	3.26E-02	1000	2.24E-02

TABLE B.3: Polarization Data: SS201 in 5.0% sodium carbonate

Velocity: 0 m/s		Velocity: 2.63 m/s		Velocity: 3.93 m/s	
Potential	Current Density	Potential	Current Density	Potential	Current Density
mV	A/cm^2	mV	A/cm^2	mV	A/cm^2
-1000	1.24E-04	-1000	7.12E-04	-1000	9.13E-04
-990	1.04E-04	-990	7.04E-04	-990	8.55E-04
-980	9.09E-05	-980	6.77E-04	-980	8.20E-04
-970	7.89E-05	-970	6.62E-04	-970	7.93E-04
-960	6.89E-05	-960	6.35E-04	-960	7.59E-04
-950	6.00E-05	-950	6.19E-04	-950	7.24E-04
-940	5.34E-05	-940	5.96E-04	-940	6.93E-04
-930	4.91E-05	-930	5.73E-04	-930	6.58E-04
-920	4.49E-05	-920	5.53E-04	-920	6.27E-04
-910	4.22E-05	-910	5.26E-04	-910	6.00E-04
-900	3.99E-05	-900	5.07E-04	-900	5.69E-04
-890	3.72E-05	-890	4.84E-04	-890	5.30E-04
-880	3.44E-05	-880	4.57E-04	-880	5.03E-04
-870	3.29E-05	-870	4.18E-04	-870	4.68E-04
-860	3.10E-05	-860	3.87E-04	-860	4.37E-04
-850	2.83E-05	-850	3.68E-04	-850	4.10E-04
-840	2.63E-05	-840	3.41E-04	-840	3.87E-04
-830	2.55E-05	-830	3.21E-04	-830	3.68E-04
-820	2.32E-05	-820	3.02E-04	-820	3.48E-04
-810	2.21E-05	-810	2.83E-04	-810	3.25E-04
-800	2.05E-05	-800	2.55E-04	-800	3.10E-04
-790	1.93E-05	-790	2.50E-04	-790	2.86E-04
-780	1.78E-05	-780	2.41E-04	-780	2.71E-04
-770	1.66E-05	-770	2.26E-04	-770	2.52E-04
-760	1.51E-05	-760	2.12E-04	-760	2.32E-04
-750	1.39E-05	-750	1.96E-04	-750	2.17E-04
-740	1.24E-05	-740	1.82E-04	-740	2.01E-04
-730	1.12E-05	-730	1.68E-04	-730	1.82E-04
-720	1.01E-05	-720	1.57E-04	-720	1.66E-04
-710	8.90E-06	-710	1.46E-04	-710	1.55E-04
-700	6.97E-06	-700	1.32E-04	-700	1.43E-04
-690	5.42E-06	-690	1.22E-04	-690	1.28E-04

Continued on next page

Potential mV	Current Density A/cm^2	Potential mV	Current Density A/cm^2	Potential mV	Current Density A/cm^2
-680	2.71E-06	-680	1.11E-04	-680	1.16E-04
-670	1.93E-06	-670	1.01E-04	-670	1.08E-04
-660	3.87E-07	-660	9.13E-05	-660	9.29E-05
-650	1.93E-06	-650	8.28E-05	-650	8.51E-05
-640	3.87E-06	-640	7.28E-05	-640	7.74E-05
-630	5.42E-06	-630	6.42E-05	-630	6.97E-05
-620	7.35E-06	-620	5.57E-05	-620	6.19E-05
-610	9.29E-06	-610	4.64E-05	-610	5.42E-05
-600	9.67E-06	-600	3.87E-05	-600	4.26E-05
-590	1.01E-05	-590	3.21E-05	-590	3.87E-05
-580	1.08E-05	-580	2.67E-05	-580	3.10E-05
-570	1.16E-05	-570	2.01E-05	-570	2.32E-05
-560	1.24E-05	-560	1.55E-05	-560	1.93E-05
-550	1.32E-05	-550	9.67E-06	-550	1.55E-05
-540	1.20E-05	-540	3.48E-06	-540	1.16E-05
-530	1.63E-05	-530	2.32E-06	-530	7.74E-06
-520	1.70E-05	-520	1.55E-06	-520	3.87E-06
-510	1.66E-05	-510	1.16E-06	-510	2.71E-06
-500	1.59E-05	-500	5.03E-06	-500	2.32E-06
-490	1.66E-05	-490	6.97E-06	-490	3.87E-06
-480	1.82E-05	-480	1.04E-05	-480	7.74E-06
-470	2.09E-05	-470	1.32E-05	-470	1.16E-05
-460	2.36E-05	-460	1.93E-05	-460	1.93E-05
-450	2.55E-05	-450	2.63E-05	-450	2.32E-05
-440	2.94E-05	-440	3.13E-05	-440	3.10E-05
-430	3.10E-05	-430	3.56E-05	-430	3.48E-05
-420	3.79E-05	-420	4.14E-05	-420	3.87E-05
-410	4.22E-05	-410	5.03E-05	-410	5.03E-05
-400	4.30E-05	-400	5.22E-05	-400	5.80E-05
-390	4.49E-05	-390	5.80E-05	-390	5.80E-05
-380	4.88E-05	-380	6.35E-05	-380	6.19E-05
-370	5.07E-05	-370	6.50E-05	-370	6.58E-05
-360	5.22E-05	-360	6.46E-05	-360	6.58E-05
-350	5.11E-05	-350	6.35E-05	-350	5.80E-05
-340	4.68E-05	-340	4.61E-05	-340	3.87E-05

Continued on next page

Potential mV	Current Density A/cm^2	Potential mV	Current Density A/cm^2	Potential mV	Current Density A/cm^2
-330	4.26E-05	-330	4.68E-05	-330	3.87E-05
-320	3.99E-05	-320	4.33E-05	-320	3.48E-05
-310	3.87E-05	-310	4.22E-05	-310	3.10E-05
-300	3.68E-05	-300	4.10E-05	-300	3.10E-05
-290	3.72E-05	-290	3.83E-05	-290	2.71E-05
-280	3.72E-05	-280	3.87E-05	-280	2.71E-05
-270	3.83E-05	-270	3.79E-05	-270	3.10E-05
-260	3.87E-05	-260	3.99E-05	-260	3.10E-05
-250	3.87E-05	-250	4.02E-05	-250	3.10E-05
-240	4.02E-05	-240	3.99E-05	-240	3.10E-05
-230	4.14E-05	-230	3.99E-05	-230	3.48E-05
-220	4.22E-05	-220	4.22E-05	-220	3.48E-05
-210	4.41E-05	-210	4.37E-05	-210	3.48E-05
-200	4.37E-05	-200	4.68E-05	-200	3.48E-05
-190	4.45E-05	-190	4.41E-05	-190	3.87E-05
-180	4.61E-05	-180	4.80E-05	-180	3.87E-05
-170	4.37E-05	-170	4.99E-05	-170	3.87E-05
-160	4.41E-05	-160	5.15E-05	-160	3.87E-05
-150	4.45E-05	-150	5.07E-05	-150	4.26E-05
-140	4.53E-05	-140	5.11E-05	-140	5.03E-05
-130	4.53E-05	-130	5.26E-05	-130	5.42E-05
-120	4.57E-05	-120	5.26E-05	-120	5.42E-05
-110	4.64E-05	-110	4.80E-05	-110	5.42E-05
-100	4.61E-05	-100	4.22E-05	-100	3.87E-05
-90	4.45E-05	-90	4.02E-05	-90	3.87E-05
-80	4.53E-05	-80	3.72E-05	-80	3.48E-05
-70	4.53E-05	-70	3.48E-05	-70	3.87E-05
-60	4.49E-05	-60	3.41E-05	-60	3.10E-05
-50	4.45E-05	-50	3.21E-05	-50	3.10E-05
-40	4.45E-05	-40	3.17E-05	-40	3.10E-05
-30	3.87E-05	-30	3.21E-05	-30	3.10E-05
-20	3.87E-05	-20	3.29E-05	-20	3.48E-05
-10	3.87E-05	-10	3.37E-05	-10	3.48E-05
0	3.87E-05	0	3.33E-05	0	3.48E-05
10	3.87E-05	10	3.41E-05	10	3.48E-05

Continued on next page

Potential mV	Current Density A/cm^2	Potential mV	Current Density A/cm^2	Potential mV	Current Density A/cm^2
20	3.87E-05	20	3.56E-05	20	3.10E-05
30	3.99E-05	30	3.75E-05	30	3.48E-05
40	3.99E-05	40	3.83E-05	40	3.48E-05
50	4.10E-05	50	4.14E-05	50	3.87E-05
60	4.10E-05	60	4.14E-05	60	3.87E-05
70	4.10E-05	70	4.18E-05	70	3.87E-05
80	4.10E-05	80	4.37E-05	80	3.87E-05
90	4.10E-05	90	4.68E-05	90	4.26E-05
100	4.10E-05	100	4.72E-05	100	3.87E-05
110	4.22E-05	110	4.88E-05	110	4.26E-05
120	4.22E-05	120	5.11E-05	120	4.64E-05
130	4.02E-05	130	5.15E-05	130	4.64E-05
140	4.06E-05	140	5.46E-05	140	5.03E-05
150	4.22E-05	150	5.73E-05	150	5.03E-05
160	4.26E-05	160	6.04E-05	160	5.42E-05
170	4.45E-05	170	6.15E-05	170	5.80E-05
180	4.37E-05	180	6.35E-05	180	5.80E-05
190	4.37E-05	190	6.89E-05	190	6.19E-05
200	4.61E-05	200	7.43E-05	200	6.58E-05
210	4.61E-05	210	7.82E-05	210	6.58E-05
220	4.80E-05	220	8.40E-05	220	6.97E-05
230	5.03E-05	230	8.90E-05	230	7.74E-05
240	5.42E-05	240	9.37E-05	240	7.74E-05
250	5.61E-05	250	9.98E-05	250	8.13E-05
260	5.80E-05	260	1.02E-04	260	8.51E-05
270	6.19E-05	270	1.06E-04	270	9.67E-05
280	6.81E-05	280	1.09E-04	280	1.04E-04
290	6.97E-05	290	1.12E-04	290	1.04E-04
300	6.97E-05	300	1.13E-04	300	1.12E-04
310	7.39E-05	310	1.13E-04	310	1.08E-04
320	7.39E-05	320	1.13E-04	320	1.16E-04
330	7.59E-05	330	1.12E-04	330	1.16E-04
340	7.78E-05	340	1.13E-04	340	1.16E-04
350	7.97E-05	350	1.15E-04	350	1.20E-04
360	8.09E-05	360	1.16E-04	360	1.24E-04

Continued on next page

Potential mV	Current Density A/cm^2	Potential mV	Current Density A/cm^2	Potential mV	Current Density A/cm^2
370	8.28E-05	370	1.15E-04	370	1.24E-04
380	8.40E-05	380	1.13E-04	380	1.24E-04
390	8.44E-05	390	1.14E-04	390	1.24E-04
400	8.67E-05	400	1.14E-04	400	1.24E-04
410	8.67E-05	410	1.11E-04	410	1.20E-04
420	8.71E-05	420	1.09E-04	420	1.24E-04
430	8.67E-05	430	1.08E-04	430	1.20E-04
440	8.71E-05	440	1.06E-04	440	1.12E-04
450	8.55E-05	450	1.06E-04	450	1.12E-04
460	8.51E-05	460	1.08E-04	460	1.12E-04
470	8.44E-05	470	1.13E-04	470	1.12E-04
480	8.44E-05	480	1.15E-04	480	1.16E-04
490	8.59E-05	490	1.14E-04	490	1.20E-04
500	8.90E-05	500	1.14E-04	500	1.24E-04
510	9.09E-05	510	1.16E-04	510	1.28E-04
520	9.13E-05	520	1.14E-04	520	1.32E-04
530	9.21E-05	530	1.13E-04	530	1.32E-04
540	9.29E-05	540	1.22E-04	540	1.35E-04
550	9.48E-05	550	1.25E-04	550	1.39E-04
560	9.37E-05	560	1.26E-04	560	1.47E-04
570	9.98E-05	570	1.30E-04	570	1.47E-04
580	9.83E-05	580	1.31E-04	580	1.43E-04
590	9.98E-05	590	1.33E-04	590	1.47E-04
600	1.04E-04	600	1.35E-04	600	1.55E-04
610	1.04E-04	610	1.34E-04	610	1.55E-04
620	1.07E-04	620	1.41E-04	620	1.55E-04
630	1.13E-04	630	1.48E-04	630	1.55E-04
640	1.13E-04	640	1.52E-04	640	1.70E-04
650	1.18E-04	650	1.61E-04	650	1.78E-04
660	1.27E-04	660	1.78E-04	660	1.90E-04
670	1.40E-04	670	1.99E-04	670	2.09E-04
680	1.60E-04	680	2.40E-04	680	2.52E-04
690	1.94E-04	690	3.20E-04	690	3.02E-04
700	2.55E-04	700	4.13E-04	700	4.88E-04
710	3.32E-04	710	7.20E-04	710	7.97E-04

Continued on next page

Potential mV	Current Density A/cm^2	Potential mV	Current Density A/cm^2	Potential mV	Current Density A/cm^2
720	4.72E-04	720	1.16E-03	720	1.39E-03
730	6.89E-04	730	1.78E-03	730	2.22E-03
740	9.25E-04	740	2.90E-03	740	3.12E-03
750	1.28E-03	750	3.78E-03	750	4.02E-03
760	1.67E-03	760	4.88E-03	760	5.30E-03
770	1.98E-03	770	5.80E-03	770	6.15E-03
780	2.26E-03	780	6.77E-03	780	7.12E-03
790	2.63E-03	790	7.82E-03	790	8.36E-03
800	3.25E-03	800	9.13E-03	800	9.40E-03
810	3.69E-03	810	1.03E-02	810	1.08E-02
820	4.13E-03	820	1.14E-02	820	1.19E-02
830	4.64E-03	830	1.24E-02	830	1.30E-02
840	5.19E-03	840	1.35E-02	840	1.45E-02
850	5.80E-03	850	1.49E-02	850	1.56E-02
860	6.46E-03	860	1.58E-02	860	1.70E-02
870	7.35E-03	870	1.70E-02	870	1.80E-02
880	8.17E-03	880	1.83E-02	880	1.92E-02
890	9.13E-03	890	1.96E-02	890	2.05E-02
900	1.02E-02	900	2.08E-02	900	2.16E-02
910	1.13E-02	910	2.20E-02	910	2.29E-02
920	1.23E-02	920	2.33E-02	920	2.41E-02
930	1.34E-02	930	2.45E-02	930	2.55E-02
940	1.43E-02	940	2.57E-02	940	2.69E-02
950	1.55E-02	950	2.68E-02	950	2.82E-02
960	1.66E-02	960	2.82E-02	960	2.96E-02
970	1.74E-02	970	2.93E-02	970	3.08E-02
980	1.89E-02	980	3.03E-02	980	3.20E-02
990	2.00E-02	990	3.17E-02	990	3.30E-02
1000	2.12E-02	1000	3.31E-02	1000	3.48E-02

TABLE B.4: Polarization Data: SS201 in $FeSO_4$

Velocity: 0 m/s		Velocity: 2.63 m/s		Velocity: 3.93 m/s	
Potential	Current Density	Potential	Current Density	Potential	Current Density
mV	A/cm^2	mV	A/cm^2	mV	A/cm^2
-1000	2.01E-04	-1000	4.68E-03	-1000	5.42E-03
-990	1.93E-04	-990	4.49E-03	-990	5.30E-03
-980	1.84E-04	-980	4.37E-03	-980	5.22E-03
-970	1.72E-04	-970	4.10E-03	-970	5.22E-03
-960	1.63E-04	-960	4.02E-03	-960	5.11E-03
-950	1.58E-04	-950	4.06E-03	-950	5.07E-03
-940	1.52E-04	-940	4.02E-03	-940	4.91E-03
-930	1.49E-04	-930	3.91E-03	-930	4.84E-03
-920	1.47E-04	-920	3.87E-03	-920	4.76E-03
-910	1.45E-04	-910	3.72E-03	-910	4.64E-03
-900	1.39E-04	-900	3.64E-03	-900	4.61E-03
-890	1.34E-04	-890	3.56E-03	-890	4.57E-03
-880	1.27E-04	-880	3.41E-03	-880	4.41E-03
-870	1.23E-04	-870	3.29E-03	-870	4.33E-03
-860	1.18E-04	-860	3.25E-03	-860	4.26E-03
-850	1.16E-04	-850	3.21E-03	-850	4.18E-03
-840	1.13E-04	-840	3.17E-03	-840	4.06E-03
-830	1.10E-04	-830	3.10E-03	-830	4.02E-03
-820	1.05E-04	-820	3.06E-03	-820	3.95E-03
-810	1.01E-04	-810	3.02E-03	-810	3.91E-03
-800	9.60E-05	-800	2.90E-03	-800	3.87E-03
-790	8.94E-05	-790	2.88E-03	-790	3.75E-03
-780	8.32E-05	-780	2.84E-03	-780	3.72E-03
-770	7.82E-05	-770	2.79E-03	-770	3.64E-03
-760	7.20E-05	-760	2.74E-03	-760	3.60E-03
-750	6.62E-05	-750	2.66E-03	-750	3.52E-03
-740	5.80E-05	-740	2.60E-03	-740	3.48E-03
-730	5.19E-05	-730	2.57E-03	-730	3.44E-03
-720	4.72E-05	-720	2.53E-03	-720	3.41E-03
-710	4.30E-05	-710	2.51E-03	-710	3.37E-03
-700	4.06E-05	-700	2.46E-03	-700	3.33E-03
-690	3.95E-05	-690	2.40E-03	-690	3.29E-03

Continued on next page

Potential mV	Current Density A/cm^2	Potential mV	Current Density A/cm^2	Potential mV	Current Density A/cm^2
-680	3.72E-05	-680	2.36E-03	-680	3.21E-03
-670	3.64E-05	-670	2.32E-03	-670	3.17E-03
-660	3.37E-05	-660	2.30E-03	-660	3.13E-03
-650	3.21E-05	-650	2.27E-03	-650	3.21E-03
-640	3.02E-05	-640	2.24E-03	-640	3.17E-03
-630	2.79E-05	-630	2.20E-03	-630	3.14E-03
-620	2.63E-05	-620	2.17E-03	-620	3.10E-03
-610	2.48E-05	-610	2.17E-03	-610	3.06E-03
-600	2.21E-05	-600	2.14E-03	-600	3.03E-03
-590	2.01E-05	-590	2.11E-03	-590	2.98E-03
-580	1.82E-05	-580	2.09E-03	-580	2.96E-03
-570	1.59E-05	-570	2.08E-03	-570	2.92E-03
-560	1.39E-05	-560	2.06E-03	-560	2.88E-03
-550	1.16E-05	-550	1.98E-03	-550	2.80E-03
-540	9.67E-06	-540	1.92E-03	-540	2.69E-03
-530	8.90E-06	-530	1.90E-03	-530	2.59E-03
-520	8.13E-06	-520	1.87E-03	-520	2.55E-03
-510	4.26E-06	-510	1.84E-03	-510	2.44E-03
-500	3.87E-07	-500	1.80E-03	-500	2.36E-03
-490	7.74E-07	-490	1.74E-03	-490	2.27E-03
-480	1.93E-06	-480	1.69E-03	-480	2.13E-03
-470	3.48E-06	-470	1.62E-03	-470	2.07E-03
-460	4.64E-06	-460	1.53E-03	-460	1.90E-03
-450	5.80E-06	-450	1.43E-03	-450	1.82E-03
-440	6.97E-06	-440	1.30E-03	-440	1.70E-03
-430	7.74E-06	-430	1.20E-03	-430	1.59E-03
-420	8.51E-06	-420	1.14E-03	-420	1.49E-03
-410	9.67E-06	-410	1.08E-03	-410	1.37E-03
-400	1.04E-05	-400	1.03E-03	-400	1.28E-03
-390	1.20E-05	-390	8.90E-04	-390	1.22E-03
-380	1.32E-05	-380	8.44E-04	-380	1.10E-03
-370	1.32E-05	-370	7.31E-04	-370	1.03E-03
-360	1.20E-05	-360	6.77E-04	-360	9.37E-04
-350	1.20E-05	-350	6.19E-04	-350	8.63E-04
-340	1.24E-05	-340	5.42E-04	-340	7.74E-04

Continued on next page

Potential mV	Current Density A/cm^2	Potential mV	Current Density A/cm^2	Potential mV	Current Density A/cm^2
-330	1.20E-05	-330	4.95E-04	-330	7.12E-04
-320	1.20E-05	-320	4.26E-04	-320	6.58E-04
-310	1.16E-05	-310	3.64E-04	-310	6.11E-04
-300	1.16E-05	-300	3.21E-04	-300	5.34E-04
-290	1.20E-05	-290	3.06E-04	-290	4.84E-04
-280	1.39E-05	-280	2.59E-04	-280	4.41E-04
-270	1.39E-05	-270	2.05E-04	-270	3.87E-04
-260	1.55E-05	-260	1.78E-04	-260	3.52E-04
-250	1.59E-05	-250	1.55E-04	-250	3.10E-04
-240	1.63E-05	-240	1.24E-04	-240	2.75E-04
-230	1.74E-05	-230	9.29E-05	-230	2.52E-04
-220	1.90E-05	-220	7.74E-05	-220	2.13E-04
-210	2.01E-05	-210	5.03E-05	-210	1.66E-04
-200	2.17E-05	-200	3.87E-05	-200	1.39E-04
-190	2.32E-05	-190	1.93E-05	-190	1.04E-04
-180	2.40E-05	-180	2.71E-05	-180	5.80E-05
-170	2.40E-05	-170	3.87E-05	-170	3.87E-05
-160	2.40E-05	-160	7.74E-05	-160	5.80E-05
-150	2.36E-05	-150	1.16E-04	-150	9.67E-05
-140	2.40E-05	-140	2.13E-04	-140	1.55E-04
-130	2.48E-05	-130	3.64E-04	-130	2.75E-04
-120	2.75E-05	-120	4.99E-04	-120	4.10E-04
-110	2.75E-05	-110	6.39E-04	-110	5.80E-04
-100	2.83E-05	-100	7.74E-04	-100	7.35E-04
-90	3.13E-05	-90	6.62E-04	-90	8.05E-04
-80	3.33E-05	-80	3.02E-04	-80	7.04E-04
-70	3.48E-05	-70	2.63E-04	-70	6.08E-04
-60	3.68E-05	-60	2.36E-04	-60	5.22E-04
-50	3.95E-05	-50	2.24E-04	-50	4.22E-04
-40	4.06E-05	-40	2.17E-04	-40	2.75E-04
-30	4.41E-05	-30	2.09E-04	-30	2.44E-04
-20	4.76E-05	-20	2.01E-04	-20	2.36E-04
-10	4.95E-05	-10	1.97E-04	-10	2.32E-04
0	5.07E-05	0	1.82E-04	0	2.24E-04
10	5.19E-05	10	1.66E-04	10	2.17E-04

Continued on next page

Potential mV	Current Density A/cm^2	Potential mV	Current Density A/cm^2	Potential mV	Current Density A/cm^2
20	5.42E-05	20	1.51E-04	20	2.01E-04
30	5.77E-05	30	1.39E-04	30	1.90E-04
40	6.00E-05	40	1.32E-04	40	1.82E-04
50	6.27E-05	50	1.28E-04	50	1.74E-04
60	6.62E-05	60	1.28E-04	60	1.63E-04
70	7.00E-05	70	1.20E-04	70	1.59E-04
80	7.35E-05	80	1.16E-04	80	1.55E-04
90	7.70E-05	90	1.16E-04	90	1.51E-04
100	8.09E-05	100	1.20E-04	100	1.43E-04
110	8.48E-05	110	1.20E-04	110	1.39E-04
120	8.90E-05	120	1.20E-04	120	1.35E-04
130	9.33E-05	130	1.24E-04	130	1.35E-04
140	9.71E-05	140	1.28E-04	140	1.35E-04
150	1.01E-04	150	1.28E-04	150	1.35E-04
160	1.06E-04	160	1.32E-04	160	1.39E-04
170	1.11E-04	170	1.35E-04	170	1.43E-04
180	1.15E-04	180	1.39E-04	180	1.47E-04
190	1.19E-04	190	1.43E-04	190	1.51E-04
200	1.23E-04	200	1.47E-04	200	1.55E-04
210	1.28E-04	210	1.51E-04	210	1.55E-04
220	1.32E-04	220	1.55E-04	220	1.59E-04
230	1.36E-04	230	1.63E-04	230	1.63E-04
240	1.40E-04	240	1.66E-04	240	1.66E-04
250	1.45E-04	250	1.70E-04	250	1.70E-04
260	1.49E-04	260	1.74E-04	260	1.74E-04
270	1.54E-04	270	1.78E-04	270	1.82E-04
280	1.58E-04	280	1.82E-04	280	1.82E-04
290	1.63E-04	290	1.90E-04	290	1.90E-04
300	1.68E-04	300	1.93E-04	300	1.93E-04
310	1.72E-04	310	1.97E-04	310	2.01E-04
320	1.77E-04	320	2.01E-04	320	2.05E-04
330	1.82E-04	330	2.09E-04	330	2.09E-04
340	1.86E-04	340	2.13E-04	340	2.13E-04
350	1.91E-04	350	2.17E-04	350	2.17E-04
360	1.96E-04	360	2.21E-04	360	2.21E-04

Continued on next page

Potential mV	Current Density A/cm^2	Potential mV	Current Density A/cm^2	Potential mV	Current Density A/cm^2
370	2.00E-04	370	2.24E-04	370	2.28E-04
380	2.05E-04	380	2.32E-04	380	2.32E-04
390	2.10E-04	390	2.36E-04	390	2.36E-04
400	2.15E-04	400	2.40E-04	400	2.40E-04
410	2.19E-04	410	2.44E-04	410	2.44E-04
420	2.23E-04	420	2.48E-04	420	2.48E-04
430	2.28E-04	430	2.52E-04	430	2.55E-04
440	2.34E-04	440	2.55E-04	440	2.59E-04
450	2.38E-04	450	2.63E-04	450	2.63E-04
460	2.43E-04	460	2.71E-04	460	2.67E-04
470	2.49E-04	470	2.71E-04	470	2.75E-04
480	2.55E-04	480	2.75E-04	480	2.83E-04
490	2.60E-04	490	2.79E-04	490	2.86E-04
500	2.66E-04	500	2.86E-04	500	2.94E-04
510	2.72E-04	510	2.94E-04	510	3.02E-04
520	2.77E-04	520	2.98E-04	520	3.06E-04
530	2.84E-04	530	3.02E-04	530	3.13E-04
540	2.91E-04	540	3.13E-04	540	3.21E-04
550	2.98E-04	550	3.21E-04	550	3.29E-04
560	3.05E-04	560	3.29E-04	560	3.41E-04
570	3.12E-04	570	3.37E-04	570	3.48E-04
580	3.21E-04	580	3.44E-04	580	3.60E-04
590	3.25E-04	590	3.56E-04	590	3.72E-04
600	3.37E-04	600	3.68E-04	600	3.83E-04
610	3.44E-04	610	3.79E-04	610	3.95E-04
620	3.56E-04	620	3.91E-04	620	4.14E-04
630	3.68E-04	630	4.06E-04	630	4.26E-04
640	3.83E-04	640	4.30E-04	640	4.45E-04
650	3.95E-04	650	4.45E-04	650	4.64E-04
660	4.10E-04	660	4.57E-04	660	4.88E-04
670	4.30E-04	670	4.84E-04	670	5.11E-04
680	4.45E-04	680	5.07E-04	680	5.38E-04
690	4.68E-04	690	5.34E-04	690	5.65E-04
700	4.95E-04	700	5.65E-04	700	6.00E-04
710	5.19E-04	710	6.04E-04	710	6.31E-04

Continued on next page

Potential mV	Current Density A/cm^2	Potential mV	Current Density A/cm^2	Potential mV	Current Density A/cm^2
720	5.50E-04	720	6.39E-04	720	6.70E-04
730	5.84E-04	730	6.70E-04	730	7.04E-04
740	6.23E-04	740	7.08E-04	740	7.47E-04
750	6.66E-04	750	7.47E-04	750	7.86E-04
760	7.20E-04	760	7.74E-04	760	8.13E-04
770	7.74E-04	770	8.09E-04	770	8.36E-04
780	8.51E-04	780	8.32E-04	780	8.71E-04
790	9.44E-04	790	8.63E-04	790	9.13E-04
800	1.03E-03	800	9.13E-04	800	9.37E-04
810	1.11E-03	810	9.48E-04	810	9.40E-04
820	1.22E-03	820	9.87E-04	820	9.29E-04
830	1.32E-03	830	1.01E-03	830	9.44E-04
840	1.43E-03	840	1.02E-03	840	9.48E-04
850	1.52E-03	850	1.03E-03	850	9.71E-04
860	1.60E-03	860	1.03E-03	860	9.52E-04
870	1.66E-03	870	1.01E-03	870	9.37E-04
880	1.68E-03	880	9.87E-04	880	9.25E-04
890	1.68E-03	890	9.67E-04	890	9.25E-04
900	1.66E-03	900	9.48E-04	900	8.86E-04
910	1.61E-03	910	9.13E-04	910	8.78E-04
920	1.55E-03	920	8.86E-04	920	8.51E-04
930	1.52E-03	930	8.71E-04	930	8.24E-04
940	1.44E-03	940	8.59E-04	940	8.09E-04
950	1.36E-03	950	8.55E-04	950	7.82E-04
960	1.32E-03	960	8.40E-04	960	7.74E-04
970	1.27E-03	970	8.28E-04	970	7.86E-04
980	1.25E-03	980	8.28E-04	980	8.01E-04
990	1.25E-03	990	8.28E-04	990	8.09E-04
1000	1.25E-03	1000	8.32E-04	1000	8.32E-04
1010	1.25E-03	1010	8.55E-04	1010	8.51E-04
1020	1.26E-03	1020	8.63E-04	1020	8.71E-04
1030	1.27E-03	1030	9.02E-04	1030	9.13E-04
1040	1.29E-03	1040	9.33E-04	1040	9.44E-04
1050	1.31E-03	1050	9.64E-04	1050	9.79E-04
1060	1.35E-03	1060	1.01E-03	1060	1.03E-03

Continued on next page

Potential mV	Current Density A/cm^2	Potential mV	Current Density A/cm^2	Potential mV	Current Density A/cm^2
1070	1.38E-03	1070	1.04E-03	1070	1.08E-03
1080	1.42E-03	1080	1.09E-03	1080	1.12E-03
1090	1.45E-03	1090	1.13E-03	1090	1.16E-03
1100	1.51E-03	1100	1.20E-03	1100	1.21E-03
1110	1.54E-03	1110	1.26E-03	1110	1.28E-03
1120	1.60E-03	1120	1.33E-03	1120	1.32E-03
1130	1.63E-03	1130	1.36E-03	1130	1.39E-03
1140	1.67E-03	1140	1.43E-03	1140	1.43E-03
1150	1.70E-03	1150	1.49E-03	1150	1.47E-03
1160	1.73E-03	1160	1.52E-03	1160	1.52E-03
1170	1.75E-03	1170	1.56E-03	1170	1.57E-03
1180	1.76E-03	1180	1.63E-03	1180	1.63E-03
1190	1.77E-03	1190	1.70E-03	1190	1.74E-03
1200	1.78E-03	1200	1.76E-03	1200	1.82E-03
1210	1.78E-03	1210	1.84E-03	1210	1.84E-03
1220	1.78E-03	1220	1.83E-03	1220	1.88E-03
1230	1.80E-03	1230	1.93E-03	1230	1.94E-03
1240	1.81E-03	1240	1.97E-03	1240	2.03E-03
1250	1.81E-03	1250	1.99E-03	1250	2.07E-03
1260	1.83E-03	1260	2.05E-03	1260	2.17E-03
1270	1.86E-03	1270	2.13E-03	1270	2.21E-03
1280	1.88E-03	1280	2.18E-03	1280	2.26E-03
1290	1.92E-03	1290	2.32E-03	1290	2.35E-03
1300	1.97E-03	1300	2.38E-03	1300	2.55E-03
1310	2.00E-03	1310	2.44E-03	1310	2.63E-03
1320	2.06E-03	1320	2.49E-03	1320	2.72E-03
1330	2.16E-03	1330	2.52E-03	1330	2.82E-03
1340	2.26E-03	1340	2.67E-03	1340	2.90E-03
1350	2.37E-03	1350	2.79E-03	1350	2.94E-03
1360	2.52E-03	1360	3.06E-03	1360	2.97E-03
1370	2.62E-03	1370	3.14E-03	1370	3.10E-03
1380	2.71E-03	1380	3.27E-03	1380	3.17E-03
1390	2.62E-03	1390	3.38E-03	1390	3.21E-03
1400	1.82E-03	1400	3.51E-03	1400	3.29E-03
1410	1.61E-03	1410	3.64E-03	1410	3.37E-03

Continued on next page

Potential mV	Current Density A/cm^2	Potential mV	Current Density A/cm^2	Potential mV	Current Density A/cm^2
1420	1.62E-03	1420	3.87E-03	1420	3.44E-03
1430	1.55E-03	1430	3.91E-03	1430	3.52E-03
1440	1.55E-03	1440	3.95E-03	1440	3.64E-03
1450	1.55E-03	1450	4.10E-03	1450	3.91E-03
1460	1.47E-03	1460	4.45E-03	1460	4.30E-03
1470	1.50E-03	1470	4.57E-03	1470	4.45E-03
1480	1.70E-03	1480	4.76E-03	1480	4.53E-03
1490	2.21E-03	1490	4.88E-03	1490	4.72E-03
1500	2.38E-03	1500	5.30E-03	1500	4.95E-03
1510	2.56E-03	1510	5.38E-03	1510	5.11E-03
1520	2.70E-03	1520	5.50E-03	1520	5.42E-03
1530	2.94E-03	1530	5.69E-03	1530	5.69E-03
1540	3.10E-03	1540	6.00E-03	1540	5.92E-03
1550	3.19E-03	1550	6.19E-03	1550	6.00E-03
1560	3.41E-03	1560	6.31E-03	1560	6.11E-03
1570	2.79E-03	1570	6.39E-03	1570	6.31E-03
1580	2.53E-03	1580	6.46E-03	1580	6.46E-03
1590	2.33E-03	1590	6.66E-03	1590	6.58E-03
1600	1.93E-03	1600	6.89E-03	1600	6.97E-03
1610	1.77E-03	1610	6.97E-03	1610	7.08E-03
1620	1.66E-03	1620	7.16E-03	1620	7.28E-03
1630	1.59E-03	1630	7.39E-03	1630	7.59E-03
1640	1.54E-03	1640	7.70E-03	1640	7.74E-03
1650	1.53E-03	1650	7.86E-03	1650	7.86E-03
1660	1.54E-03	1660	8.13E-03	1660	8.09E-03
1670	1.54E-03	1670	8.32E-03	1670	8.32E-03
1680	1.55E-03	1680	8.51E-03	1680	8.51E-03
1690	1.55E-03	1690	8.71E-03	1690	8.71E-03
1700	1.56E-03	1700	8.90E-03	1700	8.90E-03

TABLE B.5: Polarization Data: SS201 in $FeSO_4$+$FeCl_3$

Velocity: 0 m/s		Velocity: 2.63 m/s		Velocity: 3.93 m/s	
Potential	Current Density	Potential	Current Density	Potential	Current Density
mV	A/cm^2	mV	A/cm^2	mV	A/cm^2
-1000	2.28E-03	-1000	4.84E-03	-1000	5.50E-03
-990	2.21E-03	-970	4.68E-03	-990	5.46E-03
-980	2.14E-03	-960	4.61E-03	-980	5.42E-03
-970	2.09E-03	-950	4.57E-03	-950	5.38E-03
-960	2.02E-03	-940	4.53E-03	-930	5.30E-03
-950	1.97E-03	-930	4.49E-03	-920	5.26E-03
-940	1.90E-03	-910	4.45E-03	-910	5.22E-03
-930	1.85E-03	-900	4.41E-03	-900	5.19E-03
-920	1.80E-03	-750	4.33E-03	-890	5.11E-03
-910	1.73E-03	-700	4.26E-03	-880	4.99E-03
-900	1.68E-03	-680	4.18E-03	-730	4.91E-03
-890	1.62E-03	-670	4.10E-03	-720	4.88E-03
-880	1.58E-03	-660	4.06E-03	-700	4.84E-03
-870	1.52E-03	-620	4.02E-03	-690	4.80E-03
-860	1.48E-03	-600	3.95E-03	-680	4.76E-03
-850	1.46E-03	-590	3.75E-03	-670	4.61E-03
-840	1.40E-03	-540	3.60E-03	-660	4.57E-03
-830	1.36E-03	-530	3.56E-03	-650	4.53E-03
-820	1.31E-03	-520	3.52E-03	-640	4.45E-03
-810	1.27E-03	-510	3.44E-03	-630	4.37E-03
-800	1.23E-03	-500	3.33E-03	-610	4.26E-03
-790	1.20E-03	-490	3.25E-03	-600	4.10E-03
-780	1.16E-03	-480	3.21E-03	-590	4.06E-03
-770	1.12E-03	-470	3.13E-03	-580	3.99E-03
-760	1.08E-03	-460	3.02E-03	-560	3.87E-03
-750	1.05E-03	-450	2.90E-03	-550	3.83E-03
-740	1.02E-03	-440	2.79E-03	-540	3.75E-03
-730	9.87E-04	-430	2.67E-03	-530	3.72E-03
-720	9.75E-04	-420	2.55E-03	-520	3.60E-03
-710	9.48E-04	-410	2.48E-03	-510	3.44E-03
-700	9.25E-04	-400	2.36E-03	-500	3.37E-03
-690	9.06E-04	-390	2.24E-03	-490	3.29E-03

Continued on next page

Potential mV	Current Density A/cm^2	Potential mV	Current Density A/cm^2	Potential mV	Current Density A/cm^2
-680	8.94E-04	-380	2.17E-03	-480	3.13E-03
-670	8.82E-04	-370	2.01E-03	-470	3.10E-03
-660	8.63E-04	-360	1.90E-03	-460	2.98E-03
-650	8.48E-04	-350	1.78E-03	-450	2.90E-03
-640	8.36E-04	-340	1.66E-03	-440	2.75E-03
-630	8.24E-04	-330	1.55E-03	-430	2.67E-03
-620	8.13E-04	-320	1.43E-03	-420	2.55E-03
-610	8.05E-04	-310	1.32E-03	-410	2.48E-03
-600	7.97E-04	-300	1.20E-03	-400	2.32E-03
-590	7.86E-04	-290	1.12E-03	-390	2.24E-03
-580	7.74E-04	-280	1.01E-03	-380	2.13E-03
-570	7.66E-04	-270	9.29E-04	-370	1.97E-03
-560	7.62E-04	-260	8.51E-04	-360	1.86E-03
-550	7.59E-04	-250	7.74E-04	-350	1.74E-03
-540	7.55E-04	-240	6.97E-04	-340	1.63E-03
-490	7.51E-04	-230	6.58E-04	-330	1.51E-03
-480	7.47E-04	-220	6.19E-04	-320	1.39E-03
-460	7.43E-04	-210	5.80E-04	-310	1.28E-03
-410	7.35E-04	-200	5.42E-04	-300	1.16E-03
-400	7.24E-04	-190	5.03E-04	-290	1.08E-03
-390	7.20E-04	-180	4.64E-04	-280	9.67E-04
-380	7.12E-04	-170	4.26E-04	-270	8.90E-04
-370	7.00E-04	-160	3.87E-04	-260	7.74E-04
-360	6.89E-04	-150	3.48E-04	-250	6.97E-04
-350	6.73E-04	-140	3.10E-04	-240	6.58E-04
-340	6.58E-04	-130	2.71E-04	-230	5.42E-04
-330	6.39E-04	-120	2.71E-04	-220	5.03E-04
-320	6.19E-04	-110	2.32E-04	-210	4.64E-04
-310	5.84E-04	-100	1.90E-04	-200	4.26E-04
-300	5.46E-04	-90	1.43E-04	-190	3.87E-04
-290	4.95E-04	-80	9.67E-05	-180	3.48E-04
-280	4.37E-04	-70	3.87E-05	-170	3.10E-04
-270	4.02E-04	-60	5.42E-05	-160	2.71E-04
-260	3.68E-04	-50	1.01E-04	-150	2.32E-04
-250	3.48E-04	-40	2.21E-04	-140	1.93E-04

Continued on next page

Potential mV	Current Density A/cm^2	Potential mV	Current Density A/cm^2	Potential mV	Current Density A/cm^2
-240	3.37E-04	-30	2.75E-04	-130	1.55E-04
-230	3.41E-04	-20	3.33E-04	-120	1.16E-04
-220	3.41E-04	-10	4.64E-04	-110	1.32E-04
-210	3.41E-04	0	5.07E-04	-100	1.01E-04
-200	3.29E-04	10	5.61E-04	-90	7.35E-05
-190	3.10E-04	20	6.46E-04	-80	5.03E-05
-180	2.98E-04	30	7.24E-04	-70	4.26E-05
-170	2.83E-04	40	7.97E-04	-60	3.87E-05
-160	2.63E-04	50	8.78E-04	-50	5.03E-05
-150	2.40E-04	60	9.67E-04	-40	5.80E-05
-140	2.24E-04	70	1.03E-03	-30	7.35E-05
-130	2.01E-04	80	1.11E-03	-20	1.04E-04
-120	1.82E-04	90	1.19E-03	-10	1.47E-04
-110	1.16E-04	100	1.27E-03	0	1.93E-04
-100	5.03E-05	110	1.36E-03	10	2.71E-04
-90	7.74E-06	120	1.44E-03	20	3.33E-04
-80	3.87E-05	130	1.54E-03	30	3.99E-04
-70	5.03E-05	140	1.60E-03	40	4.80E-04
-60	6.58E-05	150	1.70E-03	50	5.53E-04
-50	8.51E-05	160	1.81E-03	60	6.27E-04
-40	1.08E-04	170	1.87E-03	70	7.08E-04
-30	1.66E-04	180	2.02E-03	80	7.89E-04
-20	2.21E-04	190	2.14E-03	90	8.78E-04
-10	2.86E-04	200	2.30E-03	100	9.67E-04
0	3.48E-04	210	2.43E-03	110	1.06E-03
10	4.30E-04	220	2.55E-03	120	1.15E-03
20	4.95E-04	230	2.68E-03	130	1.23E-03
30	5.80E-04	240	2.79E-03	140	1.32E-03
40	6.89E-04	250	2.86E-03	150	1.43E-03
50	7.74E-04	260	3.00E-03	160	1.52E-03
60	8.82E-04	270	3.10E-03	170	1.64E-03
70	9.71E-04	280	3.20E-03	180	1.75E-03
80	1.07E-03	290	3.32E-03	190	1.83E-03
90	1.18E-03	300	3.44E-03	200	1.95E-03
100	1.28E-03	310	3.55E-03	210	2.01E-03

Continued on next page

Potential mV	Current Density A/cm^2	Potential mV	Current Density A/cm^2	Potential mV	Current Density A/cm^2
110	1.41E-03	320	3.65E-03	220	2.10E-03
120	1.54E-03	330	3.78E-03	230	2.22E-03
130	1.68E-03	340	3.91E-03	240	2.32E-03
140	1.82E-03	350	4.06E-03	250	2.43E-03
150	2.00E-03	360	4.14E-03	260	2.57E-03
160	2.13E-03	370	4.22E-03	270	2.83E-03
170	2.27E-03	380	4.33E-03	280	3.03E-03
180	2.42E-03	390	4.49E-03	290	3.19E-03
190	2.55E-03	400	4.64E-03	300	3.32E-03
200	2.69E-03	410	4.76E-03	310	3.45E-03
210	2.83E-03	420	4.91E-03	320	3.57E-03
220	2.98E-03	430	5.03E-03	330	3.68E-03
230	3.11E-03	440	5.15E-03	340	3.79E-03
240	3.25E-03	450	5.26E-03	350	3.91E-03
250	3.39E-03	460	5.34E-03	360	4.02E-03
260	3.56E-03	470	5.53E-03	370	4.10E-03
270	3.69E-03	480	5.65E-03	380	4.22E-03
280	3.85E-03	490	5.77E-03	390	4.33E-03
290	3.99E-03	500	5.92E-03	400	4.45E-03
300	4.16E-03	510	6.04E-03	410	4.61E-03
310	4.26E-03	520	6.15E-03	420	4.76E-03
320	4.64E-03	530	6.27E-03	430	4.88E-03
330	5.15E-03	540	6.54E-03	440	4.99E-03
340	5.46E-03	550	6.62E-03	450	5.07E-03
350	6.00E-03	560	6.73E-03	460	5.22E-03
360	6.27E-03	570	6.81E-03	470	5.38E-03
370	6.46E-03	580	6.97E-03	480	5.53E-03
380	6.62E-03	590	7.16E-03	490	5.69E-03
390	6.81E-03	600	7.28E-03	500	5.77E-03
400	6.97E-03	610	7.43E-03	510	5.88E-03
410	7.20E-03	620	7.55E-03	520	6.00E-03
420	7.35E-03	630	7.74E-03	530	6.11E-03
430	7.51E-03	640	7.97E-03	540	6.23E-03
440	7.70E-03	650	8.13E-03	550	6.42E-03
450	7.86E-03	660	8.24E-03	560	6.58E-03

Continued on next page

Potential mV	Current Density A/cm^2	Potential mV	Current Density A/cm^2	Potential mV	Current Density A/cm^2
460	8.01E-03	670	8.36E-03	570	6.70E-03
470	8.17E-03	680	8.55E-03	580	6.77E-03
480	8.32E-03	690	8.63E-03	590	6.93E-03
490	8.44E-03	700	8.78E-03	600	7.08E-03
500	8.59E-03	710	8.90E-03	610	7.16E-03
510	8.75E-03	720	9.06E-03	620	7.31E-03
520	8.90E-03	730	9.29E-03	630	7.47E-03
530	9.06E-03	740	9.40E-03	640	7.59E-03
540	9.21E-03	750	9.64E-03	650	7.74E-03
550	9.37E-03	760	9.75E-03	660	7.82E-03
560	9.52E-03	770	9.87E-03	670	8.01E-03
570	9.67E-03	780	1.01E-02	680	8.17E-03
580	9.83E-03	790	1.01E-02	690	8.28E-03
590	9.95E-03	800	1.04E-02	700	8.44E-03
600	1.02E-02	810	1.04E-02	710	8.55E-03
610	1.03E-02	820	1.06E-02	720	8.67E-03
620	1.05E-02	830	1.07E-02	730	8.78E-03
630	1.06E-02	840	1.10E-02	740	8.98E-03
640	1.08E-02	850	1.11E-02	750	9.21E-03
650	1.10E-02	860	1.12E-02	760	9.29E-03
660	1.11E-02	870	1.13E-02	770	9.44E-03
670	1.13E-02	880	1.15E-02	780	9.56E-03
680	1.15E-02	890	1.16E-02	790	9.67E-03
690	1.16E-02	900	1.18E-02	800	9.83E-03
700	1.18E-02	910	1.20E-02	810	9.95E-03
710	1.19E-02	920	1.22E-02	820	1.01E-02
720	1.21E-02	930	1.23E-02	830	1.01E-02
730	1.23E-02	940	1.24E-02	840	1.03E-02
740	1.25E-02	950	1.26E-02	850	1.04E-02
750	1.27E-02	960	1.28E-02	860	1.05E-02
760	1.28E-02	970	1.28E-02	870	1.07E-02
770	1.29E-02	980	1.30E-02	880	1.10E-02
780	1.32E-02	990	1.33E-02	890	1.11E-02
790	1.33E-02	1000	1.34E-02	900	1.13E-02
800	1.35E-02			910	1.15E-02

Continued on next page

Potential mV	Current Density A/cm^2	Potential mV	Current Density A/cm^2	Potential mV	Current Density A/cm^2
810	1.37E-02			920	1.16E-02
820	1.38E-02			930	1.18E-02
830	1.40E-02			940	1.19E-02
840	1.41E-02			950	1.21E-02
850	1.43E-02			960	1.24E-02
860	1.44E-02			970	1.25E-02
870	1.46E-02			980	1.26E-02
880	1.47E-02			990	1.27E-02
890	1.49E-02			1000	1.29E-02
900	1.51E-02				
910	1.52E-02				
920	1.54E-02				
930	1.55E-02				
940	1.57E-02				
950	1.58E-02				
960	1.60E-02				
970	1.61E-02				
980	1.63E-02				
990	1.64E-02				
1000	1.66E-02				

TABLE B.6: Polarization Data: Brass in artificial seawater

Velocity: 0 m/s		Velocity: 2.63 m/s		Velocity: 3.93 m/s	
Potential	Current Density	Potential	Current Density	Potential	Current Density
mV	A/cm^2	mV	A/cm^2	mV	A/cm^2
-1000	4.80E-04	-1000	5.22E-03	-1000	6.73E-03
-990	4.53E-04	-990	4.80E-03	-990	6.27E-03
-980	4.18E-04	-980	4.57E-03	-980	5.84E-03
-970	3.95E-04	-970	4.33E-03	-970	5.53E-03
-960	3.75E-04	-960	4.14E-03	-960	5.22E-03
-950	3.60E-04	-950	3.91E-03	-950	4.95E-03
-940	3.44E-04	-940	3.68E-03	-940	4.72E-03
-930	3.25E-04	-930	3.48E-03	-930	4.45E-03
-920	3.10E-04	-920	3.37E-03	-920	4.18E-03
-910	2.94E-04	-910	3.15E-03	-910	3.99E-03
-900	2.83E-04	-900	3.00E-03	-900	3.72E-03
-890	2.63E-04	-890	2.82E-03	-890	3.56E-03
-880	2.55E-04	-880	2.61E-03	-880	3.39E-03
-870	2.48E-04	-870	2.48E-03	-870	3.21E-03
-860	2.40E-04	-860	2.34E-03	-860	3.02E-03
-850	2.32E-04	-850	2.26E-03	-850	2.81E-03
-840	2.24E-04	-840	2.12E-03	-840	2.71E-03
-830	2.09E-04	-830	2.02E-03	-830	2.59E-03
-820	2.01E-04	-820	1.94E-03	-820	2.47E-03
-810	1.86E-04	-810	1.85E-03	-810	2.37E-03
-800	1.74E-04	-800	1.76E-03	-800	2.28E-03
-790	1.63E-04	-790	1.69E-03	-790	2.23E-03
-780	1.51E-04	-780	1.66E-03	-780	2.17E-03
-770	1.39E-04	-770	1.57E-03	-770	2.11E-03
-760	1.28E-04	-760	1.54E-03	-760	2.05E-03
-750	1.12E-04	-750	1.51E-03	-750	2.03E-03
-740	1.04E-04	-740	1.47E-03	-740	1.98E-03
-730	9.29E-05	-730	1.43E-03	-730	1.97E-03
-720	8.13E-05	-720	1.41E-03	-720	1.96E-03
-710	7.35E-05	-710	1.40E-03	-710	1.90E-03
-700	6.58E-05	-700	1.35E-03	-700	1.88E-03
-690	5.80E-05	-690	1.34E-03	-690	1.88E-03

Continued on next page

Potential mV	Current Density A/cm^2	Potential mV	Current Density A/cm^2	Potential mV	Current Density A/cm^2
-680	5.42E-05	-680	1.32E-03	-680	1.87E-03
-670	5.03E-05	-670	1.31E-03	-670	1.85E-03
-660	4.64E-05	-660	1.29E-03	-660	1.85E-03
-650	4.26E-05	-650	1.27E-03	-650	1.85E-03
-640	3.87E-05	-640	1.27E-03	-640	1.82E-03
-630	3.79E-05	-630	1.26E-03	-630	1.81E-03
-620	3.72E-05	-620	1.26E-03	-620	1.80E-03
-610	3.52E-05	-610	1.25E-03	-610	1.81E-03
-600	3.37E-05	-600	1.24E-03	-600	1.82E-03
-590	3.17E-05	-590	1.26E-03	-590	1.79E-03
-580	3.02E-05	-580	1.25E-03	-580	1.78E-03
-570	2.90E-05	-570	1.25E-03	-570	1.78E-03
-560	2.79E-05	-560	1.24E-03	-560	1.79E-03
-550	2.71E-05	-550	1.25E-03	-550	1.78E-03
-540	2.63E-05	-540	1.26E-03	-540	1.79E-03
-530	2.55E-05	-530	1.26E-03	-530	1.79E-03
-520	2.48E-05	-520	1.27E-03	-520	1.82E-03
-510	2.40E-05	-510	1.24E-03	-510	1.80E-03
-500	2.32E-05	-500	1.25E-03	-500	1.80E-03
-490	2.21E-05	-490	1.28E-03	-490	1.80E-03
-480	2.13E-05	-480	1.32E-03	-480	1.78E-03
-470	2.01E-05	-470	1.28E-03	-470	1.76E-03
-460	1.86E-05	-460	1.24E-03	-460	1.73E-03
-450	1.74E-05	-450	1.22E-03	-450	1.68E-03
-440	1.55E-05	-440	1.20E-03	-440	1.66E-03
-430	1.39E-05	-430	1.19E-03	-430	1.55E-03
-420	1.24E-05	-420	1.09E-03	-420	1.34E-03
-410	1.01E-05	-410	8.82E-04	-410	1.12E-03
-400	7.74E-06	-400	7.16E-04	-400	9.44E-04
-390	5.42E-06	-390	5.42E-04	-390	7.47E-04
-380	3.87E-06	-380	4.64E-04	-380	6.39E-04
-370	1.93E-06	-370	3.87E-04	-370	5.57E-04
-360	3.87E-07	-360	3.48E-04	-360	5.15E-04
-350	1.55E-06	-350	3.21E-04	-350	4.76E-04
-340	3.48E-06	-340	2.90E-04	-340	4.41E-04

Continued on next page

Potential mV	Current Density A/cm^2	Potential mV	Current Density A/cm^2	Potential mV	Current Density A/cm^2
-330	5.80E-06	-330	2.71E-04	-330	4.10E-04
-320	7.74E-06	-320	2.48E-04	-320	3.79E-04
-310	9.67E-06	-310	2.24E-04	-310	3.52E-04
-300	1.24E-05	-300	2.01E-04	-300	3.25E-04
-290	1.47E-05	-290	1.70E-04	-290	2.94E-04
-280	1.70E-05	-280	1.51E-04	-280	2.52E-04
-270	2.05E-05	-270	1.16E-04	-270	2.13E-04
-260	2.36E-05	-260	7.35E-05	-260	1.47E-04
-250	2.86E-05	-250	2.32E-05	-250	9.29E-05
-240	3.44E-05	-240	4.26E-05	-240	4.64E-05
-230	4.26E-05	-230	1.01E-04	-230	8.13E-05
-220	5.65E-05	-220	1.90E-04	-220	1.59E-04
-210	7.16E-05	-210	2.83E-04	-210	2.98E-04
-200	1.05E-04	-200	4.06E-04	-200	4.53E-04
-190	1.68E-04	-190	5.80E-04	-190	6.66E-04
-180	2.42E-04	-180	7.97E-04	-180	8.98E-04
-170	3.44E-04	-170	1.07E-03	-170	1.20E-03
-160	5.15E-04	-160	1.39E-03	-160	1.55E-03
-150	6.97E-04	-150	1.82E-03	-150	2.00E-03
-140	8.90E-04	-140	2.38E-03	-140	2.55E-03
-130	1.13E-03	-130	2.87E-03	-130	3.15E-03
-120	1.46E-03	-120	3.52E-03	-120	3.72E-03
-110	1.80E-03	-110	4.26E-03	-110	4.41E-03
-100	2.17E-03	-100	4.91E-03	-100	4.91E-03
-90	2.67E-03	-90	5.50E-03	-90	5.57E-03
-80	3.07E-03	-80	6.27E-03	-80	6.23E-03
-70	3.55E-03	-70	6.93E-03	-70	6.93E-03
-60	4.06E-03	-60	7.74E-03	-60	7.70E-03
-50	4.53E-03	-50	8.40E-03	-50	8.32E-03
-40	5.15E-03	-40	9.21E-03	-40	9.06E-03
-30	5.80E-03	-30	9.87E-03	-30	9.71E-03
-20	6.39E-03	-20	1.07E-02	-20	1.04E-02
-10	7.00E-03	-10	1.14E-02	-10	1.11E-02
0	7.62E-03	0	1.21E-02	0	1.18E-02
10	8.32E-03	10	1.28E-02	10	1.25E-02

Continued on next page

Potential mV	Current Density A/cm^2	Potential mV	Current Density A/cm^2	Potential mV	Current Density A/cm^2
20	9.17E-03	20	1.32E-02	20	1.33E-02
30	1.01E-02	30	1.43E-02	30	1.41E-02
40	1.07E-02	40	1.49E-02	40	1.47E-02
50	1.15E-02	50	1.52E-02	50	1.53E-02
60	1.23E-02	60	1.63E-02	60	1.58E-02
70	1.30E-02	70	1.71E-02	70	1.63E-02
80	1.38E-02	80	1.80E-02	80	1.71E-02
90	1.45E-02	90	1.88E-02	90	1.81E-02
100	1.52E-02	100	1.94E-02	100	1.89E-02
110	1.58E-02	110	2.01E-02	110	1.95E-02
120	1.63E-02	120	2.05E-02	120	2.01E-02
130	1.69E-02	130	2.12E-02	130	2.11E-02
140	1.73E-02	140	2.19E-02	140	2.19E-02
150	1.78E-02	150	2.27E-02	150	2.25E-02
160	1.80E-02	160	2.35E-02	160	2.32E-02
170	1.82E-02	170	2.43E-02	170	2.41E-02
180	1.84E-02	180	2.50E-02	180	2.49E-02
190	1.85E-02	190	2.57E-02	190	2.57E-02

TABLE B.7: Polarization Data: Brass in 2.5% sodium carbonate

Velocity: 0 m/s		Velocity: 2.63 m/s		Velocity: 3.93 m/s	
Potential	Current Density	Potential	Current Density	Potential	Current Density
mV	A/cm^2	mV	A/cm^2	mV	A/cm^2
-1000	1.16E-03	-1000	1.57E-03	-1000	2.08E-03
-990	1.08E-03	-990	1.51E-03	-990	1.99E-03
-980	9.87E-04	-980	1.49E-03	-980	1.95E-03
-970	9.13E-04	-970	1.47E-03	-970	1.93E-03
-960	8.48E-04	-960	1.47E-03	-960	1.91E-03
-950	7.89E-04	-950	1.45E-03	-950	1.88E-03
-940	7.35E-04	-940	1.44E-03	-940	1.87E-03
-930	6.89E-04	-930	1.44E-03	-930	1.82E-03
-920	6.39E-04	-920	1.41E-03	-920	1.80E-03
-910	5.96E-04	-910	1.41E-03	-910	1.79E-03
-900	5.42E-04	-900	1.42E-03	-900	1.78E-03
-890	4.99E-04	-890	1.43E-03	-890	1.77E-03
-880	4.68E-04	-880	1.42E-03	-880	1.77E-03
-870	4.41E-04	-870	1.40E-03	-870	1.77E-03
-860	4.18E-04	-860	1.36E-03	-860	1.76E-03
-850	3.95E-04	-850	1.37E-03	-850	1.73E-03
-840	3.72E-04	-840	1.38E-03	-840	1.75E-03
-830	3.33E-04	-830	1.37E-03	-830	1.73E-03
-820	3.13E-04	-820	1.37E-03	-820	1.74E-03
-810	2.97E-04	-810	1.37E-03	-810	1.74E-03
-800	2.83E-04	-800	1.36E-03	-800	1.73E-03
-790	2.72E-04	-790	1.33E-03	-790	1.73E-03
-780	2.59E-04	-780	1.32E-03	-780	1.73E-03
-770	2.47E-04	-770	1.32E-03	-770	1.72E-03
-760	2.36E-04	-760	1.30E-03	-760	1.71E-03
-750	2.28E-04	-750	1.26E-03	-750	1.68E-03
-740	2.20E-04	-740	1.20E-03	-740	1.67E-03
-730	2.12E-04	-730	8.18E-04	-730	1.64E-03
-720	2.04E-04	-720	9.83E-04	-720	1.52E-03
-710	1.97E-04	-710	8.02E-04	-710	1.45E-03
-700	1.90E-04	-700	6.56E-04	-700	1.32E-03
-690	1.83E-04	-690	5.90E-04	-690	1.23E-03

Continued on next page

Potential mV	Current Density A/cm^2	Potential mV	Current Density A/cm^2	Potential mV	Current Density A/cm^2
-680	1.75E-04	-680	5.35E-04	-680	1.08E-03
-670	1.68E-04	-670	4.99E-04	-670	1.01E-03
-660	1.59E-04	-660	4.72E-04	-660	9.24E-04
-650	1.51E-04	-650	4.64E-04	-650	8.92E-04
-640	1.43E-04	-640	4.40E-04	-640	8.49E-04
-630	1.37E-04	-630	4.36E-04	-630	8.18E-04
-620	1.30E-04	-620	4.52E-04	-620	7.82E-04
-610	1.22E-04	-610	4.72E-04	-610	7.86E-04
-600	1.16E-04	-600	4.91E-04	-600	7.78E-04
-590	1.08E-04	-590	5.31E-04	-590	7.78E-04
-580	1.02E-04	-580	5.50E-04	-580	7.86E-04
-570	9.44E-05	-570	5.90E-04	-570	8.25E-04
-560	8.90E-05	-560	6.29E-04	-560	8.88E-04
-550	8.55E-05	-550	7.11E-04	-550	9.04E-04
-540	7.12E-05	-540	7.55E-04	-540	9.43E-04
-530	6.42E-05	-530	8.10E-04	-530	9.94E-04
-520	6.19E-05	-520	8.06E-04	-520	1.04E-03
-510	5.19E-05	-510	8.25E-04	-510	1.09E-03
-500	3.99E-05	-500	8.41E-04	-500	1.13E-03
-490	2.17E-05	-490	8.29E-04	-490	1.12E-03
-480	1.82E-05	-480	8.14E-04	-480	1.12E-03
-470	1.24E-05	-470	7.82E-04	-470	1.14E-03
-460	8.90E-06	-460	7.15E-04	-460	1.06E-03
-450	5.42E-06	-450	6.21E-04	-450	1.00E-03
-440	2.32E-05	-440	5.19E-04	-440	8.45E-04
-430	3.52E-05	-430	3.46E-04	-430	7.67E-04
-420	5.46E-05	-420	1.93E-04	-420	5.82E-04
-410	5.80E-05	-410	7.47E-05	-410	3.46E-04
-400	7.04E-05	-400	1.97E-05	-400	1.42E-04
-390	7.82E-05	-390	6.68E-05	-390	2.75E-05
-380	7.82E-05	-380	8.65E-05	-380	5.11E-05
-370	7.55E-05	-370	9.83E-05	-370	9.04E-05
-360	8.09E-05	-360	1.10E-04	-360	1.06E-04
-350	7.74E-05	-350	1.14E-04	-350	1.14E-04
-340	7.35E-05	-340	1.18E-04	-340	1.18E-04

Continued on next page

Potential mV	Current Density A/cm^2	Potential mV	Current Density A/cm^2	Potential mV	Current Density A/cm^2
-330	7.74E-05	-330	1.22E-04	-330	1.18E-04
-320	6.11E-05	-320	1.30E-04	-320	1.22E-04
-310	5.80E-05	-310	1.34E-04	-310	1.45E-04
-300	4.84E-05	-300	1.38E-04	-300	1.53E-04
-290	5.84E-05	-290	1.57E-04	-290	1.73E-04
-280	6.35E-05	-280	1.69E-04	-280	1.77E-04
-270	6.85E-05	-270	1.89E-04	-270	2.00E-04
-260	7.12E-05	-260	2.12E-04	-260	2.08E-04
-250	7.97E-05	-250	2.36E-04	-250	2.63E-04
-240	8.44E-05	-240	2.63E-04	-240	3.07E-04
-230	8.98E-05	-230	2.75E-04	-230	3.62E-04
-220	9.52E-05	-220	3.07E-04	-220	4.05E-04
-210	9.71E-05	-210	3.26E-04	-210	4.13E-04
-200	8.75E-05	-200	3.34E-04	-200	4.36E-04
-190	8.90E-05	-190	3.26E-04	-190	4.36E-04
-180	8.71E-05	-180	3.42E-04	-180	4.60E-04
-170	8.48E-05	-170	3.46E-04	-170	4.87E-04
-160	8.17E-05	-160	3.54E-04	-160	4.95E-04
-150	7.89E-05	-150	3.50E-04	-150	5.07E-04
-140	7.74E-05	-140	3.54E-04	-140	4.52E-04
-130	7.66E-05	-130	3.58E-04	-130	4.87E-04
-120	7.66E-05	-120	3.62E-04	-120	4.99E-04
-110	7.70E-05	-110	3.62E-04	-110	5.03E-04
-100	7.62E-05	-100	3.58E-04	-100	4.95E-04
-90	7.59E-05	-90	3.66E-04	-90	5.03E-04
-80	7.59E-05	-80	3.73E-04	-80	5.15E-04
-70	7.51E-05	-70	3.69E-04	-70	5.03E-04
-60	7.62E-05	-60	3.73E-04	-60	5.15E-04
-50	7.55E-05	-50	3.69E-04	-50	5.15E-04
-40	7.59E-05	-40	3.81E-04	-40	5.15E-04
-30	7.74E-05	-30	3.77E-04	-30	5.11E-04
-20	7.74E-05	-20	3.81E-04	-20	5.31E-04
-10	7.74E-05	-10	3.89E-04	-10	5.19E-04
0	7.74E-05	0	3.89E-04	0	5.27E-04
10	7.74E-05	10	3.77E-04	10	4.99E-04

Continued on next page

Potential mV	Current Density A/cm^2	Potential mV	Current Density A/cm^2	Potential mV	Current Density A/cm^2
20	7.74E-05	20	3.85E-04	20	5.15E-04
30	7.04E-05	30	3.93E-04	30	5.19E-04
40	7.12E-05	40	4.01E-04	40	5.27E-04
50	7.31E-05	50	4.01E-04	50	4.99E-04
60	7.43E-05	60	4.05E-04	60	5.15E-04
70	7.62E-05	70	4.05E-04	70	5.19E-04
80	7.66E-05	80	4.09E-04	80	5.31E-04
90	7.78E-05	90	4.01E-04	90	5.35E-04
100	8.01E-05	100	4.05E-04	100	5.50E-04
110	8.05E-05	110	4.09E-04	110	5.15E-04
120	8.20E-05	120	4.05E-04	120	5.31E-04
130	8.28E-05	130	4.05E-04	130	5.42E-04
140	8.20E-05	140	4.05E-04	140	5.62E-04
150	8.28E-05	150	4.09E-04	150	5.27E-04
160	8.28E-05	160	4.09E-04	160	5.42E-04
170	8.40E-05	170	4.13E-04	170	5.39E-04
180	8.24E-05	180	4.01E-04	180	5.62E-04
190	8.44E-05	190	4.01E-04	190	5.66E-04
200	8.51E-05	200	4.13E-04	200	5.50E-04
210	8.44E-05	210	4.09E-04	210	5.50E-04
220	8.20E-05	220	4.01E-04	220	5.70E-04
230	8.24E-05	230	4.17E-04	230	5.70E-04
240	8.32E-05	240	4.09E-04	240	5.54E-04
250	8.36E-05	250	4.05E-04	250	5.54E-04
260	8.44E-05	260	4.01E-04	260	5.46E-04
270	8.55E-05	270	4.13E-04	270	5.74E-04
280	8.67E-05	280	3.93E-04	280	5.50E-04
290	8.55E-05	290	4.05E-04	290	5.58E-04
300	8.59E-05	300	4.05E-04	300	5.35E-04
310	8.51E-05	310	4.05E-04	310	5.35E-04
320	8.51E-05	320	4.17E-04	320	5.23E-04
330	8.51E-05	330	4.17E-04	330	5.42E-04
340	8.63E-05	340	4.17E-04	340	5.31E-04
350	8.63E-05	350	4.21E-04	350	5.23E-04
360	8.67E-05	360	4.21E-04	360	5.23E-04

Continued on next page

Potential mV	Current Density A/cm^2	Potential mV	Current Density A/cm^2	Potential mV	Current Density A/cm^2
370	8.44E-05	370	4.21E-04	370	5.27E-04
380	8.17E-05	380	4.13E-04	380	5.23E-04
390	8.24E-05	390	4.09E-04	390	5.31E-04
400	8.36E-05	400	3.97E-04	400	5.23E-04
410	8.44E-05	410	4.09E-04	410	5.35E-04
420	8.63E-05	420	3.97E-04	420	5.46E-04
430	8.71E-05	430	3.97E-04	430	5.50E-04
440	8.75E-05	440	4.01E-04	440	5.42E-04
450	8.90E-05	450	3.85E-04	450	5.39E-04
460	8.82E-05	460	3.69E-04	460	5.42E-04
470	8.82E-05	470	3.58E-04	470	5.23E-04
480	8.71E-05	480	3.54E-04	480	5.46E-04
490	8.75E-05	490	3.50E-04	490	5.23E-04
500	8.75E-05	500	3.46E-04	500	5.23E-04
510	8.71E-05	510	3.30E-04	510	5.03E-04
520	8.67E-05	520	3.18E-04	520	4.95E-04
530	8.71E-05	530	3.11E-04	530	4.76E-04
540	8.75E-05	540	3.03E-04	540	4.52E-04
550	9.02E-05	550	2.91E-04	550	4.32E-04
560	8.94E-05	560	2.83E-04	560	4.25E-04
570	9.33E-05	570	2.79E-04	570	3.97E-04
580	9.44E-05	580	2.75E-04	580	3.93E-04
590	9.71E-05	590	2.83E-04	590	3.85E-04
600	1.01E-04	600	2.91E-04	600	3.85E-04
610	1.08E-04	610	2.99E-04	610	3.58E-04
620	1.16E-04	620	3.26E-04	620	3.54E-04
630	1.32E-04	630	3.62E-04	630	3.62E-04
640	1.56E-04	640	4.09E-04	640	3.73E-04
650	1.93E-04	650	4.80E-04	650	3.81E-04
660	2.44E-04	660	5.27E-04	660	3.97E-04
670	3.03E-04	670	6.17E-04	670	4.25E-04
680	3.70E-04	680	7.51E-04	680	4.40E-04
690	4.49E-04	690	8.53E-04	690	5.58E-04
700	5.53E-04	700	1.09E-03	700	6.56E-04
710	6.50E-04	710	1.25E-03	710	7.94E-04

Continued on next page

Potential mV	Current Density A/cm^2	Potential mV	Current Density A/cm^2	Potential mV	Current Density A/cm^2
720	7.28E-04	720	1.43E-03	720	9.12E-04
730	8.28E-04	730	1.63E-03	730	1.08E-03
740	9.25E-04	740	1.93E-03	740	1.38E-03
750	1.08E-03	750	2.06E-03	750	1.64E-03
760	1.20E-03	760	2.41E-03	760	1.74E-03
770	1.35E-03	770	2.84E-03	770	1.91E-03
780	1.51E-03	780	3.98E-03	780	2.21E-03
790	1.66E-03	790	4.64E-03	790	2.66E-03
800	1.88E-03	800	4.83E-03	800	3.08E-03
810	2.08E-03	810	5.11E-03	810	3.41E-03
820	2.28E-03	820	5.74E-03	820	4.01E-03
830	2.52E-03	830	6.13E-03	830	4.21E-03
840	2.79E-03	840	6.96E-03	840	4.44E-03
850	3.11E-03	850	7.43E-03	850	5.03E-03
860	3.72E-03	860	7.90E-03	860	5.46E-03
870	4.37E-03	870	8.73E-03	870	7.35E-03
880	4.80E-03	880	9.67E-03	880	7.82E-03
890	5.34E-03	890	1.02E-02	890	7.94E-03
900	5.65E-03	900	1.05E-02	900	9.04E-03
910	6.35E-03	910	1.09E-02	910	9.98E-03
920	6.89E-03	920	1.14E-02	920	1.04E-02
930	7.51E-03	930	1.06E-02	930	1.14E-02
940	8.05E-03	940	1.16E-02	940	1.20E-02
950	8.71E-03	950	1.19E-02	950	1.29E-02
960	9.71E-03	960	1.26E-02	960	1.34E-02
970	1.06E-02	970	1.33E-02	970	1.40E-02
980	1.12E-02	980	1.42E-02	980	1.42E-02
990	1.20E-02	990	1.45E-02	990	1.42E-02
1000	1.28E-02	1000	1.60E-02	1000	1.52E-02

TABLE B.8: Polarization Data: Brass in 5.0% sodium carbonate

Velocity: 0 m/s		Velocity: 2.63 m/s		Velocity: 3.93 m/s	
Potential	Current Density	Potential	Current Density	Potential	Current Density
mV	A/cm^2	mV	A/cm^2	mV	A/cm^2
-1000	6.97E-05	-1000	1.04E-03	-1000	1.70E-03
-990	5.80E-05	-750	9.29E-04	-990	1.66E-03
-980	5.42E-05	-740	8.90E-04	-980	1.63E-03
-970	5.03E-05	-730	8.55E-04	-970	1.59E-03
-960	4.64E-05	-720	8.28E-04	-960	1.58E-03
-950	4.64E-05	-710	8.01E-04	-950	1.55E-03
-940	4.26E-05	-700	7.74E-04	-940	1.51E-03
-930	4.26E-05	-690	7.59E-04	-930	1.53E-03
-920	3.87E-05	-680	7.35E-04	-920	1.47E-03
-910	3.87E-05	-670	7.08E-04	-910	1.50E-03
-900	3.87E-05	-660	6.89E-04	-900	1.47E-03
-890	3.87E-05	-650	6.62E-04	-890	1.47E-03
-880	3.48E-05	-640	6.39E-04	-880	1.47E-03
-870	3.48E-05	-630	6.19E-04	-870	1.45E-03
-860	3.48E-05	-620	6.04E-04	-860	1.43E-03
-850	3.48E-05	-610	5.77E-04	-850	1.43E-03
-840	3.48E-05	-600	5.57E-04	-840	1.42E-03
-830	3.10E-05	-590	5.30E-04	-830	1.40E-03
-820	3.10E-05	-580	5.03E-04	-820	1.39E-03
-810	3.10E-05	-570	4.76E-04	-810	1.41E-03
-800	3.10E-05	-560	4.61E-04	-800	1.39E-03
-790	2.71E-05	-550	4.33E-04	-790	1.39E-03
-780	2.71E-05	-540	4.14E-04	-780	1.39E-03
-770	2.71E-05	-530	3.91E-04	-770	1.38E-03
-760	2.71E-05	-520	3.79E-04	-760	1.37E-03
-750	2.32E-05	-510	3.72E-04	-750	1.37E-03
-740	2.32E-05	-500	3.64E-04	-740	1.35E-03
-730	2.32E-05	-490	3.52E-04	-730	1.35E-03
-720	2.32E-05	-480	3.37E-04	-720	1.35E-03
-710	1.93E-05	-470	3.41E-04	-710	1.29E-03
-700	1.93E-05	-460	3.41E-04	-700	1.26E-03
-690	1.93E-05	-450	3.37E-04	-690	1.22E-03

Continued on next page

Potential mV	Current Density A/cm^2	Potential mV	Current Density A/cm^2	Potential mV	Current Density A/cm^2
-680	1.93E-05	-440	3.33E-04	-680	1.18E-03
-670	1.93E-05	-430	3.29E-04	-670	1.11E-03
-660	1.93E-05	-420	2.90E-04	-660	1.07E-03
-650	1.93E-05	-410	2.32E-04	-650	1.02E-03
-640	1.93E-05	-400	1.63E-04	-640	9.98E-04
-630	1.55E-05	-390	3.87E-05	-630	9.37E-04
-620	1.55E-05	-380	1.74E-04	-620	8.98E-04
-610	1.55E-05	-370	3.68E-04	-610	8.78E-04
-600	1.55E-05	-360	5.80E-04	-600	8.44E-04
-590	1.55E-05	-350	7.35E-04	-590	8.13E-04
-580	1.16E-05	-340	1.16E-04	-580	7.93E-04
-570	1.16E-05	-330	1.32E-04	-570	7.66E-04
-560	1.16E-05	-320	1.51E-04	-560	7.51E-04
-550	1.16E-05	-310	1.63E-04	-550	7.35E-04
-540	7.74E-06	-300	1.86E-04	-540	7.20E-04
-530	3.87E-06	-290	2.17E-04	-530	7.16E-04
-520	3.87E-06	-280	2.52E-04	-520	7.35E-04
-510	1.93E-06	-270	2.98E-04	-510	7.47E-04
-500	3.10E-06	-260	3.60E-04	-500	7.51E-04
-490	3.87E-06	-250	5.03E-04	-490	7.78E-04
-480	7.74E-06	-240	6.19E-04	-480	7.74E-04
-470	1.16E-05	-230	7.39E-04	-470	7.82E-04
-460	1.93E-05	-220	8.17E-04	-460	7.86E-04
-450	3.48E-05	-210	9.02E-04	-450	7.89E-04
-440	5.42E-05	-200	9.37E-04	-440	7.82E-04
-430	8.51E-05	-190	9.67E-04	-430	7.16E-04
-420	1.24E-04	-180	9.91E-04	-420	6.85E-04
-410	1.59E-04	-170	1.01E-03	-410	5.84E-04
-400	1.93E-04	-160	1.01E-03	-400	3.99E-04
-390	2.32E-04	-150	1.06E-03	-390	1.55E-04
-380	2.71E-04	-140	1.03E-03	-380	7.35E-05
-370	3.10E-04	-130	9.06E-04	-370	3.72E-04
-360	3.21E-04	-120	9.25E-04	-360	6.50E-04
-350	3.41E-04	-110	9.29E-04	-350	1.16E-04
-340	3.64E-04	-100	9.40E-04	-340	1.24E-04

Continued on next page

Potential mV	Current Density A/cm^2	Potential mV	Current Density A/cm^2	Potential mV	Current Density A/cm^2
-330	3.68E-04	-90	9.40E-04	-330	1.43E-04
-320	3.52E-04	-80	9.29E-04	-320	1.55E-04
-310	3.48E-04	-70	9.40E-04	-310	1.78E-04
-300	3.52E-04	-60	9.48E-04	-300	2.13E-04
-290	3.48E-04	-50	9.56E-04	-290	2.59E-04
-280	2.98E-04	-40	9.67E-04	-280	3.10E-04
-270	2.71E-04	-30	9.67E-04	-270	3.91E-04
-260	2.52E-04	-20	9.75E-04	-260	5.42E-04
-250	2.32E-04	-10	9.87E-04	-250	6.77E-04
-240	1.39E-04	0	1.01E-03	-240	8.13E-04
-230	1.55E-04	10	1.01E-03	-230	9.33E-04
-220	1.66E-04	20	9.87E-04	-220	1.05E-03
-210	1.63E-04	30	1.01E-03	-210	1.11E-03
-200	1.70E-04	40	1.02E-03	-200	1.17E-03
-190	1.70E-04	50	1.03E-03	-190	1.17E-03
-180	1.70E-04	60	1.05E-03	-180	1.16E-03
-170	1.63E-04	70	1.04E-03	-170	1.16E-03
-160	1.55E-04	80	1.03E-03	-160	1.16E-03
-150	1.47E-04	90	1.03E-03	-150	1.14E-03
-140	1.43E-04	100	1.03E-03	-140	1.15E-03
-130	1.43E-04	110	1.04E-03	-130	1.14E-03
-120	1.28E-04	120	1.04E-03	-120	1.15E-03
-110	1.32E-04	130	1.04E-03	-110	1.16E-03
-100	1.32E-04	140	1.06E-03	-100	1.15E-03
-90	1.35E-04	150	1.05E-03	-90	1.17E-03
-80	1.39E-04	160	1.04E-03	-80	1.16E-03
-70	1.39E-04	170	1.05E-03	-70	1.16E-03
-60	1.43E-04	180	1.05E-03	-60	1.16E-03
-50	1.43E-04	190	1.05E-03	-50	1.18E-03
-40	1.47E-04	200	1.06E-03	-40	1.18E-03
-30	1.51E-04	210	1.06E-03	-30	1.18E-03
-20	1.51E-04	220	1.06E-03	-20	1.18E-03
-10	1.43E-04	230	1.05E-03	-10	1.19E-03
0	1.47E-04	240	1.06E-03	0	1.18E-03
10	1.51E-04	250	1.06E-03	10	1.20E-03

Continued on next page

Potential mV	Current Density A/cm^2	Potential mV	Current Density A/cm^2	Potential mV	Current Density A/cm^2
20	1.51E-04	260	1.03E-03	20	1.18E-03
30	1.51E-04	270	1.05E-03	30	1.20E-03
40	1.55E-04	280	1.03E-03	40	1.20E-03
50	1.59E-04	290	1.05E-03	50	1.21E-03
60	1.63E-04	300	1.06E-03	60	1.20E-03
70	1.63E-04	310	1.06E-03	70	1.20E-03
80	1.63E-04	320	1.04E-03	80	1.22E-03
90	1.63E-04	330	1.05E-03	90	1.20E-03
100	1.66E-04	340	1.04E-03	100	1.21E-03
110	1.70E-04	350	1.04E-03	110	1.23E-03
120	1.70E-04	360	1.04E-03	120	1.23E-03
130	1.70E-04	370	1.04E-03	130	1.23E-03
140	1.70E-04	380	1.05E-03	140	1.23E-03
150	1.74E-04	390	1.02E-03	150	1.21E-03
160	1.74E-04	400	1.04E-03	160	1.22E-03
170	1.74E-04	410	1.01E-03	170	1.22E-03
180	1.74E-04	420	1.01E-03	180	1.24E-03
190	1.74E-04	430	1.00E-03	190	1.24E-03
200	1.74E-04	440	9.83E-04	200	1.24E-03
210	1.74E-04	450	9.60E-04	210	1.24E-03
220	1.74E-04	460	9.44E-04	220	1.23E-03
230	1.74E-04	470	9.37E-04	230	1.24E-03
240	1.74E-04	480	9.17E-04	240	1.24E-03
250	1.74E-04	490	9.09E-04	250	1.24E-03
260	1.74E-04	500	8.71E-04	260	1.24E-03
270	1.78E-04	510	8.63E-04	270	1.23E-03
280	1.74E-04	520	8.36E-04	280	1.24E-03
290	1.78E-04	530	7.93E-04	290	1.24E-03
300	1.78E-04	540	7.55E-04	300	1.25E-03
310	1.82E-04	550	7.20E-04	310	1.23E-03
320	1.82E-04	560	7.00E-04	320	1.24E-03
330	1.82E-04	570	6.46E-04	330	1.24E-03
340	1.82E-04	580	6.31E-04	340	1.22E-03
350	1.86E-04	590	5.88E-04	350	1.22E-03
360	1.86E-04	600	5.42E-04	360	1.22E-03

Continued on next page

Potential mV	Current Density A/cm^2	Potential mV	Current Density A/cm^2	Potential mV	Current Density A/cm^2
370	1.90E-04	610	5.19E-04	370	1.21E-03
380	1.86E-04	620	4.88E-04	380	1.20E-03
390	1.86E-04	630	4.64E-04	390	1.20E-03
400	1.90E-04	640	4.53E-04	400	1.20E-03
410	1.90E-04	650	4.49E-04	410	1.18E-03
420	1.86E-04	660	4.84E-04	420	1.16E-03
430	1.86E-04	670	5.38E-04	430	1.14E-03
440	1.90E-04	680	6.23E-04	440	1.12E-03
450	1.90E-04	690	7.89E-04	450	1.11E-03
460	1.93E-04	700	1.01E-03	460	1.09E-03
470	1.93E-04	710	1.22E-03	470	1.08E-03
480	1.93E-04	720	1.56E-03	480	1.07E-03
490	1.93E-04	730	1.90E-03	490	1.04E-03
500	1.93E-04	740	2.29E-03	500	1.01E-03
510	1.93E-04	750	2.75E-03	510	9.75E-04
520	1.93E-04	760	3.31E-03	520	9.52E-04
530	1.90E-04	770	3.75E-03	530	9.13E-04
540	1.93E-04	780	4.30E-03	540	8.75E-04
550	1.93E-04	790	4.91E-03	550	8.36E-04
560	1.93E-04	800	5.53E-03	560	7.86E-04
570	1.97E-04	810	6.19E-03	570	7.47E-04
580	1.97E-04	820	6.97E-03	580	7.08E-04
590	1.97E-04	830	7.74E-03	590	6.62E-04
600	1.97E-04	840	8.55E-03	600	6.23E-04
610	1.97E-04	850	9.40E-03	610	5.80E-04
620	1.97E-04	860	1.03E-02	620	5.42E-04
630	2.01E-04	870	1.11E-02	630	5.15E-04
640	2.05E-04	880	1.19E-02	640	5.03E-04
650	2.13E-04	890	1.27E-02	650	5.03E-04
660	2.32E-04	900	1.37E-02	660	5.38E-04
670	2.55E-04	910	1.47E-02	670	5.65E-04
680	2.98E-04	920	1.57E-02	680	6.50E-04
690	3.75E-04	930	1.66E-02	690	7.70E-04
700	4.95E-04	940	1.75E-02	700	1.01E-03
710	6.50E-04	950	1.84E-02	710	1.22E-03

Continued on next page

Potential mV	Current Density A/cm^2	Potential mV	Current Density A/cm^2	Potential mV	Current Density A/cm^2
720	8.51E-04	960	1.94E-02	720	1.55E-03
730	1.03E-03	970	2.04E-02	730	1.83E-03
740	1.24E-03	980	2.13E-02	740	2.29E-03
750	1.47E-03	990	2.24E-02	750	2.67E-03
760	1.70E-03	1000	2.33E-02	760	3.20E-03
770	1.93E-03			770	3.72E-03
780	2.19E-03			780	4.18E-03
790	2.51E-03			790	4.68E-03
800	2.86E-03			800	5.53E-03
810	3.20E-03			810	6.19E-03
820	3.61E-03			820	6.97E-03
830	3.99E-03			830	7.82E-03
840	4.37E-03			840	8.59E-03
850	4.76E-03			850	9.48E-03
860	5.26E-03			860	1.04E-02
870	5.84E-03			870	1.11E-02
880	6.35E-03			880	1.20E-02
890	6.97E-03			890	1.29E-02
900	7.74E-03			900	1.41E-02
910	8.36E-03			910	1.52E-02
920	9.02E-03			920	1.62E-02
930	9.91E-03			930	1.70E-02
940	1.08E-02			940	1.80E-02
950	1.16E-02			950	1.91E-02
960	1.25E-02			960	2.01E-02
970	1.34E-02			970	2.09E-02
980	1.40E-02			980	2.19E-02
990	1.49E-02			990	2.28E-02
1000	1.59E-02			1000	2.38E-02

TABLE B.9: Polarization Data: Brass in $FeSO_4$

Velocity: 0 m/s		Velocity: 2.63 m/s		Velocity: 3.93 m/s	
Potential	Current Density	Potential	Current Density	Potential	Current Density
mV	A/cm^2	mV	A/cm^2	mV	A/cm^2
-1000	3.56E-04	-1000	5.26E-03	-1000	6.42E-03
-990	2.83E-04	-990	5.03E-03	-990	6.23E-03
-980	2.40E-04	-980	4.84E-03	-980	6.00E-03
-970	2.09E-04	-970	4.68E-03	-970	5.69E-03
-960	1.90E-04	-960	4.53E-03	-960	5.50E-03
-950	1.74E-04	-950	4.33E-03	-950	5.34E-03
-940	1.63E-04	-940	4.22E-03	-940	5.22E-03
-930	1.55E-04	-930	3.99E-03	-930	5.11E-03
-920	1.52E-04	-920	3.87E-03	-920	4.84E-03
-910	1.44E-04	-910	3.64E-03	-910	4.57E-03
-900	1.37E-04	-900	3.48E-03	-900	4.45E-03
-890	1.28E-04	-890	3.29E-03	-890	4.37E-03
-880	1.22E-04	-880	3.17E-03	-880	4.26E-03
-870	1.16E-04	-870	3.02E-03	-870	4.14E-03
-860	1.10E-04	-860	2.79E-03	-860	3.99E-03
-850	1.03E-04	-850	2.75E-03	-850	3.91E-03
-840	9.56E-05	-840	2.67E-03	-840	3.75E-03
-830	8.90E-05	-830	2.59E-03	-830	3.72E-03
-820	7.74E-05	-820	2.55E-03	-820	3.64E-03
-810	7.08E-05	-810	2.52E-03	-810	3.56E-03
-800	6.04E-05	-800	2.46E-03	-800	3.48E-03
-790	5.26E-05	-790	2.41E-03	-790	3.41E-03
-780	4.91E-05	-780	2.32E-03	-780	3.33E-03
-770	4.53E-05	-770	2.29E-03	-770	3.29E-03
-760	4.10E-05	-760	2.24E-03	-760	3.25E-03
-750	3.87E-05	-750	2.20E-03	-750	3.21E-03
-740	3.52E-05	-740	2.13E-03	-740	3.17E-03
-730	3.41E-05	-730	2.10E-03	-700	3.12E-03
-720	3.17E-05	-720	2.04E-03	-690	3.12E-03
-710	3.02E-05	-710	1.97E-03	-680	3.10E-03
-700	2.79E-05	-700	1.93E-03	-670	3.06E-03
-690	2.75E-05	-690	1.90E-03	-660	3.03E-03

Continued on next page

Potential mV	Current Density A/cm^2	Potential mV	Current Density A/cm^2	Potential mV	Current Density A/cm^2
-680	2.71E-05	-680	1.85E-03	-650	3.01E-03
-670	2.59E-05	-670	1.80E-03	-640	2.96E-03
-660	2.55E-05	-590	1.63E-03	-620	2.88E-03
-650	2.44E-05	-580	1.59E-03	-570	2.77E-03
-640	2.40E-05	-570	1.55E-03	-550	2.72E-03
-630	2.36E-05	-560	1.51E-03	-520	2.70E-03
-620	2.28E-05	-550	1.46E-03	-500	2.60E-03
-550	2.24E-05	-540	1.43E-03	-480	2.48E-03
-500	2.32E-05	-530	1.39E-03	-470	2.43E-03
-490	2.24E-05	-520	1.35E-03	-460	2.31E-03
-460	2.17E-05	-510	1.34E-03	-450	2.26E-03
-450	2.13E-05	-500	1.32E-03	-440	2.08E-03
-440	2.09E-05	-490	1.28E-03	-430	1.97E-03
-430	2.05E-05	-480	1.24E-03	-420	1.90E-03
-420	2.01E-05	-470	1.20E-03	-410	1.76E-03
-410	1.93E-05	-460	1.16E-03	-400	1.65E-03
-400	1.86E-05	-450	1.13E-03	-390	1.49E-03
-390	1.78E-05	-440	1.11E-03	-380	1.36E-03
-380	1.66E-05	-430	1.08E-03	-370	1.27E-03
-370	1.63E-05	-420	1.06E-03	-360	1.11E-03
-360	1.59E-05	-410	1.04E-03	-350	1.01E-03
-350	1.47E-05	-400	1.04E-03	-340	8.51E-04
-340	1.43E-05	-390	1.03E-03	-330	7.59E-04
-330	1.35E-05	-380	1.01E-03	-320	6.66E-04
-320	1.32E-05	-370	9.79E-04	-310	6.00E-04
-310	1.24E-05	-360	8.67E-04	-300	5.26E-04
-300	1.16E-05	-350	8.13E-04	-290	4.76E-04
-290	1.12E-05	-340	7.70E-04	-280	4.26E-04
-280	9.67E-06	-330	7.20E-04	-270	3.99E-04
-270	8.90E-06	-320	6.46E-04	-260	3.83E-04
-260	8.13E-06	-310	6.00E-04	-250	3.64E-04
-250	7.74E-06	-300	5.46E-04	-240	3.52E-04
-240	6.97E-06	-290	5.07E-04	-230	3.33E-04
-230	6.19E-06	-280	4.84E-04	-160	2.63E-04
-220	5.42E-06	-270	4.37E-04	-150	1.55E-04

Continued on next page

Potential mV	Current Density A/cm^2	Potential mV	Current Density A/cm^2	Potential mV	Current Density A/cm^2
-210	5.03E-06	-260	4.22E-04	-140	7.74E-05
-200	3.87E-06	-250	3.95E-04	-130	1.32E-04
-190	2.32E-06	-240	3.87E-04	-120	3.87E-04
-180	3.87E-07	-230	3.75E-04	-110	8.01E-04
-170	1.93E-06	-220	3.68E-04	-100	1.21E-03
-160	5.42E-06	-160	3.21E-04	-90	1.80E-03
-150	1.55E-05	-150	1.97E-04	-80	2.26E-03
-140	2.71E-05	-140	6.19E-05	-70	2.75E-03
-130	4.64E-05	-130	2.13E-04	-60	3.25E-03
-120	7.35E-05	-120	5.22E-04	-50	3.79E-03
-110	1.08E-04	-110	7.93E-04	-40	4.33E-03
-100	1.66E-04	-100	1.23E-03	-30	4.99E-03
-90	2.86E-04	-90	1.74E-03	-20	5.61E-03
-80	4.57E-04	-80	2.25E-03	-10	6.23E-03
-70	7.51E-04	-70	2.83E-03	0	6.81E-03
-60	1.07E-03	-60	3.39E-03	10	7.24E-03
-50	1.47E-03	-50	3.84E-03	20	7.89E-03
-40	1.89E-03	-40	4.41E-03	30	8.51E-03
-30	2.32E-03	-30	4.91E-03	40	8.98E-03
-20	2.69E-03	-20	5.38E-03	50	9.60E-03
-10	3.12E-03	-10	6.00E-03	60	1.01E-02
0	3.54E-03	0	6.42E-03	70	1.04E-02
10	4.07E-03	10	6.77E-03	80	1.07E-02
20	4.45E-03	20	7.04E-03	90	1.11E-02
30	4.99E-03	30	7.62E-03	100	1.14E-02
40	5.38E-03	40	7.89E-03	110	1.18E-02
50	5.84E-03	50	8.13E-03	120	1.25E-02
60	6.19E-03	60	8.63E-03	160	1.30E-02
70	6.39E-03	70	8.94E-03	170	1.32E-02
80	6.70E-03	80	9.52E-03	190	1.34E-02
90	7.08E-03	90	9.98E-03	200	1.35E-02
100	7.59E-03	100	1.03E-02	210	1.36E-02
110	8.09E-03	110	1.07E-02	220	1.38E-02
120	8.48E-03	120	1.11E-02		
130	8.90E-03	130	1.15E-02		

Continued on next page

Potential mV	Current Density A/cm^2	Potential mV	Current Density A/cm^2	Potential mV	Current Density A/cm^2
140	9.37E-03	140	1.19E-02		
150	9.91E-03	150	1.21E-02		
160	1.04E-02	160	1.23E-02		
170	1.08E-02	170	1.25E-02		
180	1.13E-02	180	1.26E-02		
190	1.18E-02	190	1.27E-02		
200	1.23E-02	200	1.30E-02		
210	1.27E-02	210	1.32E-02		
220	1.32E-02	220	1.34E-02		
230	1.37E-02	230	1.37E-02		
240	1.42E-02	240	1.41E-02		
250	1.48E-02				
260	1.53E-02				
270	1.59E-02				
280	1.64E-02				
290	1.68E-02				
300	1.74E-02				
310	1.80E-02				
320	1.84E-02				

TABLE B.10: Polarization Data: Brass in $FeSO_4$+$FeCl_3$

Velocity: 0 m/s		Velocity: 2.63 m/s		Velocity: 3.93 m/s	
Potential	Current Density	Potential	Current Density	Potential	Current Density
mV	A/cm^2	mV	A/cm^2	mV	A/cm^2
-500	8.32E-04	-490	3.75E-02	-500	3.34E-02
-490	8.17E-04	-480	3.60E-02	-490	3.23E-02
-480	8.09E-04	-470	3.52E-02	-480	3.20E-02
-470	8.05E-04	-460	3.44E-02	-470	3.10E-02
-460	8.01E-04	-450	3.37E-02	-460	2.99E-02
-450	7.93E-04	-440	3.27E-02	-450	2.88E-02
-440	7.89E-04	-430	3.08E-02	-440	2.78E-02
-430	7.86E-04	-420	3.02E-02	-430	2.68E-02
-420	7.82E-04	-410	2.90E-02	-420	2.57E-02
-410	7.78E-04	-400	2.79E-02	-410	2.45E-02
-400	7.74E-04	-390	2.74E-02	-400	2.33E-02
-390	7.70E-04	-380	2.59E-02	-390	2.23E-02
-380	7.66E-04	-370	2.47E-02	-380	2.09E-02
-370	7.62E-04	-360	2.33E-02	-370	2.00E-02
-360	7.59E-04	-350	2.21E-02	-360	1.86E-02
-350	7.55E-04	-340	2.09E-02	-350	1.74E-02
-340	7.47E-04	-330	1.92E-02	-340	1.61E-02
-330	7.39E-04	-320	1.83E-02	-330	1.50E-02
-320	7.31E-04	-310	1.66E-02	-320	1.39E-02
-310	7.16E-04	-300	1.55E-02	-310	1.28E-02
-300	7.00E-04	-290	1.40E-02	-300	1.16E-02
-290	6.77E-04	-280	1.24E-02	-290	1.06E-02
-280	6.46E-04	-270	1.10E-02	-280	9.40E-03
-270	6.11E-04	-260	9.67E-03	-270	8.28E-03
-260	5.69E-04	-250	8.13E-03	-260	6.97E-03
-250	5.03E-04	-240	7.16E-03	-250	6.00E-03
-240	3.87E-04	-230	5.73E-03	-240	4.41E-03
-230	2.67E-04	-220	4.37E-03	-230	3.25E-03
-220	7.74E-05	-210	2.59E-03	-220	2.01E-03
-210	1.55E-05	-200	1.43E-03	-210	1.08E-03
-200	2.71E-04	-190	8.13E-04	-200	7.74E-04
-190	5.80E-04	-180	1.86E-03	-190	1.20E-03

Continued on next page

Potential mV	Current Density A/cm^2	Potential mV	Current Density A/cm^2	Potential mV	Current Density A/cm^2
-180	1.12E-03	-170	3.02E-03	-180	2.36E-03
-170	1.46E-03	-160	4.41E-03	-170	3.48E-03
-160	1.96E-03	-150	5.57E-03	-160	4.61E-03
-150	2.82E-03	-140	6.70E-03	-150	5.73E-03
-140	3.25E-03	-130	7.89E-03	-140	6.93E-03
-130	4.22E-03	-120	9.21E-03	-130	7.97E-03
-120	5.42E-03	-110	1.03E-02	-120	9.21E-03
-110	6.70E-03	-100	1.15E-02	-110	1.03E-02
-100	7.59E-03	-90	1.28E-02	-100	1.13E-02
-90	8.98E-03	-80	1.39E-02	-90	1.25E-02
-80	1.03E-02	-70	1.49E-02	-80	1.35E-02
-70	1.16E-02	-60	1.60E-02	-70	1.47E-02
-60	1.26E-02	-50	1.72E-02	-60	1.60E-02
-50	1.37E-02	-40	1.84E-02	-50	1.72E-02
-40	1.47E-02	-30	1.95E-02	-40	1.81E-02
-30	1.58E-02	-20	2.07E-02	-30	1.93E-02
-20	1.71E-02	-10	2.16E-02	-20	2.03E-02
-10	1.82E-02	0	2.30E-02	-10	2.14E-02
0	1.90E-02			0	2.26E-02

TABLE B.11: Polarization Data: Aluminum in artificial seawater

Velocity: 0 m/s		Velocity: 2.63 m/s		Velocity: 3.93 m/s	
Potential	Current Density	Potential	Current Density	Potential	Current Density
mV	A/cm^2	mV	A/cm^2	mV	A/cm^2
-1000	1.23E-05	-1000	1.66E-04	-1000	2.75E-04
-990	1.07E-05	-990	1.61E-04	-990	2.65E-04
-980	1.00E-05	-980	1.58E-04	-980	2.59E-04
-970	9.44E-06	-970	1.51E-04	-970	2.55E-04
-960	8.90E-06	-960	1.49E-04	-960	2.47E-04
-950	8.44E-06	-950	1.46E-04	-950	2.35E-04
-940	8.01E-06	-940	1.44E-04	-940	2.31E-04
-930	7.62E-06	-930	1.40E-04	-930	2.26E-04
-920	7.28E-06	-920	1.38E-04	-920	2.24E-04
-910	6.89E-06	-910	1.34E-04	-910	2.17E-04
-900	6.58E-06	-900	1.31E-04	-900	2.14E-04
-890	6.19E-06	-890	1.28E-04	-890	2.07E-04
-880	5.80E-06	-880	1.25E-04	-880	2.01E-04
-870	5.46E-06	-870	1.23E-04	-870	1.97E-04
-860	4.99E-06	-860	1.22E-04	-860	1.93E-04
-850	4.72E-06	-850	1.20E-04	-850	1.87E-04
-840	4.37E-06	-840	1.16E-04	-840	1.83E-04
-830	4.02E-06	-830	1.15E-04	-830	1.80E-04
-820	3.72E-06	-820	1.12E-04	-820	1.75E-04
-810	3.44E-06	-810	1.10E-04	-810	1.67E-04
-800	3.17E-06	-800	1.10E-04	-800	1.57E-04
-790	2.86E-06	-790	1.03E-04	-790	1.45E-04
-780	2.55E-06	-780	1.01E-04	-780	1.36E-04
-770	2.17E-06	-770	9.37E-05	-770	1.18E-04
-760	1.55E-06	-760	8.44E-05	-760	9.79E-05
-750	8.90E-07	-750	6.97E-05	-750	6.97E-05
-740	4.84E-06	-740	4.64E-05	-740	2.94E-05
-730	6.42E-06	-730	1.59E-05	-730	1.93E-05
-720	1.04E-05	-720	2.71E-06	-720	1.16E-06
-710	1.18E-05	-710	5.80E-06	-710	5.42E-06
-700	1.84E-05	-700	7.74E-06	-700	6.19E-06
-690	2.28E-05	-690	1.16E-05	-690	1.55E-05

Continued on next page

Potential mV	Current Density A/cm^2	Potential mV	Current Density A/cm^2	Potential mV	Current Density A/cm^2
-680	2.79E-05	-680	3.87E-05	-680	4.10E-05
-670	5.34E-05	-670	5.19E-05	-670	5.80E-05
-660	7.82E-05	-660	6.97E-05	-660	7.00E-05
-650	1.08E-04	-650	7.55E-05	-650	8.90E-05
-640	1.47E-04	-640	1.08E-04	-640	1.07E-04
-630	1.97E-04	-630	1.42E-04	-630	1.36E-04
-620	2.44E-04	-620	1.82E-04	-620	1.78E-04
-610	2.84E-04	-610	2.29E-04	-610	2.23E-04
-600	3.37E-04	-600	2.76E-04	-600	2.60E-04
-590	3.95E-04	-590	3.16E-04	-590	3.16E-04
-580	4.49E-04	-580	3.83E-04	-580	3.58E-04
-570	4.99E-04	-570	4.30E-04	-570	3.99E-04
-560	5.57E-04	-560	4.84E-04	-560	4.72E-04
-550	6.08E-04	-550	5.38E-04	-550	5.26E-04
-540	6.66E-04	-540	5.84E-04	-540	5.84E-04
-530	7.16E-04	-530	6.11E-04	-530	6.31E-04
-520	7.74E-04	-520	6.50E-04	-520	6.81E-04
-510	8.36E-04	-510	7.28E-04	-510	7.35E-04
-500	8.86E-04	-500	7.82E-04	-500	8.05E-04
-490	9.44E-04	-490	8.40E-04	-490	8.55E-04
-480	9.91E-04	-480	8.86E-04	-480	8.98E-04
-470	1.05E-03	-470	9.37E-04	-470	9.48E-04
-460	1.11E-03	-460	9.75E-04	-460	1.00E-03
-450	1.16E-03	-450	1.03E-03	-450	1.07E-03
-440	1.22E-03	-440	1.09E-03	-440	1.08E-03
-430	1.27E-03	-430	1.15E-03	-430	1.15E-03
-420	1.32E-03	-420	1.18E-03	-420	1.22E-03
-410	1.38E-03	-410	1.25E-03	-410	1.27E-03
-400	1.44E-03	-400	1.30E-03	-400	1.32E-03
-390	1.49E-03	-390	1.35E-03	-390	1.36E-03
-380	1.57E-03	-380	1.40E-03	-380	1.43E-03
-370	1.63E-03	-370	1.46E-03	-370	1.49E-03
-360	1.69E-03	-360	1.52E-03	-360	1.56E-03
-350	1.75E-03	-350	1.57E-03	-350	1.59E-03
-340	1.80E-03	-340	1.61E-03	-340	1.63E-03

Continued on next page

Potential mV	Current Density A/cm^2	Potential mV	Current Density A/cm^2	Potential mV	Current Density A/cm^2
-330	1.87E-03	-330	1.67E-03	-330	1.72E-03
-320	1.92E-03	-320	1.73E-03	-320	1.76E-03
-310	1.97E-03	-310	1.77E-03	-310	1.81E-03
-300	2.04E-03	-300	1.83E-03	-300	1.89E-03

TABLE B.12: Polarization Data: Aluminum in 2.5% sodium carbonate

Velocity: 0 m/s		Velocity: 2.63 m/s		Velocity: 3.93 m/s	
Potential	Current Density	Potential	Current Density	Potential	Current Density
mV	A/cm^2	mV	A/cm^2	mV	A/cm^2
-1665	3.87E-03	-1696	3.87E-03	-1752	3.87E-03
-1665	3.83E-03	-1696	3.83E-03	-1747	3.83E-03
-1664	3.79E-03	-1695	3.79E-03	-1743	3.79E-03
-1664	3.75E-03	-1695	3.75E-03	-1739	3.75E-03
-1664	3.72E-03	-1694	3.72E-03	-1736	3.72E-03
-1663	3.68E-03	-1693	3.68E-03	-1734	3.68E-03
-1663	3.64E-03	-1694	3.64E-03	-1731	3.64E-03
-1662	3.60E-03	-1693	3.60E-03	-1728	3.60E-03
-1662	3.56E-03	-1692	3.56E-03	-1725	3.56E-03
-1662	3.52E-03	-1690	3.52E-03	-1723	3.52E-03
-1661	3.48E-03	-1689	3.48E-03	-1722	3.48E-03
-1661	3.44E-03	-1690	3.44E-03	-1720	3.44E-03
-1660	3.41E-03	-1688	3.41E-03	-1718	3.41E-03
-1659	3.37E-03	-1687	3.37E-03	-1716	3.37E-03
-1658	3.33E-03	-1687	3.33E-03	-1714	3.33E-03
-1658	3.29E-03	-1686	3.29E-03	-1713	3.29E-03
-1657	3.25E-03	-1685	3.25E-03	-1712	3.25E-03
-1657	3.21E-03	-1684	3.21E-03	-1709	3.21E-03
-1656	3.17E-03	-1683	3.17E-03	-1708	3.17E-03
-1655	3.13E-03	-1681	3.13E-03	-1706	3.13E-03
-1655	3.10E-03	-1681	3.10E-03	-1705	3.10E-03
-1654	3.06E-03	-1680	3.06E-03	-1703	3.06E-03
-1653	3.02E-03	-1679	3.02E-03	-1702	3.02E-03
-1652	2.98E-03	-1678	2.98E-03	-1701	2.98E-03
-1652	2.94E-03	-1677	2.94E-03	-1699	2.94E-03
-1651	2.90E-03	-1676	2.90E-03	-1697	2.90E-03
-1650	2.86E-03	-1675	2.86E-03	-1695	2.86E-03
-1650	2.83E-03	-1674	2.83E-03	-1694	2.83E-03
-1649	2.79E-03	-1673	2.79E-03	-1693	2.79E-03
-1649	2.75E-03	-1672	2.75E-03	-1691	2.75E-03
-1648	2.71E-03	-1671	2.71E-03	-1690	2.71E-03
-1648	2.67E-03	-1670	2.67E-03	-1688	2.67E-03

Continued on next page

Potential mV	Current Density A/cm^2	Potential mV	Current Density A/cm^2	Potential mV	Current Density A/cm^2
-1648	2.63E-03	-1669	2.63E-03	-1687	2.63E-03
-1647	2.59E-03	-1668	2.59E-03	-1686	2.59E-03
-1647	2.55E-03	-1667	2.55E-03	-1684	2.55E-03
-1646	2.52E-03	-1666	2.52E-03	-1683	2.52E-03
-1646	2.48E-03	-1665	2.48E-03	-1681	2.48E-03
-1645	2.44E-03	-1664	2.44E-03	-1680	2.44E-03
-1645	2.40E-03	-1663	2.40E-03	-1678	2.40E-03
-1644	2.36E-03	-1662	2.36E-03	-1677	2.36E-03
-1644	2.32E-03	-1661	2.32E-03	-1675	2.32E-03
-1644	2.28E-03	-1660	2.28E-03	-1674	2.28E-03
-1643	2.24E-03	-1659	2.24E-03	-1673	2.24E-03
-1643	2.21E-03	-1658	2.21E-03	-1671	2.21E-03
-1642	2.17E-03	-1657	2.17E-03	-1670	2.17E-03
-1642	2.13E-03	-1656	2.13E-03	-1668	2.13E-03
-1641	2.09E-03	-1655	2.09E-03	-1666	2.09E-03
-1640	2.05E-03	-1654	2.05E-03	-1665	2.05E-03
-1639	2.01E-03	-1653	2.01E-03	-1664	2.01E-03
-1639	1.97E-03	-1652	1.97E-03	-1663	1.97E-03
-1639	1.93E-03	-1651	1.93E-03	-1662	1.93E-03
-1638	1.90E-03	-1650	1.90E-03	-1660	1.90E-03
-1637	1.86E-03	-1649	1.86E-03	-1659	1.86E-03
-1637	1.82E-03	-1648	1.82E-03	-1657	1.82E-03
-1636	1.78E-03	-1647	1.78E-03	-1656	1.78E-03
-1635	1.74E-03	-1646	1.74E-03	-1655	1.74E-03
-1634	1.70E-03	-1645	1.70E-03	-1653	1.70E-03
-1634	1.66E-03	-1643	1.66E-03	-1652	1.66E-03
-1633	1.63E-03	-1642	1.63E-03	-1651	1.63E-03
-1632	1.59E-03	-1641	1.59E-03	-1650	1.59E-03
-1631	1.55E-03	-1640	1.55E-03	-1649	1.55E-03
-1630	1.51E-03	-1639	1.51E-03	-1647	1.51E-03
-1629	1.47E-03	-1638	1.47E-03	-1645	1.47E-03
-1628	1.43E-03	-1637	1.43E-03	-1644	1.43E-03
-1628	1.39E-03	-1636	1.39E-03	-1643	1.39E-03
-1627	1.35E-03	-1635	1.35E-03	-1642	1.35E-03
-1625	1.32E-03	-1634	1.32E-03	-1641	1.32E-03

Continued on next page

Potential mV	Current Density A/cm^2	Potential mV	Current Density A/cm^2	Potential mV	Current Density A/cm^2
-1625	1.28E-03	-1633	1.28E-03	-1640	1.28E-03
-1624	1.24E-03	-1632	1.24E-03	-1638	1.24E-03
-1624	1.20E-03	-1630	1.20E-03	-1637	1.20E-03
-1623	1.16E-03	-1630	1.16E-03	-1636	1.16E-03
-1621	1.12E-03	-1629	1.12E-03	-1634	1.12E-03
-1620	1.08E-03	-1628	1.08E-03	-1633	1.08E-03
-1619	1.04E-03	-1627	1.04E-03	-1632	1.04E-03
-1618	1.01E-03	-1626	1.01E-03	-1631	1.01E-03
-1617	9.67E-04	-1624	9.67E-04	-1630	9.67E-04
-1616	9.29E-04	-1623	9.29E-04	-1628	9.29E-04
-1615	8.90E-04	-1622	8.90E-04	-1627	8.90E-04
-1615	8.51E-04	-1621	8.51E-04	-1626	8.51E-04
-1614	8.13E-04	-1620	8.13E-04	-1624	8.13E-04
-1614	7.74E-04	-1619	7.74E-04	-1623	7.74E-04
-1613	7.35E-04	-1618	7.35E-04	-1622	7.35E-04
-1612	6.97E-04	-1617	6.97E-04	-1621	6.97E-04
-1611	6.58E-04	-1616	6.58E-04	-1619	6.58E-04
-1610	6.19E-04	-1615	6.19E-04	-1618	6.19E-04
-1610	5.80E-04	-1614	5.80E-04	-1617	5.80E-04
-1610	5.42E-04	-1613	5.42E-04	-1616	5.42E-04
-1609	5.03E-04	-1611	5.03E-04	-1615	5.03E-04
-1609	4.64E-04	-1610	4.64E-04	-1612	4.64E-04
-1609	4.26E-04	-1609	4.26E-04	-1611	4.26E-04
-1608	3.87E-04	-1608	3.87E-04	-1610	3.87E-04
-1607	3.48E-04	-1607	3.48E-04	-1609	3.48E-04
-1605	3.10E-04	-1606	3.10E-04	-1608	3.10E-04
-1603	2.71E-04	-1605	2.71E-04	-1607	2.71E-04
-1603	2.32E-04	-1604	2.32E-04	-1606	2.32E-04
-1602	1.93E-04	-1602	1.93E-04	-1604	1.93E-04
-1602	1.55E-04	-1601	1.55E-04	-1603	1.55E-04
-1601	1.16E-04	-1600	1.16E-04	-1602	1.16E-04
-1601	7.74E-05	-1599	7.74E-05	-1601	7.74E-05
-1601	3.87E-05	-1598	3.87E-05	-1598	3.87E-05
-1598	3.87E-05	-1595	3.87E-05	-1597	3.87E-05
-1597	7.74E-05	-1594	7.74E-05	-1596	7.74E-05

Continued on next page

Potential mV	Current Density A/cm^2	Potential mV	Current Density A/cm^2	Potential mV	Current Density A/cm^2
-1595	1.16E-04	-1593	1.16E-04	-1595	1.16E-04
-1594	1.55E-04	-1592	1.55E-04	-1594	1.55E-04
-1592	1.93E-04	-1591	1.93E-04	-1592	1.93E-04
-1590	2.32E-04	-1590	2.32E-04	-1591	2.32E-04
-1588	2.71E-04	-1589	2.71E-04	-1590	2.71E-04
-1587	3.10E-04	-1588	3.10E-04	-1588	3.10E-04
-1585	3.48E-04	-1586	3.48E-04	-1587	3.48E-04
-1584	3.87E-04	-1585	3.87E-04	-1586	3.87E-04
-1582	4.26E-04	-1584	4.26E-04	-1585	4.26E-04
-1580	4.64E-04	-1583	4.64E-04	-1584	4.64E-04
-1578	5.03E-04	-1582	5.03E-04	-1582	5.03E-04
-1575	5.42E-04	-1581	5.42E-04	-1581	5.42E-04
-1572	5.80E-04	-1580	5.80E-04	-1579	5.80E-04
-1570	6.19E-04	-1579	6.19E-04	-1578	6.19E-04
-1566	6.58E-04	-1577	6.58E-04	-1577	6.58E-04
-1563	6.97E-04	-1576	6.97E-04	-1576	6.97E-04
-1560	7.35E-04	-1575	7.35E-04	-1575	7.35E-04
-1556	7.74E-04	-1574	7.74E-04	-1574	7.74E-04
-1552	8.13E-04	-1573	8.13E-04	-1572	8.13E-04
-1548	8.51E-04	-1571	8.51E-04	-1571	8.51E-04
-1545	8.90E-04	-1570	8.90E-04	-1570	8.90E-04
-1521	9.29E-04	-1569	9.29E-04	-1568	9.29E-04
-1489	9.67E-04	-1568	9.67E-04	-1566	9.67E-04
-1449	1.01E-03	-1567	1.01E-03	-1565	1.01E-03
-1400	1.04E-03	-1566	1.04E-03	-1564	1.04E-03
-512	1.08E-03	-1565	1.08E-03	-1563	1.08E-03
-451	1.12E-03	-1564	1.12E-03	-1561	1.12E-03
-303	1.16E-03	-1562	1.16E-03	-1560	1.16E-03
-223	1.20E-03	-1561	1.20E-03	-1559	1.20E-03
-159	1.24E-03	-1560	1.24E-03	-1557	1.24E-03
-135	1.28E-03	-1558	1.28E-03	-1556	1.28E-03
-128	1.32E-03	-1557	1.32E-03	-1554	1.32E-03
-102	1.35E-03	-1555	1.35E-03	-1553	1.35E-03
-88	1.39E-03	-1554	1.39E-03	-1551	1.39E-03
-82	1.43E-03	-1553	1.43E-03	-1550	1.43E-03

Continued on next page

Potential mV	Current Density A/cm^2	Potential mV	Current Density A/cm^2	Potential mV	Current Density A/cm^2
-71	1.47E-03	-1552	1.47E-03	-1549	1.47E-03
-60	1.51E-03	-1550	1.51E-03	-1547	1.51E-03
-52	1.55E-03	-1549	1.55E-03	-1546	1.55E-03
-46	1.59E-03	-1548	1.59E-03	-1544	1.59E-03
-39	1.63E-03	-1547	1.63E-03	-1543	1.63E-03
-37	1.66E-03	-1546	1.66E-03	-1542	1.66E-03
-37	1.70E-03	-1546	1.70E-03	-1540	1.70E-03
-37	1.74E-03	-1545	1.74E-03	-1539	1.74E-03
-32	1.78E-03	-1543	1.78E-03	-1537	1.78E-03
-36	1.82E-03	-1541	1.82E-03	-1536	1.82E-03
-43	1.86E-03	-1539	1.86E-03	-1535	1.86E-03
-40	1.90E-03	-1538	1.90E-03	-1533	1.90E-03
-35	1.93E-03	-1536	1.93E-03	-1531	1.93E-03
-42	1.97E-03	-1534	1.97E-03	-1529	1.97E-03
-51	2.01E-03	-1533	2.01E-03	-1528	2.01E-03
-59	2.05E-03	-1532	2.05E-03	-1526	2.05E-03
-60	2.09E-03	-1530	2.09E-03	-1525	2.09E-03
-60	2.13E-03	-1528	2.13E-03	-1523	2.13E-03
-60	2.17E-03	-1527	2.17E-03	-1522	2.17E-03
-60	2.21E-03	-1526	2.21E-03	-1521	2.21E-03
-57	2.24E-03	-1523	2.24E-03	-1519	2.24E-03
-50	2.28E-03	-1522	2.28E-03	-1517	2.28E-03
-40	2.32E-03	-1520	2.32E-03	-1515	2.32E-03
-38	2.36E-03	-1520	2.36E-03	-1513	2.36E-03
-44	2.40E-03	-1518	2.40E-03	-1512	2.40E-03
-44	2.44E-03	-1516	2.44E-03	-1510	2.44E-03
-37	2.48E-03	-1514	2.48E-03	-1509	2.48E-03
-21	2.52E-03	-1513	2.52E-03	-1506	2.52E-03
-31	2.55E-03	-1512	2.55E-03	-1505	2.55E-03
-35	2.59E-03	-1510	2.59E-03	-1503	2.59E-03
-36	2.63E-03	-1508	2.63E-03	-1502	2.63E-03
-33	2.67E-03	-1506	2.67E-03	-1500	2.67E-03
-29	2.71E-03	-1505	2.71E-03	-1498	2.71E-03
-24	2.75E-03	-1503	2.75E-03	-1497	2.75E-03
-19	2.79E-03	-1502	2.79E-03	-1495	2.79E-03

Continued on next page

Potential mV	Current Density A/cm^2	Potential mV	Current Density A/cm^2	Potential mV	Current Density A/cm^2
-11	2.83E-03	-1501	2.83E-03	-1493	2.83E-03
-17	2.86E-03	-1500	2.86E-03	-1492	2.86E-03
-21	2.90E-03	-1497	2.90E-03	-1490	2.90E-03
-20	2.94E-03	-1499	2.94E-03	-1488	2.94E-03
-10	2.98E-03	-1495	2.98E-03	-1486	2.98E-03
-5	3.02E-03	-1494	3.02E-03	-1484	3.02E-03
-6	3.06E-03	-1490	3.06E-03	-1482	3.06E-03
-4	3.10E-03	-1489	3.10E-03	-1481	3.10E-03
2	3.13E-03	-1488	3.13E-03	-1479	3.13E-03
4	3.17E-03	-1487	3.17E-03	-1477	3.17E-03
11	3.21E-03	-1483	3.21E-03	-1476	3.21E-03
13	3.25E-03	-1481	3.25E-03	-1473	3.25E-03
22	3.29E-03	-1478	3.29E-03	-1472	3.29E-03
30	3.33E-03	-1477	3.33E-03	-1469	3.33E-03
26	3.37E-03	-1476	3.37E-03	-1467	3.37E-03
28	3.41E-03	-1475	3.41E-03	-1465	3.41E-03
30	3.44E-03	-1472	3.44E-03	-1464	3.44E-03
34	3.48E-03	-1470	3.48E-03	-1462	3.48E-03
40	3.52E-03	-1467	3.52E-03	-1461	3.52E-03
40	3.56E-03	-1468	3.56E-03	-1458	3.56E-03
41	3.60E-03	-1465	3.60E-03	-1457	3.60E-03
42	3.64E-03	-1462	3.64E-03	-1455	3.64E-03
44	3.68E-03	-1460	3.68E-03	-1453	3.68E-03
49	3.72E-03	-1458	3.72E-03	-1452	3.72E-03
52	3.75E-03	-1457	3.75E-03	-1452	3.75E-03
61	3.79E-03	-1456	3.79E-03	-1451	3.79E-03
63	3.83E-03	-1454	3.83E-03	-1450	3.83E-03
64	3.87E-03	-1452	3.87E-03	-1448	3.87E-03

TABLE B.13: Polarization Data: Aluminum in 5.0% sodium carbonate

Velocity: 0 m/s		Velocity: 2.63 m/s		Velocity: 3.93 m/s	
Potential	Current Density	Potential	Current Density	Potential	Current Density
mV	A/cm^2	mV	A/cm^2	mV	A/cm^2
-1696	3.87E-03	-1696	3.87E-03	-1678	3.87E-03
-1692	3.83E-03	-1693	3.83E-03	-1677	3.83E-03
-1690	3.79E-03	-1691	3.79E-03	-1676	3.79E-03
-1688	3.75E-03	-1690	3.75E-03	-1675	3.75E-03
-1686	3.72E-03	-1689	3.72E-03	-1674	3.72E-03
-1684	3.68E-03	-1688	3.68E-03	-1672	3.68E-03
-1682	3.64E-03	-1687	3.64E-03	-1671	3.64E-03
-1680	3.60E-03	-1686	3.60E-03	-1670	3.60E-03
-1679	3.56E-03	-1685	3.56E-03	-1669	3.56E-03
-1677	3.52E-03	-1683	3.52E-03	-1668	3.52E-03
-1675	3.48E-03	-1682	3.48E-03	-1666	3.48E-03
-1673	3.44E-03	-1681	3.44E-03	-1665	3.44E-03
-1671	3.41E-03	-1680	3.41E-03	-1664	3.41E-03
-1670	3.37E-03	-1679	3.37E-03	-1663	3.37E-03
-1668	3.33E-03	-1678	3.33E-03	-1662	3.33E-03
-1666	3.29E-03	-1676	3.29E-03	-1661	3.29E-03
-1665	3.25E-03	-1675	3.25E-03	-1660	3.25E-03
-1663	3.21E-03	-1674	3.21E-03	-1659	3.21E-03
-1662	3.17E-03	-1673	3.17E-03	-1658	3.17E-03
-1660	3.13E-03	-1671	3.13E-03	-1657	3.13E-03
-1659	3.10E-03	-1670	3.10E-03	-1656	3.10E-03
-1657	3.06E-03	-1669	3.06E-03	-1655	3.06E-03
-1656	3.02E-03	-1667	3.02E-03	-1655	3.02E-03
-1654	2.98E-03	-1666	2.98E-03	-1654	2.98E-03
-1652	2.94E-03	-1665	2.94E-03	-1653	2.94E-03
-1651	2.90E-03	-1664	2.90E-03	-1652	2.90E-03
-1650	2.86E-03	-1663	2.86E-03	-1651	2.86E-03
-1648	2.83E-03	-1662	2.83E-03	-1650	2.83E-03
-1647	2.79E-03	-1660	2.79E-03	-1649	2.79E-03
-1646	2.75E-03	-1659	2.75E-03	-1648	2.75E-03
-1644	2.71E-03	-1658	2.71E-03	-1648	2.71E-03
-1643	2.67E-03	-1657	2.67E-03	-1647	2.67E-03

Continued on next page

Potential mV	Current Density A/cm^2	Potential mV	Current Density A/cm^2	Potential mV	Current Density A/cm^2
-1642	2.63E-03	-1655	2.63E-03	-1646	2.63E-03
-1641	2.59E-03	-1654	2.59E-03	-1644	2.59E-03
-1639	2.55E-03	-1653	2.55E-03	-1643	2.55E-03
-1638	2.52E-03	-1652	2.52E-03	-1642	2.52E-03
-1637	2.48E-03	-1650	2.48E-03	-1642	2.48E-03
-1635	2.44E-03	-1649	2.44E-03	-1641	2.44E-03
-1634	2.40E-03	-1647	2.40E-03	-1640	2.40E-03
-1633	2.36E-03	-1646	2.36E-03	-1639	2.36E-03
-1632	2.32E-03	-1645	2.32E-03	-1638	2.32E-03
-1631	2.28E-03	-1644	2.28E-03	-1636	2.28E-03
-1630	2.24E-03	-1642	2.24E-03	-1635	2.24E-03
-1628	2.21E-03	-1641	2.21E-03	-1634	2.21E-03
-1627	2.17E-03	-1640	2.17E-03	-1633	2.17E-03
-1626	2.13E-03	-1639	2.13E-03	-1631	2.13E-03
-1625	2.09E-03	-1638	2.09E-03	-1630	2.09E-03
-1624	2.05E-03	-1637	2.05E-03	-1630	2.05E-03
-1623	2.01E-03	-1635	2.01E-03	-1629	2.01E-03
-1622	1.97E-03	-1634	1.97E-03	-1627	1.97E-03
-1620	1.93E-03	-1633	1.93E-03	-1626	1.93E-03
-1619	1.90E-03	-1631	1.90E-03	-1625	1.90E-03
-1618	1.86E-03	-1630	1.86E-03	-1624	1.86E-03
-1617	1.82E-03	-1629	1.82E-03	-1622	1.82E-03
-1616	1.78E-03	-1627	1.78E-03	-1621	1.78E-03
-1615	1.74E-03	-1626	1.74E-03	-1620	1.74E-03
-1614	1.70E-03	-1625	1.70E-03	-1619	1.70E-03
-1613	1.66E-03	-1624	1.66E-03	-1617	1.66E-03
-1611	1.63E-03	-1623	1.63E-03	-1615	1.63E-03
-1610	1.59E-03	-1621	1.59E-03	-1614	1.59E-03
-1609	1.55E-03	-1620	1.55E-03	-1613	1.55E-03
-1608	1.51E-03	-1619	1.51E-03	-1611	1.51E-03
-1607	1.47E-03	-1617	1.47E-03	-1610	1.47E-03
-1606	1.43E-03	-1616	1.43E-03	-1609	1.43E-03
-1604	1.39E-03	-1615	1.39E-03	-1608	1.39E-03
-1603	1.35E-03	-1614	1.35E-03	-1607	1.35E-03
-1602	1.32E-03	-1612	1.32E-03	-1605	1.32E-03

Continued on next page

Potential mV	Current Density A/cm^2	Potential mV	Current Density A/cm^2	Potential mV	Current Density A/cm^2
-1600	1.28E-03	-1611	1.28E-03	-1604	1.28E-03
-1599	1.24E-03	-1610	1.24E-03	-1603	1.24E-03
-1598	1.20E-03	-1609	1.20E-03	-1602	1.20E-03
-1596	1.16E-03	-1607	1.16E-03	-1601	1.16E-03
-1596	1.12E-03	-1606	1.12E-03	-1599	1.12E-03
-1594	1.08E-03	-1604	1.08E-03	-1598	1.08E-03
-1593	1.04E-03	-1603	1.04E-03	-1597	1.04E-03
-1592	1.01E-03	-1602	1.01E-03	-1595	1.01E-03
-1590	9.67E-04	-1600	9.67E-04	-1594	9.67E-04
-1589	9.29E-04	-1599	9.29E-04	-1593	9.29E-04
-1588	8.90E-04	-1598	8.90E-04	-1591	8.90E-04
-1587	8.51E-04	-1597	8.51E-04	-1590	8.51E-04
-1585	8.13E-04	-1595	8.13E-04	-1589	8.13E-04
-1584	7.74E-04	-1594	7.74E-04	-1588	7.74E-04
-1583	7.35E-04	-1592	7.35E-04	-1587	7.35E-04
-1581	6.97E-04	-1591	6.97E-04	-1585	6.97E-04
-1580	6.58E-04	-1590	6.58E-04	-1584	6.58E-04
-1579	6.19E-04	-1589	6.19E-04	-1583	6.19E-04
-1577	5.80E-04	-1587	5.80E-04	-1581	5.80E-04
-1576	5.42E-04	-1586	5.42E-04	-1580	5.42E-04
-1575	5.03E-04	-1584	5.03E-04	-1578	5.03E-04
-1573	4.64E-04	-1583	4.64E-04	-1577	4.64E-04
-1572	4.26E-04	-1582	4.26E-04	-1575	4.26E-04
-1571	3.87E-04	-1580	3.87E-04	-1573	3.87E-04
-1569	3.48E-04	-1579	3.48E-04	-1572	3.48E-04
-1567	3.10E-04	-1577	3.10E-04	-1571	3.10E-04
-1566	2.71E-04	-1576	2.71E-04	-1569	2.71E-04
-1564	2.32E-04	-1575	2.32E-04	-1568	2.32E-04
-1563	1.93E-04	-1573	1.93E-04	-1566	1.93E-04
-1561	1.55E-04	-1572	1.55E-04	-1564	1.55E-04
-1559	1.16E-04	-1570	1.16E-04	-1563	1.16E-04
-1557	7.74E-05	-1568	7.74E-05	-1561	7.74E-05
-1555	3.87E-05	-1567	3.87E-05	-1560	3.87E-05
-1553	3.87E-05	-1563	3.87E-05	-1557	3.87E-05
-1551	7.74E-05	-1562	7.74E-05	-1555	7.74E-05

Continued on next page

Potential mV	Current Density A/cm^2	Potential mV	Current Density A/cm^2	Potential mV	Current Density A/cm^2
-1549	1.16E-04	-1560	1.16E-04	-1554	1.16E-04
-1548	1.55E-04	-1559	1.55E-04	-1552	1.55E-04
-1545	1.93E-04	-1557	1.93E-04	-1550	1.93E-04
-1543	2.32E-04	-1556	2.32E-04	-1548	2.32E-04
-1540	2.71E-04	-1554	2.71E-04	-1546	2.71E-04
-1538	3.10E-04	-1553	3.10E-04	-1544	3.10E-04
-1535	3.48E-04	-1550	3.48E-04	-1543	3.48E-04
-1532	3.87E-04	-1548	3.87E-04	-1541	3.87E-04
-1529	4.26E-04	-1547	4.26E-04	-1539	4.26E-04
-1526	4.64E-04	-1545	4.64E-04	-1537	4.64E-04
-1521	5.03E-04	-1543	5.03E-04	-1535	5.03E-04
-1518	5.42E-04	-1542	5.42E-04	-1533	5.42E-04
-1513	5.80E-04	-1540	5.80E-04	-1531	5.80E-04
-1509	6.19E-04	-1538	6.19E-04	-1529	6.19E-04
-1501	6.58E-04	-1536	6.58E-04	-1527	6.58E-04
-1495	6.97E-04	-1534	6.97E-04	-1525	6.97E-04
-1488	7.35E-04	-1532	7.35E-04	-1523	7.35E-04
-1478	7.74E-04	-1530	7.74E-04	-1521	7.74E-04
-1400	8.13E-04	-1528	8.13E-04	-1519	8.13E-04
-1317	8.51E-04	-1526	8.51E-04	-1516	8.51E-04
-1194	8.90E-04	-1524	8.90E-04	-1515	8.90E-04
-1117	9.29E-04	-1522	9.29E-04	-1512	9.29E-04
-1060	9.67E-04	-1520	9.67E-04	-1510	9.67E-04
-985	1.01E-03	-1517	1.01E-03	-1508	1.01E-03
-880	1.04E-03	-1515	1.04E-03	-1506	1.04E-03
-774	1.08E-03	-1513	1.08E-03	-1503	1.08E-03
-684	1.12E-03	-1511	1.12E-03	-1501	1.12E-03
-545	1.16E-03	-1509	1.16E-03	-1498	1.16E-03
-400	1.20E-03	-1507	1.20E-03	-1495	1.20E-03
250	1.24E-03	-1505	1.24E-03	-1493	1.24E-03
290	1.28E-03	-1502	1.28E-03	-1492	1.28E-03
347	1.32E-03	-1500	1.32E-03	-1490	1.32E-03
361	1.35E-03	-1497	1.35E-03	-1487	1.35E-03
430	1.39E-03	-1495	1.39E-03	-1484	1.39E-03
497	1.43E-03	-1492	1.43E-03	-1482	1.43E-03

Continued on next page

Potential mV	Current Density A/cm^2	Potential mV	Current Density A/cm^2	Potential mV	Current Density A/cm^2
547	1.47E-03	-1490	1.47E-03	-1478	1.47E-03
560	1.51E-03	-1487	1.51E-03	-1477	1.51E-03
565	1.55E-03	-1484	1.55E-03	-1474	1.55E-03
583	1.59E-03	-1481	1.59E-03	-1471	1.59E-03
607	1.63E-03	-1479	1.63E-03	-1469	1.63E-03
613	1.66E-03	-1477	1.66E-03	-1466	1.66E-03
652	1.70E-03	-1475	1.70E-03	-1463	1.70E-03
687	1.74E-03	-1471	1.74E-03	-1461	1.74E-03
693	1.78E-03	-1469	1.78E-03	-1458	1.78E-03
695	1.82E-03	-1467	1.82E-03	-1456	1.82E-03
706	1.86E-03	-1464	1.86E-03	-1454	1.86E-03
719	1.90E-03	-1461	1.90E-03	-1450	1.90E-03
724	1.93E-03	-1458	1.93E-03	-1448	1.93E-03
737	1.97E-03	-1455	1.97E-03	-1445	1.97E-03
755	2.01E-03	-1452	2.01E-03	-1441	2.01E-03
773	2.05E-03	-1450	2.05E-03	-1439	2.05E-03
779	2.09E-03	-1446	2.09E-03	-1437	2.09E-03
783	2.13E-03	-1444	2.13E-03	-1434	2.13E-03
789	2.17E-03	-1442	2.17E-03	-1431	2.17E-03
795	2.21E-03	-1437	2.21E-03	-1428	2.21E-03
800	2.24E-03	-1434	2.24E-03	-1426	2.24E-03
805	2.28E-03	-1432	2.28E-03	-1423	2.28E-03
840	2.32E-03	-1429	2.32E-03	-1421	2.32E-03

TABLE B.14: Polarization Data: Aluminum in $FeSO_4$

Velocity: 0 m/s		Velocity: 2.63 m/s		Velocity: 3.93 m/s	
Potential	Current Density	Potential	Current Density	Potential	Current Density
mV	A/cm^2	mV	A/cm^2	mV	A/cm^2
-1000	6.27E-05	-1000	1.66E-03	-1000	2.67E-03
-990	6.11E-05	-950	1.63E-03	-970	2.63E-03
-980	5.96E-05	-900	1.59E-03	-940	2.59E-03
-970	5.84E-05	-850	1.55E-03	-920	2.55E-03
-960	5.73E-05	-780	1.51E-03	-900	2.52E-03
-950	5.65E-05	-540	1.37E-03	-890	2.48E-03
-940	5.61E-05	-530	1.33E-03	-880	2.44E-03
-930	5.57E-05	-520	1.21E-03	-840	2.40E-03
-920	5.50E-05	-510	1.13E-03	-820	2.36E-03
-910	5.46E-05	-500	1.04E-03	-790	2.32E-03
-900	5.38E-05	-490	9.33E-04	-680	2.29E-03
-890	5.30E-05	-480	8.44E-04	-650	2.28E-03
-880	5.26E-05	-470	7.93E-04	-630	2.26E-03
-870	5.22E-05	-460	7.16E-04	-620	2.24E-03
-860	5.22E-05	-450	6.62E-04	-610	2.23E-03
-850	5.19E-05	-440	6.00E-04	-600	2.21E-03
-840	5.19E-05	-430	5.57E-04	-590	2.17E-03
-830	5.15E-05	-420	5.07E-04	-580	2.09E-03
-820	5.11E-05	-410	4.53E-04	-570	2.04E-03
-810	5.07E-05	-400	4.22E-04	-560	1.96E-03
-800	5.03E-05	-390	3.79E-04	-550	1.86E-03
-790	4.99E-05	-380	3.52E-04	-540	1.75E-03
-780	4.91E-05	-370	3.33E-04	-530	1.62E-03
-770	4.88E-05	-360	3.25E-04	-520	1.51E-03
-760	4.80E-05	-350	3.13E-04	-510	1.41E-03
-750	4.76E-05	-340	3.02E-04	-500	1.31E-03
-740	4.72E-05	-330	2.86E-04	-490	1.21E-03
-730	4.68E-05	-320	2.79E-04	-480	1.12E-03
-720	4.64E-05	-310	2.71E-04	-470	1.04E-03
-710	4.57E-05	-300	2.52E-04	-460	9.75E-04
-700	4.53E-05	-290	2.44E-04	-450	8.98E-04
-690	4.49E-05	-280	2.36E-04	-440	8.20E-04

Continued on next page

Potential mV	Current Density A/cm^2	Potential mV	Current Density A/cm^2	Potential mV	Current Density A/cm^2
-680	4.45E-05	-270	2.28E-04	-430	7.74E-04
-670	4.41E-05	-260	2.13E-04	-420	7.08E-04
-660	4.37E-05	-250	2.01E-04	-410	6.46E-04
-650	4.33E-05	-240	1.86E-04	-400	5.96E-04
-640	4.26E-05	-230	1.70E-04	-390	5.57E-04
-630	4.22E-05	-220	1.55E-04	-380	5.19E-04
-620	4.18E-05	-210	1.39E-04	-370	4.88E-04
-610	4.10E-05	-200	1.12E-04	-360	4.53E-04
-600	4.02E-05	-190	8.90E-05	-350	4.26E-04
-590	3.99E-05	-180	6.58E-05	-340	3.91E-04
-580	3.95E-05	-170	4.64E-05	-330	3.64E-04
-570	3.95E-05	-160	1.93E-05	-320	3.41E-04
-560	3.91E-05	-150	3.87E-06	-310	3.21E-04
-550	3.87E-05	-140	7.74E-06	-300	2.98E-04
-540	3.83E-05	-130	1.16E-05	-290	2.83E-04
-530	3.79E-05	-120	1.55E-05	-280	2.67E-04
-520	3.75E-05	-80	1.93E-05	-270	2.48E-04
-510	3.64E-05	-30	2.32E-05	-260	2.36E-04
-500	3.56E-05	20	2.71E-05	-250	2.21E-04
-490	3.37E-05	30	3.10E-05	-240	2.01E-04
-480	3.21E-05	60	3.48E-05	-230	1.86E-04
-470	2.90E-05	70	3.48E-05	-220	1.74E-04
-460	2.52E-05	80	3.87E-05	-210	1.51E-04
-450	2.13E-05	90	3.87E-05	-200	1.39E-04
-440	1.86E-05	100	4.26E-05	-190	1.12E-04
-430	1.74E-05	110	4.26E-05	-180	8.90E-05
-420	1.66E-05	120	4.64E-05	-170	6.58E-05
-410	1.51E-05	130	4.64E-05	-160	3.48E-05
-400	1.39E-05	140	5.03E-05	-150	3.87E-06
-390	1.28E-05	150	5.42E-05	-140	1.16E-05
-380	1.16E-05	160	5.42E-05	-130	1.55E-05
-370	1.01E-05	170	5.80E-05	-100	1.93E-05
-360	8.90E-06	180	5.80E-05	-80	2.32E-05
-350	7.74E-06	190	5.80E-05	-70	2.32E-05
-340	6.97E-06	200	6.19E-05	-50	2.71E-05

Continued on next page

Potential mV	Current Density A/cm^2	Potential mV	Current Density A/cm^2	Potential mV	Current Density A/cm^2
-330	6.19E-06	210	6.58E-05	-40	3.10E-05
-320	5.03E-06	220	6.97E-05	-30	3.10E-05
-310	4.64E-06	230	6.97E-05	-20	3.48E-05
-300	3.87E-06	240	7.35E-05	-10	3.48E-05
-290	2.71E-06	250	7.35E-05	0	3.48E-05
-280	2.32E-06	260	7.74E-05	10	3.87E-05
-270	1.55E-06	270	8.13E-05	20	4.26E-05
-260	1.16E-06	280	8.51E-05	30	4.26E-05
-250	7.74E-07	290	8.51E-05	40	4.26E-05
-240	3.87E-07	300	8.51E-05	50	4.64E-05
-230	7.74E-07	310	8.90E-05	60	4.64E-05
-220	1.55E-06	320	9.29E-05	70	5.42E-05
-210	1.93E-06	330	9.29E-05	80	5.80E-05
-200	2.71E-06	340	9.29E-05	90	6.19E-05
-190	3.48E-06	350	9.67E-05	100	6.19E-05
-180	4.26E-06	360	1.04E-04	110	6.58E-05
-170	5.03E-06	370	1.04E-04	120	6.97E-05
-160	6.19E-06	380	1.12E-04	130	7.35E-05
-150	6.58E-06	390	1.12E-04	140	7.74E-05
-140	7.74E-06	400	1.16E-04	150	8.13E-05
-130	7.74E-06	410	1.20E-04	160	8.51E-05
-120	7.74E-06	420	1.28E-04	170	8.90E-05
-110	8.51E-06	430	1.35E-04	180	9.29E-05
-100	8.51E-06	440	1.43E-04	190	1.01E-04
-90	8.90E-06	450	1.51E-04	200	1.04E-04
-80	9.67E-06	460	1.63E-04	210	1.08E-04
-70	1.01E-05	470	1.74E-04	220	1.12E-04
-60	1.16E-05	480	1.86E-04	230	1.16E-04
-50	1.20E-05	490	1.93E-04	240	1.24E-04
-40	1.32E-05	500	2.17E-04	250	1.32E-04
-30	1.47E-05	510	2.32E-04	260	1.35E-04
-20	1.70E-05	520	2.52E-04	270	1.47E-04
-10	1.86E-05	530	2.75E-04	280	1.55E-04
0	2.05E-05	540	2.90E-04	290	1.66E-04
10	2.09E-05	550	3.10E-04	300	1.70E-04

Continued on next page

Potential mV	Current Density A/cm^2	Potential mV	Current Density A/cm^2	Potential mV	Current Density A/cm^2
20	2.17E-05	560	3.37E-04	310	1.74E-04
30	2.32E-05	570	3.56E-04	320	1.78E-04
40	2.59E-05	580	3.75E-04	330	1.86E-04
50	2.79E-05	590	3.91E-04	340	1.93E-04
60	3.06E-05	600	4.06E-04	350	2.01E-04
70	3.21E-05	610	4.26E-04	360	2.13E-04
80	3.37E-05	620	4.41E-04	370	2.24E-04
90	3.64E-05	630	4.57E-04	380	2.28E-04
100	3.87E-05	640	4.68E-04	390	2.40E-04
110	4.10E-05	650	4.80E-04	400	2.52E-04
120	4.33E-05	660	4.84E-04	410	2.55E-04
130	4.57E-05	670	4.91E-04	420	2.63E-04
140	4.84E-05	680	4.95E-04	430	2.79E-04
150	5.07E-05	690	5.11E-04	440	2.90E-04
160	5.34E-05	700	5.22E-04	450	3.02E-04
170	5.57E-05	710	5.22E-04	460	3.10E-04
180	5.80E-05	720	5.26E-04	470	3.17E-04
190	6.04E-05	730	5.26E-04	480	3.21E-04
200	6.35E-05	740	5.30E-04	490	3.29E-04
210	6.58E-05	750	5.34E-04	500	3.37E-04
220	6.85E-05	760	5.38E-04	510	3.44E-04
230	7.12E-05	770	5.42E-04	520	3.60E-04
240	7.35E-05	780	5.50E-04	530	3.68E-04
250	7.62E-05	790	5.61E-04	540	3.75E-04
260	7.93E-05	800	5.69E-04	550	3.79E-04
270	8.17E-05	810	5.77E-04	560	3.91E-04
280	8.51E-05	820	5.80E-04	570	3.95E-04
290	8.78E-05	830	5.84E-04	580	3.99E-04
300	9.25E-05	840	5.88E-04	590	4.02E-04
310	9.44E-05	850	5.92E-04	600	4.18E-04
320	9.83E-05	860	6.00E-04	610	4.30E-04
330	1.01E-04	870	6.04E-04	620	4.33E-04
340	1.04E-04	880	6.04E-04	630	4.45E-04
350	1.08E-04	890	6.11E-04	640	4.57E-04
360	1.12E-04	900	6.19E-04	650	4.64E-04

Continued on next page

Potential mV	Current Density A/cm^2	Potential mV	Current Density A/cm^2	Potential mV	Current Density A/cm^2
370	1.16E-04	910	6.27E-04	660	4.68E-04
380	1.22E-04	920	6.31E-04	670	4.72E-04
390	1.27E-04	930	6.35E-04	680	4.84E-04
400	1.32E-04	940	6.42E-04	690	4.88E-04
410	1.39E-04	950	6.46E-04	700	4.99E-04
420	1.46E-04	960	6.54E-04	710	5.07E-04
430	1.56E-04	970	6.62E-04	720	5.19E-04
440	1.70E-04	980	6.70E-04	730	5.22E-04
450	1.82E-04	990	6.77E-04	740	5.34E-04
460	1.96E-04	1000	6.85E-04	750	5.50E-04
470	2.11E-04			760	5.61E-04
480	2.29E-04			770	5.65E-04
490	2.48E-04			780	5.69E-04
500	2.63E-04			790	5.77E-04
510	2.85E-04			800	5.88E-04
520	3.00E-04			810	5.96E-04
530	3.25E-04			820	6.00E-04
540	3.44E-04			830	6.15E-04
550	3.64E-04			840	6.19E-04
560	3.87E-04			850	6.23E-04
570	4.06E-04			860	6.42E-04
580	4.30E-04			870	6.58E-04
590	4.45E-04			880	6.73E-04
600	4.64E-04			890	6.85E-04
610	4.80E-04			900	6.85E-04
620	4.99E-04			910	7.08E-04
630	5.03E-04			920	7.24E-04
640	5.15E-04			930	7.31E-04
650	5.34E-04			940	7.35E-04
660	5.38E-04			950	7.47E-04
670	5.50E-04			960	7.62E-04
680	5.69E-04			970	7.66E-04
690	5.77E-04			980	7.70E-04
700	5.84E-04			990	7.89E-04
710	5.88E-04			1000	8.05E-04

Continued on next page

Potential mV	Current Density A/cm^2	Potential mV	Current Density A/cm^2	Potential mV	Current Density A/cm^2
720	6.04E-04				
730	6.11E-04				
740	6.15E-04				
750	6.27E-04				
760	6.27E-04				
770	6.35E-04				
780	6.35E-04				
790	6.39E-04				
800	6.46E-04				
810	6.46E-04				
820	6.46E-04				
830	6.58E-04				
840	6.62E-04				
850	6.62E-04				
860	6.70E-04				
870	6.73E-04				
880	6.73E-04				
890	6.77E-04				
900	6.81E-04				
910	6.89E-04				
920	7.00E-04				
930	7.04E-04				
940	7.08E-04				
950	7.16E-04				
960	7.28E-04				
970	7.31E-04				
980	7.43E-04				
990	7.55E-04				
1000	7.62E-04				

TABLE B.15: Polarization Data: Aluminum in $FeSO_4$+$FeCl_3$

Velocity: 0 m/s		Velocity: 2.63 m/s		Velocity: 3.93 m/s	
Potential	Current Density	Potential	Current Density	Potential	Current Density
mV	A/cm^2	mV	A/cm^2	mV	A/cm^2
-1000	1.71E-03	-1000	9.33E-03	-1000	1.12E-02
-990	1.64E-03	-990	8.86E-03	-990	1.07E-02
-980	1.61E-03	-980	8.71E-03	-980	1.04E-02
-970	1.53E-03	-970	7.93E-03	-970	9.83E-03
-960	1.48E-03	-960	7.78E-03	-960	9.52E-03
-950	1.45E-03	-950	7.55E-03	-950	8.86E-03
-940	1.37E-03	-940	7.24E-03	-940	7.78E-03
-930	1.30E-03	-930	7.04E-03	-930	7.59E-03
-920	1.24E-03	-920	6.77E-03	-920	7.16E-03
-910	1.20E-03	-910	6.58E-03	-910	6.93E-03
-900	1.16E-03	-900	6.11E-03	-900	6.58E-03
-890	1.15E-03	-890	5.84E-03	-890	6.15E-03
-880	1.13E-03	-880	5.34E-03	-880	5.80E-03
-870	1.12E-03	-870	5.03E-03	-870	5.57E-03
-860	1.07E-03	-860	4.64E-03	-860	5.34E-03
-850	1.02E-03	-850	4.45E-03	-850	4.88E-03
-840	9.75E-04	-840	4.14E-03	-840	4.61E-03
-830	9.40E-04	-830	3.95E-03	-830	4.22E-03
-820	9.06E-04	-820	3.75E-03	-820	3.91E-03
-810	8.67E-04	-810	3.37E-03	-810	3.60E-03
-800	8.28E-04	-800	2.98E-03	-800	3.29E-03
-790	7.78E-04	-790	2.52E-03	-790	3.02E-03
-780	7.35E-04	-780	2.21E-03	-780	2.71E-03
-770	6.42E-04	-770	1.66E-03	-770	2.17E-03
-760	5.11E-04	-760	1.28E-03	-760	1.90E-03
-750	3.44E-04	-750	8.90E-04	-750	1.63E-03
-740	1.82E-04	-740	4.26E-04	-740	1.32E-03
-730	4.26E-05	-730	2.32E-04	-730	1.16E-03
-720	2.21E-04	-720	1.55E-04	-720	5.03E-04
-710	4.72E-04	-710	3.87E-04	-710	2.32E-04
-700	7.20E-04	-700	8.51E-04	-700	3.87E-04
-690	1.06E-03	-690	1.24E-03	-690	7.74E-04

Continued on next page

Potential mV	Current Density A/cm^2	Potential mV	Current Density A/cm^2	Potential mV	Current Density A/cm^2
-680	1.39E-03	-680	1.63E-03	-680	1.01E-03
-670	1.75E-03	-670	2.09E-03	-670	1.32E-03
-660	2.15E-03	-660	2.32E-03	-660	1.47E-03
-650	2.48E-03	-650	2.59E-03	-650	1.74E-03
-640	2.79E-03	-640	3.02E-03	-640	2.21E-03
-630	3.17E-03	-630	3.48E-03	-630	2.40E-03
-620	3.53E-03	-620	3.68E-03	-620	2.90E-03
-610	3.91E-03	-610	4.14E-03	-610	3.41E-03
-600	4.18E-03	-600	4.45E-03	-600	3.68E-03
-590	4.53E-03	-590	4.88E-03	-590	4.06E-03
-580	4.95E-03	-580	5.19E-03	-580	4.26E-03
-570	5.26E-03	-570	5.57E-03	-570	4.80E-03
-560	5.61E-03	-560	5.92E-03	-560	5.38E-03
-550	6.08E-03	-550	6.39E-03	-550	5.57E-03
-540	6.42E-03	-540	6.73E-03	-540	5.77E-03
-530	6.77E-03	-530	7.08E-03	-530	5.96E-03
-520	7.12E-03	-520	7.43E-03	-520	6.39E-03
-510	7.55E-03	-510	7.74E-03	-510	6.54E-03
-500	7.89E-03	-500	8.01E-03	-500	6.73E-03
-490	8.32E-03	-490	8.75E-03	-490	7.00E-03
-480	8.71E-03	-480	8.90E-03	-480	7.55E-03
-470	9.06E-03	-470	9.29E-03	-470	7.86E-03
-460	9.44E-03	-460	9.64E-03	-460	8.13E-03
-450	9.87E-03	-450	9.83E-03	-450	8.71E-03
-440	1.06E-02	-440	1.01E-02	-440	8.98E-03
-430	1.09E-02	-430	1.03E-02	-430	9.33E-03
-420	1.13E-02	-420	1.07E-02	-420	9.83E-03
-410	1.17E-02	-410	1.09E-02	-410	1.04E-02
-400	1.23E-02	-400	1.12E-02	-400	1.06E-02
-390	1.27E-02	-390	1.18E-02	-390	1.10E-02
-380	1.32E-02	-380	1.21E-02	-380	1.14E-02
-370	1.36E-02	-370	1.24E-02	-370	1.16E-02
-360	1.40E-02	-360	1.27E-02	-360	1.18E-02
-350	1.44E-02	-350	1.31E-02	-350	1.23E-02
-340	1.55E-02	-340	1.34E-02	-340	1.28E-02

Continued on next page

Potential mV	Current Density A/cm^2	Potential mV	Current Density A/cm^2	Potential mV	Current Density A/cm^2
-330	1.61E-02	-330	1.37E-02	-330	1.34E-02
-320	1.64E-02	-320	1.38E-02	-320	1.37E-02
-270	1.71E-02	-310	1.43E-02	-310	1.40E-02
-250	1.73E-02	-300	1.46E-02	-300	1.42E-02
-240	1.75E-02	-290	1.50E-02	-290	1.47E-02
-230	1.78E-02	-280	1.54E-02	-280	1.49E-02
-220	1.82E-02	-270	1.57E-02	-270	1.51E-02
-210	1.84E-02	-260	1.59E-02	-260	1.53E-02
-200	1.90E-02	-250	1.63E-02	-250	1.57E-02
-190	1.95E-02	-240	1.66E-02	-240	1.59E-02
-180	1.98E-02	-230	1.68E-02	-230	1.63E-02
-170	2.02E-02	-220	1.72E-02	-220	1.65E-02
-160	2.04E-02	-210	1.75E-02	-210	1.67E-02
-150	2.07E-02	-200	1.77E-02	-200	1.69E-02
-140	2.12E-02	-190	1.79E-02	-190	1.72E-02
-130	2.16E-02	-180	1.83E-02	-180	1.75E-02
-120	2.19E-02	-170	1.88E-02	-170	1.77E-02
-110	2.22E-02	-160	1.92E-02	-160	1.79E-02
-100	2.24E-02	-150	1.96E-02	-150	1.82E-02
-90	2.29E-02	-140	1.99E-02	-140	1.86E-02
-80	2.34E-02	-130	2.03E-02	-130	1.90E-02
-70	2.38E-02	-120	2.05E-02	-120	1.98E-02
-60	2.43E-02	-110	2.09E-02	-110	2.02E-02
-50	2.53E-02	-100	2.11E-02	-100	2.07E-02
-40	2.84E-02	-90	2.14E-02	-90	2.11E-02
-30	2.94E-02	-80	2.17E-02	-80	2.14E-02
-20	2.98E-02	-70	2.20E-02	-70	2.15E-02
-10	3.02E-02	-60	2.23E-02	-60	2.18E-02
0	3.05E-02	-50	2.28E-02	-50	2.21E-02
		-40	2.33E-02	-40	2.23E-02
		-30	2.37E-02	-30	2.26E-02
		-20	2.40E-02	-20	2.28E-02
		-10	2.43E-02	-10	2.32E-02
		0	2.46E-02	0	2.37E-02

References

[1] Viscount J, *The Grand Fleet 1914-1916: its creation, development and work*, Cassell, London, 1919

[2] Postlethwaite J and Nesic S, *Uhlig's Corrosion Handbook*, Ch. Erosion-Corrosion in Single and Multiphase Flow, John Wiley & Sons, 2nd edition, 2000. pp. 249–272

[3] Poulson B, *Corrosion*, Vol. 1, Ch. Erosion Corrosion, Butterworth-Heinemann, 1994. pp. 1:293–1:303

[4] Wood RJK, *Comprehensive Structure Integrity: Environmentally Assisted Fatigue*, Vol. 6, Ch. Erosion/Corrosion, Elsevier, Amsterdam, 1st edition, 2003. pp. 395–427

[5] Gabe D, Wilcox G, Gonzalez-Garcia J and Walsh F, *The rotating cylinder electrode: its continued development and application*, Journal of Applied Electrochemistry, 1998. **28**(8):pp. 759–780

[6] Silverman DC, *The Rotating Cylinder Electrode for Examining Velocity-Sensitive Corrosion - A Review*, Corrosion, 2004. **60**(11):pp. 1003–1023

[7] Matsumara M, Oka Y, Okumoto S and Furuya H, *Laboratory Corrosion Tests and Standards*, Ch. Jet-in-Slit Test for Studying Erosion-Corrosion, ASTM International, 1985. pp. 358–372

[8] Zu J, Hutchings I and Burstein G, *Design of a Slurry Erosion Test Rig*, Wear, 1990. **140**(2):pp. 331–344

[9] Burstein GT and Sasaki K, *Effect of impact angle on the slurry erosion-corrosion of 304L stainless steel*, Wear, 2000. **240**(1-2):pp. 80–94

[10] Sasaki K and Burstein G, *Erosioncorrosion of stainless steel under impingement by a fluid jet*, Corrosion Science, 2007. **49**(1):pp. 92–102

[11] Gant A, Gee M and Plint G, *A new concept in liquid jet erosion: Commissioning and probing trials*, Wear, 2007. **263**(1-6):pp. 284–288

[12] Matsumara M, Noishiki K and Sakamoto A, *Jet-in-slit test for reproducing flow-induced localized corrosion on copper alloys*, Corrosion, 1998. **54**(1):pp. 79–88

[13] Efird KD, *Jet Impingement Testing for Flow Accelerated Corrosion, in Corrosion/2000*, Paper No. 00052, NACE, Houston

[14] Demoz A, Revie W, Papavinasam S, Dabros T and Michaelian K, *A New Impinging Jet Device for Corrosion Studies*, Corrosion, 2004. **60**(5):pp. 455–464

[15] Poulson BS, *Electrochemical measurements in flowing solutions*, Corrosion Science, 1983. **23**(4):pp. 391–430

[16] Moniz B and Zhang SH, *Corrosion Tests and Standards: Application and Interpretation*, Ch. Chemical Processing, ASTM International, 2nd edition, 2005. pp. 779–794

[17] *Standard Terminology Relating to Corrosion and Corrosion Testing*, 2006

[18] Poulson B, *Complexities in Predicting Erosion Corrosion*, Wear, 1999. **233-235**:pp. 497–504

[19] Bird RB, Stewart WE and Lightfoot EN, *Transport Phenomena*, John Wiley & Sons, New York, USA, 2nd edition, 2002

[20] Massoud M, *Engineering Thermofluids: Thermodynamics, Fluid Mechanics, and Heat Transfer*, Springer, 2005

[21] Efird KD, *Uhlig's Corrosion Handbook*, Ch. Flow-Induced Corrosion, John Wiley & Sons, 2nd edition, 2000. pp. 233–248

[22] Schlichting H, *Boundary-Layer Theory*, McGraw-Hill Book Company, New Yprk, USA, 7th edition, 1979

[23] Efird KD, *Effect of Fluid Dynamics on the Corrosion of Copper-Based Alloys in Seawater*, Corrosion, 1977. **33**(1):pp. 3–8

[24] Syrett BC and Wing SS, *Effect of Flow on Corrosion of Copper-Nickel Alloys in Aerated Seawater and in Sulfide-Polluted Seawater*, Corrosion, 1980. **36**(2):pp. 73–84

[25] Skold RV and Larson TE, *Measurement of the Instantaneous Corrosion Rate by Means of Polarization Data*, Corrosion, 1957. **13**(2):pp. 139t–142t

[26] Luce WA and Fontana MG, *Erosion-Corrosion of Metals and Alloys*, Corrosion, 1949. **5**(6):pp. 189–193

[27] Berger F and Hau KFL, *Mass transfer in turbulent pipe flow measured by the electrochemical method*, International Journal of Heat and Mass Transfer, 1977. **20**(11):pp. 1185–1194

[28] Stack MM, Chacon-Nava J and Stott FH, *Relationship between the effects of velocity and alloy corrosion resistance in erosion-corrosion environments at elevated temperatures*, Wear, 1995. **180**(1-2):pp. 91–99

[29] Roe FL, Lewandowski Z and Funk T, *Simulating Microbiologically Influenced Corrosion by Depositing Extracellular Biopolymers on Mild Steel Surfaces*, Corrosion, 1996. **52**(10):pp. 744–752

[30] Fontana M, *Corrosion Engineering*, McGraw-Hill Book Company, 3rd edition, 1986

[31] Bremhorst K and Lai JCS, *The Role of Flow Characteristics in Corrosion-Erosion of Tube Inlets in the Inlet Channel of Shell and Tube Heat Exchangers*, Wear, 1979. **54**(1):pp. 87–100

[32] Dawson DA and Trass O, *Mass transfer at rough surfaces*, International Journal of Heat and Mass Transfer, 1972. **15**(7):pp. 1317–1336

[33] Heymann FJ, *ASM Handbook Volume 18: Friction, Lubrication, and Wear Technology*, Ch. Liquid Impingement Erosion, American Society for Metals (ASM) International, 1992. pp. 221–235

[34] Sasaki K and Burstein GT, *The Generation of Surface Roughness During Slurry Erosion-Corrosion and Its Effect on the Pitting Potential*, Corrosion Science, 1996. **38**(12):pp. 2111–2120

[35] Al Hossani HI, Saber TMH, Mohammed RA and Shams El Din AM, *Galvanic corrosion of copper-base alloys in contact with molybdenum-containing stainless steels in Arabian Gulf water*, Desalination, 1997. **109**(1):pp. 25–37

[36] Wood RJK, Wharton JA, Speyer AJ and Tan KS, *Investigation of erosion-corrosion processes using electrochemical noise measurements*, Tribology International, 2002. **35**(10):pp. 631–641

[37] Lotz U and Heitz E, *Flow-dependent corrosion. I. Current understanding of the mechanisms involved*, Materials and Corrosion, 1983. **34**(9):pp. 454–461

[38] Syrett BC, *Erosion-Corrosion of Copper-Nickel Alloys in Seawater and Other Aqueous Environments A Literature Review*, Corrosion, 1976. **32**(6):pp. 242–252

[39] Danek GJ, *The Effect of Sea-Water Velocity on the Corrosion Behavior of Metals*, Naval Engineers Journal, 1966. **78**(5):pp. 763–769

[40] Kosel TH, *ASM Handbook Volume 18: Friction, Lubrication, and Wear Technology*, Ch. Solid Particle Erosion, American Society for Metals (ASM) International, 1992. p. 95

[41] Nesic S, *Computation of localized erosion-corrosion in disturbed two-phase flow*, Ph.D. thesis, The University of Saskatchewan, Canada, 1991

[42] Postlethwaite J, Brady BJ, Hawrylak MW and Tinker EB, *Effects of Corrosion on the Wear Patterns in Horizontal Slurry Pipelines*, Corrosion, 1978. **34**(7):pp. 245–250

[43] Postlethwaite J and Nesic S, *Erosion in Disturbed Liquid/Particle Pipe Flow: Effects of Flow Geometry and Particle Surface Roughness*, Corrosion, 1993. **49**(10):pp. 850–857

[44] Heymann FJ, *ASM Handbook Volume 18: Friction, Lubrication, and Wear Technology*, Ch. Liquid Impingement Erosion, American Society for Metals (ASM) International, 1992

[45] Hansson CM, *ASM Handbook Volume 18: Friction, Lubrication, and Wear Technology*, Ch. Cavitation Erosion, American Society for Metals (ASM) International, 1992

[46] Madsen BW, *Measurement of erosion-corrosion synergism with a slurry wear test apparatus*, Wear, 1988. **123**(2):pp. 127–142

[47] Wood R and Hutton S, *The synergistic effect of erosion and corrosion: trends in published results*, Wear, 1990. **140**(2):pp. 387–394

[48] Wood RJK, *The Synergistic Effect of Cavitation Erosion and Corrosion For Copper and Cupro-Nickel in Seawater*, Journal of fluids engineering, 1989. **111**(3):pp. 271–277

[49] Oka Y, Matsumara M and Yamawaki M, *Slurry erosion-corrosion on commercially pure iron in a vibratory testing facility - mechanism of erosion-corrosion under predominantly erosion conditions, in 7th international conference on erosion by liquid and solid impact*, University of Cambridge, Cambridge, UK

[50] Fry SA and Wood RJK, *The synergistic effect of cavitation erosion and corrosion*, Technical Report ME/85/21, Department of Mechanical Engineeing, The University of Southampton, 1985

[51] Zheng Y, Yao Z, Wei X and Ke W, *The synergistic effect between erosion and corrosion in acidic slurry medium*, Wear, 1995. **186-187**(Part 2):pp. 555–561

[52] Watson SW, Friedersdorf FJ, Madsen BW and Cramer SD, *Methods of measuring wear-corrosion synergism*, Wear, 1995. **181-183**(Part 2):pp. 476–484

[53] Zhou S, Stack MM and Newman RC, *Characterization of Synergistic Effects Between Erosion and Corrosion in an Aqueous Environment Using Electrochemical Techniques*, Corrosion, 1996. **52**(12):pp. 934–946

[54] Ferng YM, Ma YP, Ma KT and Chung NM, *A New Approach for Investigation of Erosion-Corrosion Using Local Flow Models*, Corrosion, 1999. **55**(4):pp. 332–342

[55] Bozzini B, Ricotti ME, Boniardi M and Mele C, *Evaluation of erosion-corrosion in multi-phase flow via CFD and experimental analysis*, Wear, 2003. **255**(1-6):pp. 237–245

[56] Wood RJK, *Erosion-corrosion synergism for multi-phase flowline materials*, La Houille blanche, 1992. **47**(7-8):pp. 605–610

[57] Neville A and Hu X, *Mechanical and electrochemical interactions during liquid-solid impingement on high-alloy stainless steels*, Wear, 2001. **251**(1-12):pp. 1284–1294

[58] Wood RJ, *Erosion-corrosion interactions and their effect on marine and offshore materials*, Wear, 2006. **261**(9):pp. 1012–1023

[59] Hogmark S, Hammersten A and Soderberg S, *On the Combined Effects of Erosion and Corrosion, in 6th international conference on erosion by liquid and solid impact*, University of Cambridge, Cambridge, UK

[60] Kang C, Pettit F and Birks N, *Mechanisms in the simultaneous erosion-oxidation attack of nickel and cobalt at high temperature*, Metallurgical and Materials Transactions A, 1987. **18**(10):pp. 1785–1803

[61] Stack MM, Lekatos S and Stott FH, *Erosion-corrosion regimes: number, nomenclature and justification?*, Tribology International, 1995. **28**(7):pp. 445–451

[62] Sundararajan G, *The Solid Particle Erosion of Metallic Materials at Elevated Temperatures, in Proceedings of Corrosion-Erosion-Wear of Materials at Elevated Temperatures*, ed. Levy AV, Paper No. 11, Berkeley, California, pp. 1–11

[63] Stack MM, Zhou S and Newman RC, *Identification of transitions in erosion-corrosion regimes in aqueous environments*, Wear, 1995. **186-187**(Part 2):pp. 523–532

[64] Stack MM, Corlett N and Zhou S, *A methodology for the construction of the erosion-corrosion map in aqueous environments*, Wear, 1997. **203-204**:pp. 474–488

[65] Stack MM, Corlett N and Turgoose S, *Some recent advances in the development of theoretical approaches for the construction of erosion-corrosion maps in aqueous conditions*, Wear, 1999. **233-235**:pp. 535–541

[66] Stack MM and Pungwiwat N, *Particulate erosion-corrosion of Al in aqueous conditions: some perspectives on pH effects on the erosion-corrosion map*, Tribology International, 2002. **35**(10):pp. 651–660

[67] Stack MM, Corlett N and Turgoose S, *Some thoughts on modelling the effects of oxygen and particle concentration on the erosion-corrosion of steels in aqueous slurries*, Wear, 2003. **255**(1-6):pp. 225–236

[68] Stack MM and Pungwiwat N, *Erosion-corrosion mapping of Fe in aqueous slurries: some views on a new rationale for defining the erosion-corrosion interaction*, Wear, 2004. **256**(5):pp. 565–576

[69] Keller H, *Erosionskorrosion an Nassdampfturbinen*, VGB Kraftwerkstechnik, 1974. **54**(5):pp. 292–295

[70] Cottis R, *Techniques for Corrosion Monitoring*, Ch. Electrochemical Noise for Corrosion Monitoring, Woodhead Publishing, Cambridge, UK, 2008. pp. 86–110

[71] Huet F, *Analytical Methods in Corrosion Science and Engineering*, Ch. Electrochemical Noise Technique, Taylor and Francis, Boca Raton, FL, USA, 2006. pp. 507–570

[72] Pots BF, Hollenberg J and Hendriksen E, *What are the Real Influences of Flow on Corrosion?, in Corrosion/2006*, Paper No. 06591, NACE, Houston, Texas, USA

[73] *State-of-the-Art Report on Controlled-flow Laboratory Corrosion Tests*, Technical Report NACE Publication 5A195, NACE, 1995

[74] Liu G, Tree D and High M, *Relationships between rotating disk corrosion measurements and corrosion in pipe flow*, Corrosion, 1994. **50**(8):pp. 584–593

[75] Levich VG, *Physicochemical hydrodynamics*, Prentice-Hall, Englewood Cliffs, NJ, USA, 1962

[76] Chin D and Litt M, *An electrochemical study of flow instability on a rotating disk*, Journal of Fluid Mechanics, 1972. **54**(4):pp. 613–625

[77] Maciel J and Agostinho S, *Use of a rotating cylinder electrode in corrosion studies of a 90/10 CuNi alloy in 0.5 mol L 1 H2SO4 media*, Journal of Applied Electrochemistry, 2000. **30**(8):pp. 981–985

[78] Kear G, Barker B and Walsh F, *Electrochemical study of UNS S32550 super duplex stainless steel corrosion in turbulent seawater using the rotating cylinder electrode*, CORROSION-HOUSTON TX-, 2004. **60**:pp. 561–572

[79] Silverman DC, *Rotating Cylinder Electrode for Velocity Sensitivity Testing*, Corrosion, 1984. **40**(5):pp. 220–226

[80] Adams RN, *Electrochemistry at solid electrodes*, M. Dekker, New York, 1969

[81] Newman J, *Electrochemical Systems*, Prentice-Hall, New York, 1973

[82] Eisenberg M, Tobias CW and Wilke CR, *Ionic Mass Transfer and Concentration Polarization at Rotating Electrodes*, Journal of the Electrochemical Society, 1954. **101**(6):pp. 306–320

[83] Esteban J, Hickey G and Orazem M, *Impinging Jet Electrode: Measurement of the Hydrodynamic Constant and Its Use for Evaluating Film Persistency*, Corrosion, 1990. **46**(11):pp. 896–901

[84] Efird KD, Wright EJ, Boros JA and Hailey TG, *Correlation of Steel Corrosion in Pipe Flow with Jet Impingement and Rotating Cylinder Tests*, Corrosion, 1993. **49**(12):pp. 992–1003

[85] Lush P, *Relation Between Impingement Corrosion and Fluid Turbulence Intensity, in EUROCOR'77, 6 th European Congress on Metallic Corrosion*, London, pp. 137–146

[86] Giralt F and Trass O, *Mass transfer from crystalline surfaces in a turbulent impinging jet part I. Transfer by erosion*, The Canadian Journal of Chemical Engineering, 1975. **53**(5):pp. 505–511

[87] Giralt F and Trass O, *Mass transfer from crystalline surfaces in a turbulent impinging jet. part 2: Erosion and diffusional transfer*, The Canadian Journal of Chemical Engineering, 1976. **54**(3):pp. 148–155

[88] Efird K, Wright E, Boros J and Hailey T, *Wall shear stress and flow accelerated corrosion of carbon steel in sweet production, in Proceedings of the 12th International Corrosion Congress*, Houston, pp. 2662–2679

[89] Orazem M, Cardoso Filho J and Tribollet B, *Application of a submerged impinging jet for corrosion studies: development of models for the impedance response*, Electrochimica Acta, 2001. **46**(24-25):pp. 3685–3698

[90] Diem C and Orazem M, *Influence of velocity on corrosion of copper in alkaline chloride solutions*, Corrosion, 1994. **50**(04):pp. 290–300

[91] Abayarathna D, Naraghi A and Grahmann N, *Inhibitor Evaluations Using Various Corrosion Measurement Techniques in Laboratory Flow Loops, in Corrosion/2000*, Paper No. 00021, NACE, Houston

[92] Ross TK, Wood GC and Mahmud I, *The Anodic Behavior of Iron-Carbon Alloys in Moving Acid Media*, Journal of the Electrochemical Society, 1966. **113**(4):pp. 334–345

[93] Shadley J, Shirazi S, Dayalan E, Ismail M and Rybicki E, *Erosion-corrosion of a carbon steel elbow in a carbon dioxide environment*, Corrosion, 1996. **52**(09):pp. 715–723

[94] Hong T and Jepson W, *Corrosion inhibitor studies in large flow loop at high temperature and high pressure*, Corrosion Science, 2001. **43**(10):pp. 1839–1849

[95] Heitz E, *Analytical Methods in Corrosion Science and Engineering*, Ch. DC Electrochemical Methods, CRC Press, Boca Raton, FL, 2006. pp. 435–462

[96] Gonzales JA, Benito M and Feliu S, *Suitability of Assessment Methods for Identifying Active and Passive Zones in Reinforced Concrete*, Corrosion, 1995. **51**:pp. 145–152

[97] Heitz E, Henkhaus R and Rahmel A, *Corrosion Science: an Experimental Approach*, Ellis Horwood, Chichester, UK, 1992

[98] Song HW and Saraswathy V, *Corrosion Monitoring of Reinforced Concrete Structures - A Review*, International Journal of Electrochemcal Science, 2007. **2**(1):pp. 1–28

[99] Stellwag WB and Wieling N, *Electrochemical Corrosion Testing*, Vol. 101, Ch. Electrode potential monitoring in hot water systems a method to identify critical corrosion conditions, DECHEMA, 1986. pp. 17–26

[100] Truong V, Lai P, Moore B, Muscat R and Russo M, *Corrosion protection of magnesium by electroactive polypyrrole/paint coatings*, Synthetic Metals, 2000. **110**(1):pp. 7–15

[101] Stern M and Geary AL, *Electrochemical Polarization*, Journal of the Electrochimical Society, 1957. **104**(1):pp. 56–63

[102] Grauer R, Moreland PR and Pini G, *A Literature Review of Polarization Resistance Constant (B) Values for the Measurement of Corrosion Rate*, Technical Report Publication No. 52405, NACE, Houston, Texas, 1982

[103] Afshar A, Dolati A and Ghorbani M, *Electrochemical characterization of the NiFe alloy electrodeposition from chloridecitrateglycolic acid solutions*, Materials Chemistry & Physics, 2003. **77**(2):pp. 352–358

[104] Jaki J, Vojnovi M and Krstaji N, *Kinetic analysis of hydrogen evolution at NiMo alloy electrodes*, Electrochimica acta, 2000. **45**(25-26):pp. 4151–4158

[105] Broli A and Holtan H, *Determination of Characteristic Pitting Potentials for Aluminum by Use of the Potentiostatic Methods*, Corrosion Science, 1977. **17**(1):pp. 59–69

[106] Broli A and Holtan H, *Use of Potentiokinetic Methods for the Determination of Characteristic Potentials for Pitting Corrosion of Aluminum in a Deaerated Solution of 3 Percent NaCl*, Corrosion Science, 1973. **13**(4):pp. 237–246

[107] Evans K, Yilmaz A, Day S, Wong L, Estill J and Rebak R, *Using electrochemical methods to determine alloy 22s crevice corrosion repassivation potential*, Journal of the Minerals, Metals and Materials Society, 2005. **57**(1):pp. 56–61

[108] Parkins R, *Predictive approaches to stress corrosion cracking failure*, Corrosion Science, 1980. **20**(2):pp. 147–166

[109] Cihal V and tefec R, *On the development of the electrochemical potentiokinetic method*, Electrochimica acta, 2001. **46**(24-25):pp. 3867–3877

[110] Wang W, Hartt W and Chen S, *Sacrificial Anode Cathodic Polarization of Steel in Seawater: Part 1 A Novel Experimental and Analysis Methodology*, Corrosion, 1996. **52**(6):pp. 419–427

[111] Tan C and Blackwood D, *Corrosion protection by multilayered conducting polymer coatings*, Corrosion Science, 2003. **45**(3):pp. 545–557

[112] Eriksurd E and Heitz E, *Guidelines on Electrochemical Corrosion Measurements*, Ch. Reference Electrodes, Institute of Metals, London, 1990. pp. 34–36

[113] Bard AJ and Faulkner LR, *Electrochemical Methods: Fundamentals and Applications*, John Wiley & Sons, New York, 2nd edition, 2001

[114] Easin ABM, *Erosion-Corrosion Studies of Steel*, Master's thesis, Department of Chemical Engineering, Bangladesh University of Engineering and Technology, Dhaka, Bangladesh, 1986

[115] Burstein GT and Ilevbare GO, *The effect of specimen size on the measured pitting potential of stainless steel*, Corrosion Science, 1996. **38**(12):pp. 2257–2265

[116] Vargel C, *Corrosion of Aluminium*, Elsevier, 2004

[117] Uhlig H, *The Cost of Corrosion to the United States*, Corrosion, 1950. **6**(1):pp. 29–33

[118] Fraser J, *Corrosion Economics*, Materials Performance, 1974. **13**(4):pp. 15–17

[119] Bhaskaran R, Palaniswamy N and Rengaswamy N, *Corrosion: Materials, ASM Handbook*, Vol. 13B, Ch. Global Cost of Corrosion - A Historical Review, ASM International, 2005. pp. 621–628

[120] Verink E, Kolts J, Rumble J and Ugiansky G, *Corrosion Data Program Workshop Summary*, Materials Performance, 1987. **26**(4):pp. 55–60

[121] Koch G, Brongers M, Thompson N, Virmani Y and Payer J, *Corrosion Cost and Preventive Strategies in the United States*, Technical Report FHWA Report RD-01-156, Federal Highway Administration, U.S. Department of Transportation, 2002

[122] Behrens D, *Research and Development Program on Corrosion and Corrosion Protection in the German Federal Republic*, British Corrosion Journal, 1975. **10**(3):pp. 122–127

[123] Javaherdashti R, *How Corrosion Affects Industry and Life*, Anti-Corrosion Methods and Materials, 2000. **47**(1):pp. 30–34

[124] Hoar T, *Report of the Committee on Corrosion and ProtectionA Survey of Corrosion and Protection in the United Kingdom,*, Technical report, Her Majesty's Stationery Office, London, 1971

[125] Hoar T, *Corrosion of Metals: Its Cost and Control*, Proceedings of the Royal Society A, 1976. **348**(1652):pp. 1–18

[126] Worner HK, *The Cost of Corrosion*, Anti-Corrosion Methods and Materials, 1956. **3**(9):pp. 289–292

[127] Revie R and Uhlig H, *The Cost of Corrosion to Australia*, Journal of Institute of Engineers (Australia), 1974. **46**(3-4):pp. 3–5

[128] Rajagopalan K, *Metallic Corrosion: Cost and Prevention*, Journal of Scientific and Industrial Research, 1958. **17**(A):pp. 191–193

[129] Rajagopalan K, *Application of NBS-BCL Analysis to Cost of Corrosion in Various Sectors of Indian Economy*, Paint India, 1986. **36**(3):pp. 35–40

[130] Bhaskaran R, Rengaswamy N and Palaniswamy N, *Impact of Metallic Corrosion, Part II: Economic Impact*, Corrosion Update, 2001. (60):pp. 2–4

[131] *Report of the Committee on Corrosion and Protection*, Corrosion Engineering (in Japanese), 1977. **26**(7):pp. 401–428

[132] Shibata T, *Cost of Corrosion in Japan*, Corrosion Science and Technology, 2002. **31**(2):pp. 97–102

[133] Smith H, *What Corrosion Costs Canada*, Canadian Chemical Processing, 1953. **37**(10):p. 10

[134] Palmer J, *Corrosion: Our $1 Billion Write-Off*, Canadian Chemical Processing, 1966. **50**(3):pp. 55–57

[135] Slabbert M and Robinson F, *Economic Effects of Metallic Corrosion in South Africa*, Corrosion and Coatings, SA, 1985. **12**:pp. 3–8